NUMERICAL MODELING OF TRACE MERCURY DYNAMICS BASED ON NEW ANALYSIS OF MERCURY IN SEDIMENTS IN MINAMATA BAY AND THE YATSUSHIRO SEA, JAPAN

遅, 百鑫

NUMERICAL MODELING OF TRACE MERCURY DYNAMICS BASED ON NEW ANALYSIS OF MERCURY IN SEDIMENTS IN MINAMATA BAY AND THE YATSUSHIRO SEA, JAPAN

Baixin CHI

Abstract

With rapid industrialization, the pollution of heavy metals has aroused widespread concern in human society. Among these heavy metals, mercury is one of the most well-known and harmful heavy metals. It is widely distributed in the environment and exists in both inorganic and organic forms and is released into the environment through natural causes as well as human activities. After mercury enters the natural environment, it continuously migrates and transforms through the mercury cycle, mainly including transportation in the atmosphere, deposition from the atmosphere to land and ocean, volatilization from land and sea, and accumulation in organisms. After mercury is released into the environment and absorbed by primary organisms, it can bioaccumulate and biomagnify through the food web. Meanwhile, mercury poses a severe threat to the ecosystem and human health due to its environmental persistence.

One of the most severe environmental pollution incidents caused by mercury was the Minamata disease that occurred in Minamata Bay area in 1956. Since the factory discharged methylmercury produced during the production process into the bay along with sewage, shellfish and fish in the sea were polluted with mercury. Mercury was continuously enriched in higher fish through the food web, and eventually, humans experienced symptoms of mercury poisoning after eating these mercury-contaminated fish. As of the end of April 2022, the total number of confirmed patients was 2,284, and more than 40,000 people showed symptoms such as sensory disturbances affected by mercury. To deal with mercury pollution, in 1977, the Minamata Bay Pollution Prevention Project was initiated to dispose of sedimentary sludge containing over 25 ppm of total mercury (T-Hg).

Although the sediments with a concentration of more than 25 ppm had been dredged,

some studies have shown that the total mercury concentration in the bay area is still high, much higher than the background concentration in the natural environment. Moreover, some studies have found that the mercury levels in benthic organisms (*e.g.*, Gaetice and Snail) and fish (*e.g.*, Japanese stickleback and Bamboo wrasse) near the bay fish are higher than in other regions. Furthermore, many studies have shown that mercury in the bay migrated to the Yatsushiro Sea along with the sediment. Therefore, the concentration of residual mercury in the bay area and the dynamic migration of mercury need to be grasped.

Mercury is mainly distributed in sediments and will also migrate to other places along with them. Therefore, in this study, the migration of mercury with sediments from Minamata Bay to the Yatsushiro Sea was studied by numerical modelling. At the same time, the mercury concentration in the sediment was grasped by experimental determination, and the influence of the sediment properties on the mercury content was analyzed.

The study was divided into some chapters in this thesis, which were described as follows:

Chapter 1 explained about research background, research status and issues, research objectives, and the overview of the thesis as an introduction.

Chapter 2 is the literature review related to this study. The chapter explained mercury in the natural environment, the source, the cycle, the effects on the ecosystem and health, and mercury pollution problems worldwide. Furthermore, the occurrence of Minamata disease, the cause and process of occurrence, the impacts and the treatment measures after the occurrence, and the current situation of mercury pollution after treatment were introduced.

Chapter 3 described a transport model for mercury-containing sediments based on measured data. The calculation domain, calculation grid, governing equations, open boundary conditions, freshwater inflows, initial conditions, and application of in-situ measurement are explained in detail. The simulation result agreed with the measured total mercury concentration distribution of surface sediment. The results showed a clear migration of mercury-containing sediments from the bay to the northeast and southwest of the Yatsushiro Sea. The sediments migrated from the bay to the coastal

area around the bay and gradually spread to the entire Yatsushiro Sea. The migration is not a static process. The sediments were mainly deposited in the southwest and northeast Yatsushiro Sea and coastal sea area surrounding Nagashima Island and Amakusa over time. The deposition gradually declined over time and finally stabilized at a low level in the middle of the Yatsushiro Sea. The mercury-containing sediments trended to deposit along the seacoast, which was mainly considered due to the terrain effect.

Chapter 4 described a novel particle size classification-based method to comprehend both horizontal and vertical distribution of the T-Hg concentration in sediment fractions in the Yatsushiro Sea. The results showed that in the horizontal direction, the T-Hg concentration became smaller and smaller along two lines from the sampling point near Minamata Bay, indicating the mercury transport from the bay to the Yatsushiro Sea. Moreover, it suggested that the migrated mercury was mainly deposited in the upper sediments. In addition, according to the classification experiment results, it could be concluded that overall, the smaller the particle size, the higher the T-Hg concentration. Furthermore, very fine silt to fine silt particles are the main particles that are transferred.

In Chapter 5, the relationships between the T-Hg concentration and sediment particle size as well as particle specific surface area were analyzed. The results showed that the T-Hg concentration was inversely correlated with the particle size but was positively correlated with the specific surface area.

In Chapter 6, dependent on sediment classification, the numerical simulations of sediment migration with different particle sizes were established to study the effect of particle size on the migration of mercury-containing sediments. Furthermore, based on the simulation results, combined with the relationship between T-Hg and particle size, the simulation realized the distribution of T-Hg in the Yatsushiro Sea. The results showed that the smaller the sediment particle size, the faster the migration speed and the more comprehensive the migration range. The mercury was mainly distributed in the southwest and northeast of the Yatsushiro Sea near the bay. Meanwhile, the amount of mercury distributed in the southwest area of the Yatsushiro Sea was more than that in the northeast area.

In Chapter 7, all chapters in this thesis are concluded, and some recommendations for future work are proposed.

Acknowledgment

I would like to sincerely appreciate my supervisor, Prof. Shinichiro Yano, Department of Urban and Environmental Engineering, Kyushu University. I am very grateful and honored to be able to engage in the research under your guidance. During the research journey of PhD, you taught me a lot of knowledge and skills related to numerical simulations and experimental measurements. Thank you very much for your confidence, patience, and enthusiasm for me. Thank you for your selfless support and help in my research and life during my doctoral period. Besides, your enthusiasm and optimistic attitude will continue to inspire me to move forward and support me to keep climbing new heights in life.

I would love to thank significantly Professors Takahiro Kuba and Masaru Yamashiro, Faculty of Engineering, Kyushu University, as the dissertation evaluation committee members. I am thankful that they spend their precious time and effort in reviewing my thesis. Because of their vast knowledge and experiences, they undoubtedly help provide great ideas and improve my research work as well as my dissertation. Moreover, I express my gratitude to Assistant Prof. Yasuyuki Maruya of Kyushu University and Associate Prof. Akira Tai of Fukuoka Institute of Technology for their advice and support for my research.

I want to express my gratitude to Dr. Akito Matsuyama of the National Institute for Minamata Disease, Ministry of the Environment, for your support in the experiments of mercury. I have learned a lot about mercury sampling, pretreatment, and determination from you.

I would like to say thanks and appreciation for the financial support from the program “Support for Pioneering Research Initiated by the Next Generation (SPRING)” of the Japan Science and Technology Agency (JST) (JPMJSP2136). Dependent on this

support, I can concentrate on scientific research without any worries. It is also a great honor for me to receive your approval.

I would also express my gratitude to administrative assistant Kaneko for her assistance. I would love to acknowledge all students in Environmental Fluid Dynamic Laboratory, Kyushu University. I appreciate your helps with my research and all kinds of concern for my life. The years spent with you are significant and memorable. I am especially thankful to Mr. Abe, a “Mercury Team” member. Without your great help, the good results can’t be obtained so quickly and smoothly.

I would also like to express my sincere appreciation to all professors and staff in Graduate School of Engineering, Kyushu University. Also, I am very thankful to Kyushu University, Japan, for providing good facilities in the campus.

Finally, I want to thank all my family members for their support and encouragement in every aspect of my work. Life is a journey that requires constant exploration. Even if it is a flatboat in the sea, the support of my family is the motivation for me to ride the wind and waves.

Baixin Chi

Fukuoka, July 2023

Contents

List of Figures

List of Tables

Chapter 1
Introduction

1.1 Research Background

With the development of industrialization, many environmental problems, such as environmental pollution, climate change, and loss of biodiversity, are becoming more and more severe to human society. These issues pose significant risks to ecosystems and further pose serious threats to life on Earth, including humans (Ali and Khan, 2017). Since the 1940s, rapid industrialization and urbanization have caused heavy metal pollution to the environment. At the same time, due to human intervention, the migration and transportation speed of these heavy metals in the environment has also been greatly accelerated (Khan et al., 2004). Heavy metals persist in the environment, contaminate the food chain, and cause various health problems due to toxicity. Due to their long-term existence in the environment, these heavy metals can continuously threaten organisms (Wieczorek-Dąbrowska et al., 2013). Mercury is one of the heavy metals that fall into this category with severe environmental impacts.

Mercury (Hg) is a liquid metal at ambient temperatures and pressures. Mercury has many forms, mainly elemental mercury, monovalent mercury, divalent mercury, methylmercury, etc. Different mercury is distributed differently in different environmental systems. In general, mercury is present predominantly in the atmosphere as Hg(0), in water, soil, and sediment as inorganic Hg(II), and in biota as methylmercury (MeHg) (Ullrich et al., 2001).

Mercury is released into the air, water, and soil through natural causes and human activities, where mercury emission to the atmosphere is usually the primary way for mercury to enter the environment (Jiang et al., 2006; Bookman et al., 2008; Streets et al., 2009; Cheng and Hu, 2010). Mercury released into the environment through natural means mainly comes from the release of marine and terrestrial environments, geological activities such as volcanic eruptions and geothermal, and the release of forest fires, etc (Nriagu, 1989; Lindqvist et al., 1991; Nriagu, 1994; Camargo, 2002; Gustin, 2003; Gray and Hines, 2006). Anthropogenic mercury emissions are mainly

from the incineration of solid waste, the combustion of chemical fuels, emissions from metallurgical processes, and releases from the production of metals such as gold (Pirrone et al., 1996; Pai et al., 2000). It is estimated that 5,000-6,000 t of mercury are released into the atmosphere every year worldwide through natural and anthropogenic means. About half of mercury emissions are caused by human factors (Mason et al., 1994; Lamborg et al., 2002; Gray and Hines, 2006).

After mercury enters the environment, it undergoes a series of complex migration and transformation in the biogeochemical cycle, mainly including the transport of mercury in the atmosphere, the deposition of mercury from the atmosphere to the land and ocean, the volatilization of mercury from the land and ocean, the mercury accumulation in organisms (Pavithra et al., 2022). In addition, mercury between different forms can also be transformed into each other. Elemental mercury can be oxidized to divalent mercury, and divalent mercury can be reduced to elemental mercury. Inorganic mercury can form highly toxic methylmercury through methylation, continuously enriched through the food chain after being absorbed by organisms. At the same time, methylmercury can also become inorganic mercury through demethylation (Zhu et al. 2018). Mercury is one of the most toxic elements and therefore poses a severe threat to the environment when it enters the environment. Mercury in the environment can be rapidly converted into organic compounds (such as methylmercury, etc.) by microorganisms and thus continuously enriched and amplified in organisms (Ronchetti et al., 2006). Humans at the top of the food chain are susceptible to the worst effects due to the biomagnifying effects of mercury. At the same time, due to the environmental persistence of mercury, the impact of mercury pollution on the environment as well as humans can last for a long time (Azimi and Moghaddam, 2013).

Methylmercury is produced during the production of acetaldehyde at the Chisso plant in Minamata city using mercury sulfate as a catalyst. These methylmercuries are discharged into Minamata Bay along with the sewage, polluting shellfish and fish in the sea and continuously enriching in the body of higher fish through the food chain. Eventually, people developed symptoms of mercury poisoning after eating this mercury-contaminated seafood (Minamata City, 2022). The incident of mercury poisoning is known as the Minamata disease. Patients with Minamata disease present with symptoms such as neurological disturbances, including sensory disorders, ataxia,

dysarthria, narrowed vision, and hearing difficulties (Yorifuji et al., 2008; Eto et al., 2010). As of the end of April 2022, the total number of confirmed patients was 2,284 (Minamata City, 2022). In addition, more than 40,000 individuals exhibited symptoms such as sensory disturbances predominantly in the peripheral limbs (Hachiya, 2012).

From 1932, it was reported that about 70-150 t or more of mercury was mixed with sewage from factories and discharged into Minamata Bay (Premakumara et al., 2011). To deal with mercury pollution, in 1977, Kumamoto Prefecture started the Minamata Bay Pollution Prevention Project. The government dredged and transferred sediments exceeding 25 ppm of total mercury (calculated based on the sediment removal regulatory standards established by the Environmental Agency) into a strictly segregated area of the bay near the wastewater outlet and landfilled this area (Sakamoto et al. 2020).

Although the sediments with a mercury concentration of more than 25 ppm had been dredged, a study by Matsuyama et al. (2014) showed that the weighted average of the total mercury concentration in the bottom sediment of Minamata Bay was 2.3 mg/kg (ppm). In addition, the study by Tomiyasu et al. (2014) has shown that the maximum concentration of total mercury in sediments of undredged areas was almost up to 10 ppm. The level was much higher than the background concentration in the natural environment (about 0.2 ppm). Moreover, some studies have found significantly higher levels of mercury in benthic organisms (e.g., Gaetice and Snail) (Yasuda et al., 2010) and fish (e.g., Japanese stickleback and Bamboo wrasse) (Matsuyama et al., 2013) near Minamata Bay than in other areas. Furthermore, many studies have shown that mercury in Minamata Bay migrated along with the sediment to the nearby Yatsushiro Sea (Tomiyasu et al., 2000; Yano, 2013; Matsuyama et al., 2019). Therefore, the residual mercury in Minamata Bay and the Yatsushiro Sea still needs continuous attention.

Mercury is mainly distributed in sediments, and mercury will also migrate to other places along with sediments. Therefore, in this study, the migration of mercury with sediments from Minamata Bay to the Yatsushiro Sea was studied by numerical simulation. At the same time, the mercury content in the sediment was grasped by the method of experimental determination, and the influence of the sediment properties

on the mercury content was analyzed. Experimental measurements are generally considered one of the most effective methods for determining the distribution and dynamics of mercury in sediments. However, since field data are sometimes not abundant and sufficient for regional and temporal extrapolation, mathematical models have become an important tool that may provide more information and improve the precision of the analysis (Knightes, 2009). Therefore, in this study, the distribution of mercury in sediments and the migration of mercury with sediments were investigated by combining experimental measurement analysis and numerical simulation.

1.2 Research Status and Issues

It has been a long time since the Minamata disease occurred. The high concentration in the Minamata Bay area has also been dredged, but the mercury content in the sediment of the Minamata Bay area and the mercury content in fish and other organisms are still much higher than in other regions (Yasuda et al., 2010; Matsuyama et al., 2013). Due to the toxicity, bioaccumulation, and environmental sustainability of mercury, even residual mercury in the Minamata Bay area still needs continuous attention and monitoring. In addition, studies have shown that mercury has migrated from Minamata Bay to the Yatsushiro Sea (Tomiyasu et al., 2000; Yano, 2013; Matsuyama et al., 2019). Therefore, it is essential to grasp the distribution and dynamics of residual mercury.

Several studies have simulated the transport of mercury-containing sediments in Minamata Bay using numerical models (Fathya et al., 2016; Matsunoshita et al., 2018). However, many of the parameters used in these simulations are fixed empirical and constant parameters that could not entirely accurately reflect actual mercury migration. Therefore, we need to develop models that use field-measured data to more accurately simulate mercury migration from Minamata Bay to the Yatsushiro Sea.

In addition, mercury migrates from Minamata Bay to the Yatsushiro Sea along with the sediment. However, the properties of different sediments in the Yatsushiro Sea (such as particle size and specific surface area) are different. At present, the influence of the properties of the sediment on the mercury content in the sediment is not clear. Therefore, it is necessary to analyze the influence of these factors through experiments.

Furthermore, the current mercury migration model simulates the erosion and deposition of mercury-containing sediments to respect the mercury distribution in various locations, which cannot directly reflect actual mercury concentrations at different locations. Therefore, we need to develop a model that translates directly from the erosion and accumulation laws of mercury-contained sediments to the transport and distribution of mercury.

1.3 Research Objectives

The main objective is to develop a simulation model based on measured data to achieve a more accurate simulation of mercury migration from Minamata Bay to the Yatsushiro Sea. At the same time, a direct transformation from the accumulation and erosion of mercury-containing sediments to the distribution and transport of mercury is realized by combining experiments and simulations. In addition, a new experimental method is used to investigate the concentration of mercury in sediments, the influence of sediment properties (such as particle size and specific surface area) on the mercury concentration in the sediment, and the effect on mercury transport. The detailed purposes of this research are presented in the following points:

1. To develop a model based on measured data to simulate the migration of mercury-containing sediments from Minamata Bay to the Yatsushiro Sea and analyze the migration laws.

2. To develop a novel method based on particle size classification to comprehend both horizontal and vertical distribution of the total-Hg (T-Hg) concentration in sediment fractions in the Yatsushiro Sea.

3. To investigate the relationship of the T-Hg concentration and sediment particle size as well as particle specific surface area dependent on sedimentation classification.

4. To investigate the different laws of sediment migration with different particle sizes by establishing sediment migration models with different particle sizes. Furthermore, based on the simulation results, combined with the relationship between T-Hg and particle size, to reflect the distribution and migration of mercury directly.

1.4 Research Overview

The specific contents of this thesis are as follows:

Chapter 1 contains the research background, research status and issues, research objective, and research overview.

Chapter 2 is a literature review that explains mercury in the natural environment, the source of mercury, the cycle of mercury in the environment, the effects of mercury on the ecosystem and health, and mercury pollution problems worldwide. Furthermore, the occurrence of Minamata disease, the cause and process of occurrence, the consequences and impacts, the treatment measures after the occurrence, and the current situation of mercury pollution after treatment are introduced.

Chapter 3 describes a transport model for mercury-containing sediments based on measured data. The calculation domain, calculation grid, governing equations, open boundary conditions, freshwater inflows, initial conditions, and application of *in-situ* measurement are explained in detail. The simulation agreed with the measured total mercury concentration distribution of surface sediment. Results reflect the regularity of migration of mercury-containing sediments from Minamata Bay to the Yatsushiro Sea.

Chapter 4 describes a novel particle size classification-based method for analyzing total mercury concentration distribution in the Yatsushiro Sea. In the chapter, collection and pre-processing for sediment samples, particle size classification, analysis of particle size, and analysis of the total mercury concentration are described in detail. The results reflect the distribution of sediment particle size, the background concentrations of T-Hg in sediment, the total mercury concentrations of different particle size fractions, and the vertical distribution.

Chapter 5 analysis the relationships between the T-Hg concentration and sediment particle size as well as particle specific surface area. The results show that the T-Hg concentration in the sediment is inversely correlated with the particle size of the sediment, but is positively correlated with the specific surface area of the sediment.

Chapter 6 describes the numerical simulations of sediment migration with different

particle sizes dependent on sedimentation classification. The results reflect the different migration laws of mercury-containing sediments with different particle sizes. Furthermore, based on the simulation results, combined with the relationship between T-Hg and particle size, the simulation realized the distribution of T-Hg in the Yatsushiro Sea.

Chapter 7 is the conclusions and recommendations. The entire thesis is summarized in this chapter, and some suggestions for future work are given.

The structure of the thesis is shown in **Fig.1.1**.

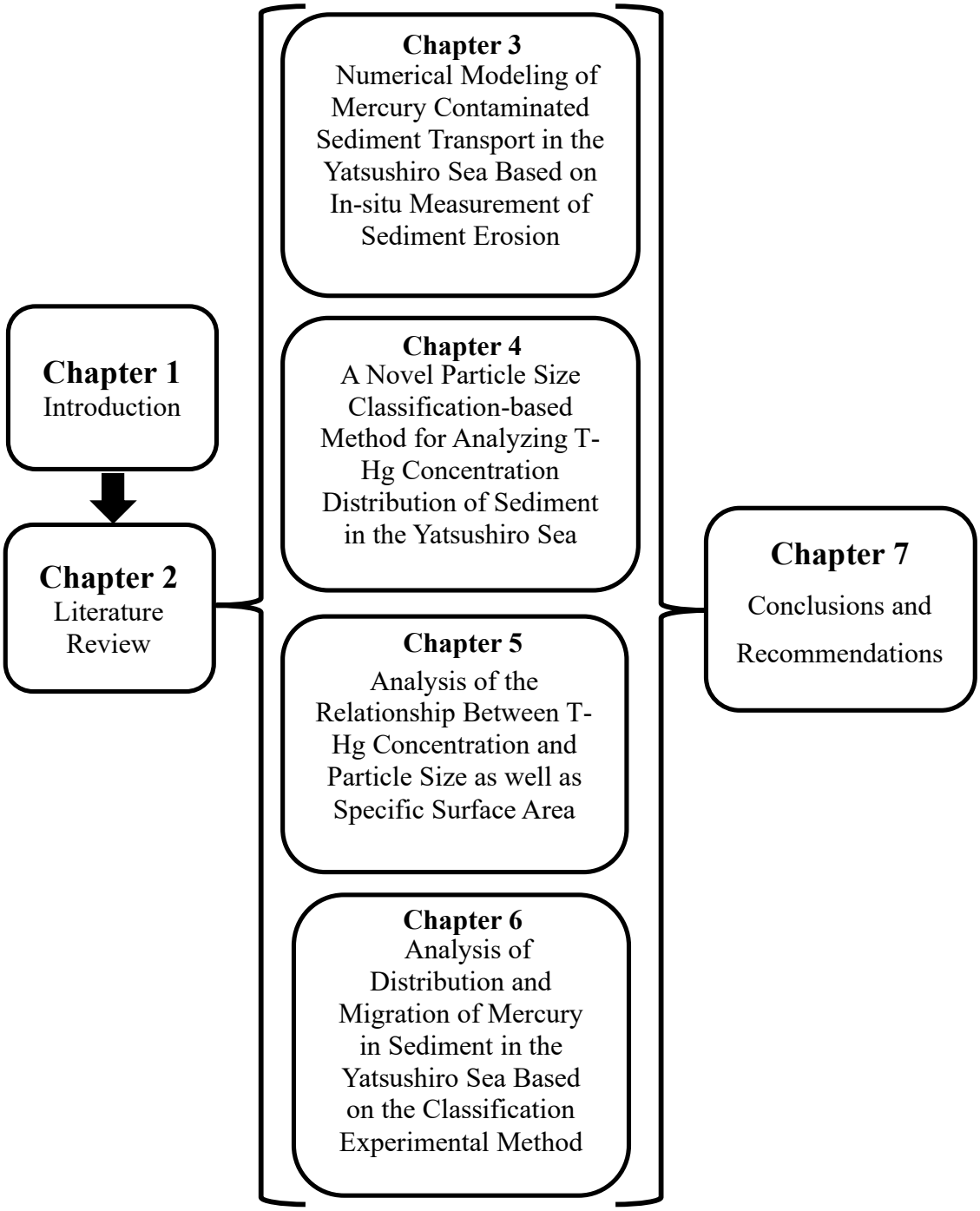

Figure 1.1 The framework of this thesis.

References

Ali, H., & Khan, E. (2017). Environmental chemistry in the twenty-first century. *Environmental Chemistry Letters*, 15(2), 329-346.

Azimi, S., & Moghaddam, M. S. (2013). Effect of mercury pollution on the urban environment and human health. *Environment and Ecology Research*, 1(1), 12-20.

Bookman, R., Driscoll, C. T., Engstrom, D. R., & Effler, S. W. (2008). Local to regional emission sources affecting mercury fluxes to New York lakes. *Atmospheric Environment*, 42(24), 6088-6097.

Camargo, J. A. (2002). Contribution of Spanish–American silver mines (1570–1820) to the present high mercury concentrations in the global environment: a review. *Chemosphere*, 48(1), 51-57.

Cheng, H., & Hu, Y. (2010). China needs to control mercury emissions from municipal solid waste (MSW) incineration. *Environmental Science & Technology*, 44, 7994-7995.

Eto, K., Marumoto, M., & Takeya, M. (2010) The pathology of methylmercury poisoning (Minamata disease). *Neuropathology*, 30(5), 471-47.

Fathya, E.N., Yano, S., Matsuyama, A., Tada, A., & Riogilang, H. (2016). Impact of reclamation project on mercury contaminated sediment transport from Minamata Bay into the Yatsushiro Sea. *Journal of Japan Society of Civil Engineers, Ser. B2(Coastal Engineering)*, 72(2), I_1285-I_1290.

Gray, J. E., & Hines, M. E. (2006). Mercury: distribution, transport, and geochemical and microbial transformations from natural and anthropogenic sources. *Applied Geochemistry*, 21(11), 1819-1820.

Gustin, M. S. (2003). Are mercury emissions from geologic sources significant? A status report. *Science of the Total Environment*, 304(1-3), 153-167.

Hachiya, N. (2012). Epidemiological update of methylmercury and Minamata disease. *Methylmercury and Neurotoxicity*, 1-11.

Jiang, G. B., Shi, J. B., & Feng, X. B. (2006). Mercury pollution in China. *Environmental science & technology*, 40(12), 3672-3678.

Khan, F. U., Rahman, A. U., Jan, A., & Riaz, M. (2004). Toxic and trace metals (Pb, Cd, Zn, Cu, Mn, Ni, Co and Cr) in dust, dustfall/soil. *Journal of the Chemical Society of Pakistan*, 26 (4), 453-456.

Knightes, C. D., Sunderland, E. M., Barber, M. C., Johnston, J. M., & Ambrose Jr, R. B. (2009). Application of ecosystem‐scale fate and bioaccumulation models to predict fish mercury response times to changes in atmospheric deposition. *Environmental Toxicology and Chemistry*, 28(4), 881-893.

Lamborg, C. H., Fitzgerald, W. F., O'Donnell, J., & Torgersen, T. (2002). A non-steady-state compartmental model of global-scale mercury biogeochemistry with interhemispheric atmospheric gradients. *Geochimica et Cosmochimica Acta*, 66(7), 1105-1118.

Lindqvist, O., Johansson, K., Bringmark, L., Timm, B., Aastrup, M., Andersson, A., Hovsenius, G., Håkanson, L., Iverfeldt, Å., & Meili, M. (1991). Mercury in the Swedish environment—recent research on causes, consequences and corrective methods. *Water, Air, and Soil Pollution*, 55, xi-261.

Mason, R. P., Fitzgerald, W. F., & Morel, F. M. (1994). The biogeochemical cycling of elemental mercury: anthropogenic influences. *Geochimica et Cosmochimica Acta*, 58(15), 3191-3198.

Matsunoshita, K., Yano, S., Matsuyama, A., Kitaoka, T., & Tada, A. (2018). Analysis on dispersion of mercury in bottom sediments in Minamata Bay by long-term numerical simulation of sediment transport using particle size classification model. *Journal of Japan Society of Civil Engineers, Ser. B2 (Coastal Engineering)*, 74(2), I_1153-I_1158 (in Japanese).

Matsuyama, A., Yokoyama, S., Kindaichi, M., Sonoda, I., & Koyama, J. (2013). Effect of seasonal variation in seawater dissolved mercury concentrations on mercury accumulation in the muscle of red sea bream (Pagrus major) held in

Minamata Bay, Japan. *Environmental monitoring and assessment*, 185, 7215-7224.

Matsuyama, A., Yano, S., Hisano, A., Kindaichi, M., Sonoda, I., Tada, A., & Akagi, H. (2014). Reevaluation of Minamata Bay, 25 years after the dredging of mercury-polluted sediments, *Marine Pollution Bulletin*, 89, 112-120.

Matsuyama, A., Yano, S., Matsunoshita, K., Kindaichi, M., Tada, A., & Akagi, H. (2019). The spatial distribution of total mercury in sediments in the Yatsushiro Sea, Japan. *Marine Pollution Bulletin*, 149, 110539.

Minamata City. (2022). Minamata Disease -Its History and Lessons-2022, 66p.

Nriagu, J. O. (1989). A global assessment of natural sources of atmospheric trace metals. *Nature*, 338, 47-49.

Nriagu, J. O. (1994). Mechanistic steps in the photoreduction of mercury in natural waters. *Science of the Total Environment*, 154(1), 1-8.

Pai, P., Niemi, D., & Powers, B. (2000). A North American inventory of anthropogenic mercury emissions. *Fuel Processing Technology*, 65, 101-115.

Pavithra, K. G., SundarRajan, P., Kumar, P. S., & Rangasamy, G. (2022). Mercury sources, contaminations, mercury cycle, detection and treatment techniques: A review. *Chemosphere*, 137314.

Pirrone, N., Keeler, G. J., & Nriagu, J. O. (1996). Regional differences in worldwide emissions of mercury to the atmosphere. *Atmospheric Environment*, 30(17), 2981-2987.

Premakumara, D. G. J., Yoshimura, T., & Clatterbuck, A. (2011). Local Governance and Environmental Sustainability in Minamata City: Beyond Deadlock and Conflict to Multi-Stakeholder Collaboration. *APSA congress 2011*, 1063-1074.

Ronchetti, R., Zuurbier, M., Jesenak, M., Koppe, J. G., Ahmed, U. F., Ceccatelli, S., & Villa, M. P. (2006). Children's health and mercury exposure. *Acta Paediatrica*, 95, 36-44.

Sakamoto, M., Itai, T., Marumoto, K., Marumoto, M., Kodamatani, H., Tomiyasu, T., Nagasaka, H., Mori K., Poulain, A.J., Domingo, J. L., Horvat, M., & Matsuyama, A. (2020). Mercury speciation in preserved historical sludge: Potential risk from sludge contained within reclaimed land of Minamata Bay, Japan. *Environmental Research*, 180, 108668.

Streets, D. G., Zhang, Q., & Wu, Y. (2009). Projections of global mercury emissions in 2050. *Environmental science & technology*, 43(8), 2983-2988.

Tomiyasu, T., Nagano, A., Yonehara, N., Sakamoto, H., Ōki, K., & Akagi, H. (2000). Mercury contamination in the Yatsushiro Sea, south-western Japan: spatial variations of mercury in sediment. *Science of the Total Environment*, 257(2-3), 121-132.

Tomiyasu, T., Takenaka, S., Noguchi, Y., Kodamatani, H., Matsuyamab, A., Oki, K., Kono, Y., Kanzaki, R., & Akagi, H. (2014). Estimation of the residual total mercury in marine sediments of Minamata Bay after a pollution prevention project. *Marine Chemistry*, 159, 19-24.

Ullrich S.M., Tanton T.W., & Abdrashitova S.A. (2001). Mercury in the aquatic environment: a review of factors affecting methylation. *Critical Reviews in Environmental Science and Technology*, 31(3), 241-293.

Wieczorek-Dąbrowska, M., Tomza-Marciniak, A., Pilarczyk, B., & Balicka-Ramisz, A. (2013). Roe and red deer as bioindicators of heavy metals contamination in north-western Poland. *Chemistry and Ecology*, 29(2), 100-110.

Yano, S. (2013). In-situ measurement of mercury transport in the sea water of Minamata Bay. *Procedia Earth and Planetary Science*, 6, 448-456.

Yasuda, Y., & Mori, K. (2010). Mercury deposit distribution in Minamata Bay. *Coastal marine science*, 34(1), 223-229.

Yorifuji, T., Tsuda, T., Takao, S., & Harada, M. (2008). Long-term exposure to methylmercury and neurologic signs in Minamata and neighboring communities. *Epidemiology*, 3-9.

Zhu, S., Zhang, Z., & Žagar, D. (2018). Mercury transport and fate models in aquatic systems: A review and synthesis. *Science of the Total Environment*, 639, 538-549.

Chapter 2
Literature Review

2.1 Mercury in the Environment

Mercury is a well-known toxic heavy metal. Mercury mainly includes organic mercury and inorganic mercury. Organic mercury primarily refers to compounds that combine mercury with structures containing carbon atoms (methyl, ethyl, phenyl, or similar groups). Inorganic mercury includes metallic mercury and mercury vapor (Hg^0) and mercurous (Hg^{2++}) or mercuric (Hg^{++}) salts (Bernhoft, 2012). In general, the predominant form of mercury in water, soil, and sediment is the inorganic Hg(II) form, and in biota as methylmercury (MeHg), while in the atmosphere, Hg(0) is the main form (USEPA, 1997; Ullrich et al., 2001).

Mercury can be found in organic, inorganic, or elemental forms in aquatic systems. Inorganic mercury in water mainly has two valence states, which are monovalent and divalent. Divalent mercury is more widely distributed (Loux, 1998). Organic mercury in water can be divided into two groups. One is covalently bonded organic mercury, such as methylmercury and dimethylmercury, and the other is complexes of mercury with organic matter (such as humic substances) (Gill et al., 1990). In aquatic systems, mercury can dissolve in the water or remain in particulate form. Suspended organics are believed to play an essential role in whether mercury dissolves or remains in particulate form (Meili, 1997). In addition, in aquatic systems, sediments are important sinks and sources of mercury (Hg) and are also considered to be a major source of methylmercury (MeHg) (Shi et al., 2005).

Mercury exists in the atmosphere in elemental and oxidized chemical forms. The predominant form in the atmosphere is usually elemental mercury (Hg^0). The low solubility of elemental mercury makes it difficult to dissolve in atmospheric water droplets. At the same time, its relative volatility means that tiny amounts of mercury will be adsorbed to the surface of aerosol particles. Therefore, atmospheric mercury exists primarily in the gaseous phase in the atmosphere (Cohen et al., 2004). According to the simulation results (**Fig. 2.1**) of Selin et al. (2007), it can be seen that mercury in the atmosphere is ubiquitous, and the mercury content is high in some

areas. Due to atmospheric movement, atmospheric mercury can be transported to the global environment and deposited locally, regionally, or even on another continent, causing global problems (Schroeder & Munthe, 1998; Lin & Pehkonen, 1999).

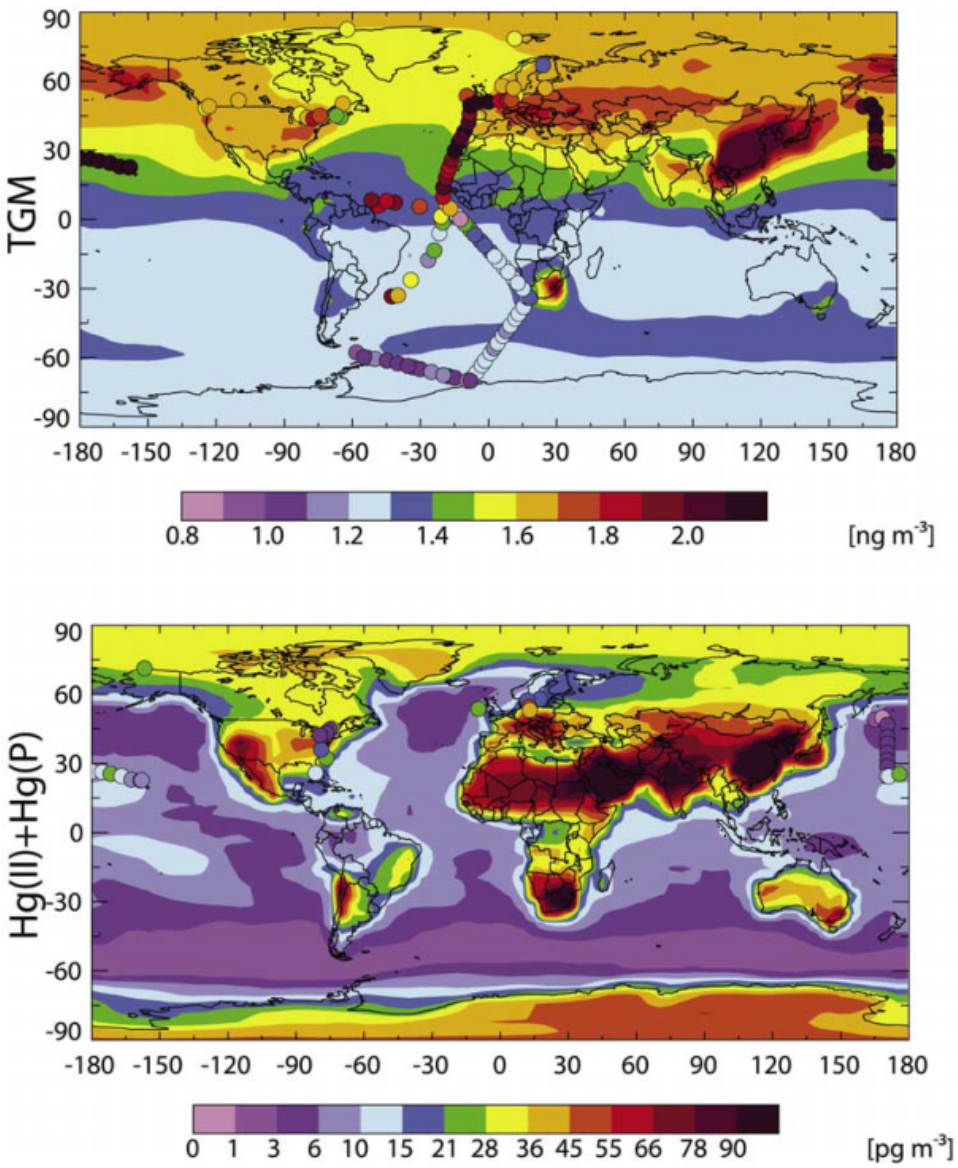

Figure 2.1 Annual average mercury concentrations in surface air (Selin et al., 2007).

After transporting mercury in the atmosphere for a certain distance, through wet and dry deposition, more than 90% of the emitted mercury eventually returns to the ground and enters the terrestrial ecosystem, making the soil the largest recipient of emitted mercury (Lindqvist et al.,1991). The global mean background levels of Hg in different types of soils ranged from 0.58 to 1.8 mg/kg, with higher Hg concentrations in Histosols and Cambisols (Kabata-Pendias, 2010). Moreover, it is noteworthy that

mercury is much more persistent in soil than in lakes, oceans, and other biomes (Padmavathiamma and Li, 2007; Tangahu et al., 2011).

Mercury in living organisms is mainly in the form of methylmercury, which is the most toxic form of mercury. In addition, methylmercury accumulates in animal and human food chains more easily than inorganic substances (Shi et al., 2005). In aquatic systems, bioaccumulation through the food chain can lead to high levels of mercury contamination in fish, even at low concentrations of MeHg in the water (Wang et al., 2004). Methylmercury has an affinity for sulfur-containing proteins and amino acids such as cysteine and is frequently associated with protein tissues (Harris et al., 2003). Consequently, concentrations of mercury, especially the methylated form, are commonly highest in muscle tissue (Bloom, 1992).

2.2 Source of Mercury

Mercury is released into the air, water, and soil from both natural causes and human activities, and emissions to the atmosphere are usually the main route of entry of mercury into the environment (Jiang et al., 2006; Bookman et al., 2008; Streets et al., 2009; Cheng and Hu, 2010). It is estimated that 5,000-6,000 t of mercury are released into the atmosphere worldwide each year from natural sources and anthropogenic emissions. About 50% of these releases may come from anthropogenic sources (Mason et al., 1994; Lamborg et al., 2002a; Gray and Hines, 2006).

2.2.1 Natural sources of mercury

Many natural processes can lead to the release of mercury into the environment. The main naturally occurring mercury emission processes include (1) mercury release from mercury deposits; (2) mercury release from marine and terrestrial environments (by reduction of Hg^{2+} to Hg^{0}); (3) geological activities such as volcanic eruptions and geothermal activity; (4) Forest fire (Nriagu, 1989; Lindqvist et al., 1991; Nriagu, 1994; Camargo, 2002; Gustin, 2003; Gray and Hines, 2006). The quantity of mercury emitted by various natural processes also varies. **Fig. 2.2** shows the global distribution of mercury mines. It can be seen that the mercury belts (red) with high mercury production are distributed in relatively few regions of the world (Rytuba, 2003). In addition, there are large mercury deposits in the Mediterranean region (Bailey et al., 1973). Natural mercury emissions from the area were estimated to be 110 t per year (Pirrone et al., 2001). Ocean mercury emissions were estimated at 800-2600 t per year (Mason and Sheu, 2002; Fitzgerald et al., 2007). Terrestrial mercury emissions were estimated at 1000-3200 t annually (Lindberg et al., 1998). The amount of mercury released by geological activities was estimated to be about 60-700 t (Ferrara et al., 2000; Nriagu and Becker, 2003; Pyle and Mather, 2003). In addition, it was estimated that 590-930 t of mercury were emitted worldwide annually from biomass burning (e.g., forest fires) (Brunke et al., 2001). It should be noted that since natural mercury emissions are generally non-point sources and widely distributed, it is extremely difficult to estimate natural mercury emissions accurately (Wang et al., 2004).

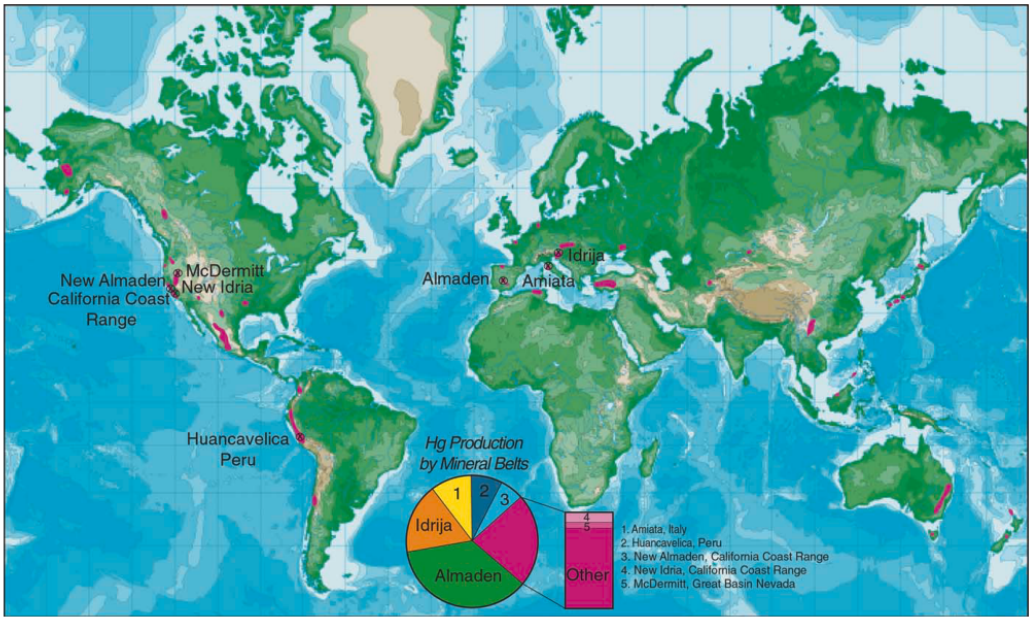

Figure 2.2 The distribution of mercury mines in the world (Rytuba, 2003).

2.2.2 Anthropogenic sources of mercury

Anthropogenic mercury emissions are mainly from (1) incineration of solid waste (municipal and medical waste), (2) combustion of coal and oil, (3) releases from pyrometallurgical processes (iron, lead, and zinc), and (4) production of mercury and gold (Pirrone et al., 1996; Pai et al., 2000). Due to human activities, there is a significant impact on global mercury emissions. The measurements of mercury levels in sediments from remote locations worldwide showed that mercury deposition has roughly tripled since the industrial age (Bindler et al., 2001; Biester et al., 2002; Lamborg et al., 2002b). According to the comparison of mercury flux simulations before and after industrialization (**Fig. 2.3**) from Mason and Sheu (2002), it can be seen that the flux of mercury increased significantly after industrialization. Meanwhile, it can also be seen that about half of the fugitive flux from land and sea after industrialization was anthropogenic. In addition, different anthropogenic activities in different regions have contributed to different degrees of mercury release. In most parts of the world, anthropogenic mercury comes primarily from the burning of fossil fuels for power generation and heating, but in South America, gold mining accounts for more than half of total anthropogenic mercury emissions (**Fig. 2.4**, from AMAP/UNEP, 2008).

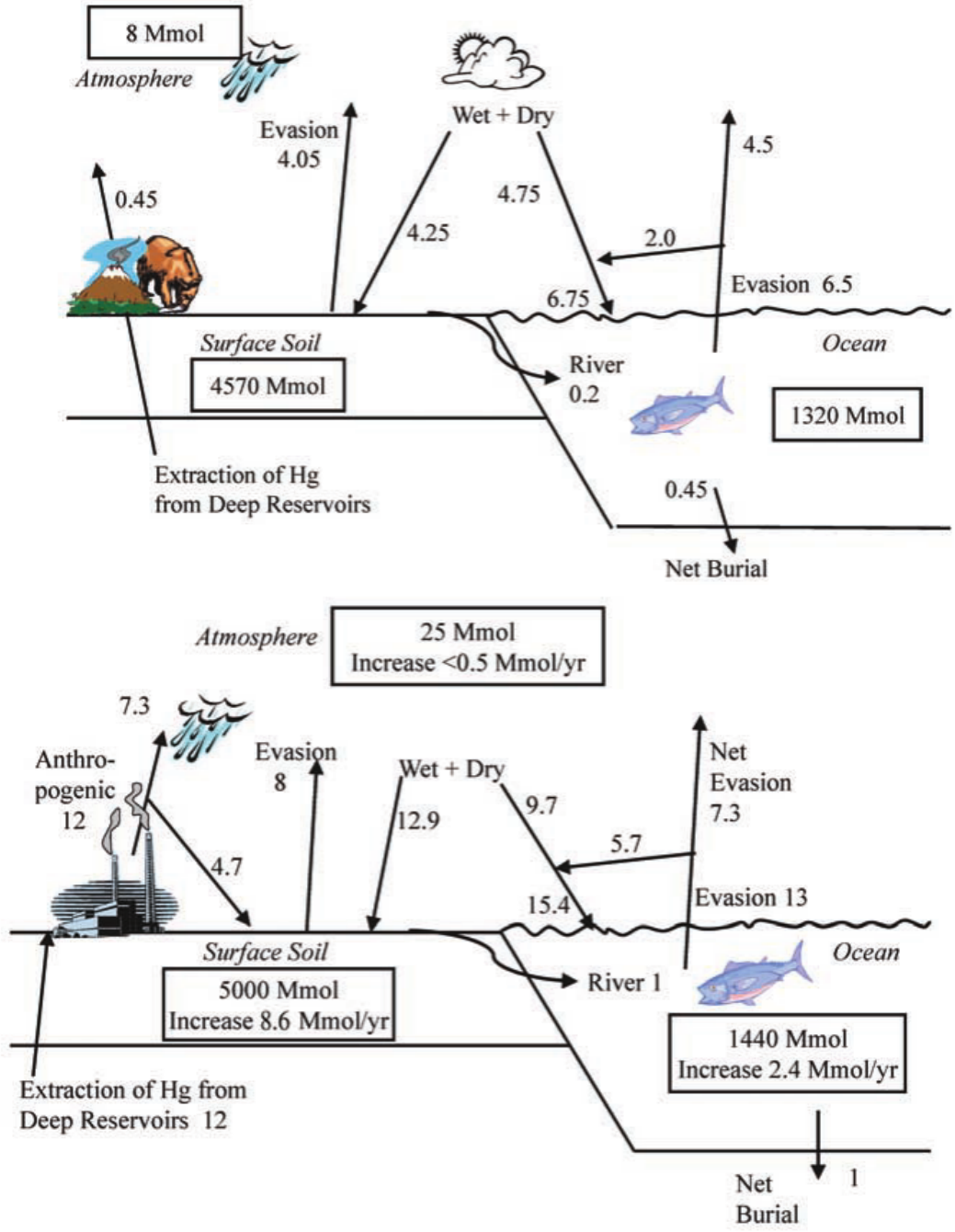

Figure 2.3 Mercury fluxes before and after industrialization (from Mason and Sheu, 2002). The upper figure shows the mercury flux before industrialization, and the lower figure shows the mercury flux after industrialization. All fluxes are in Mmol yr^{-1}.

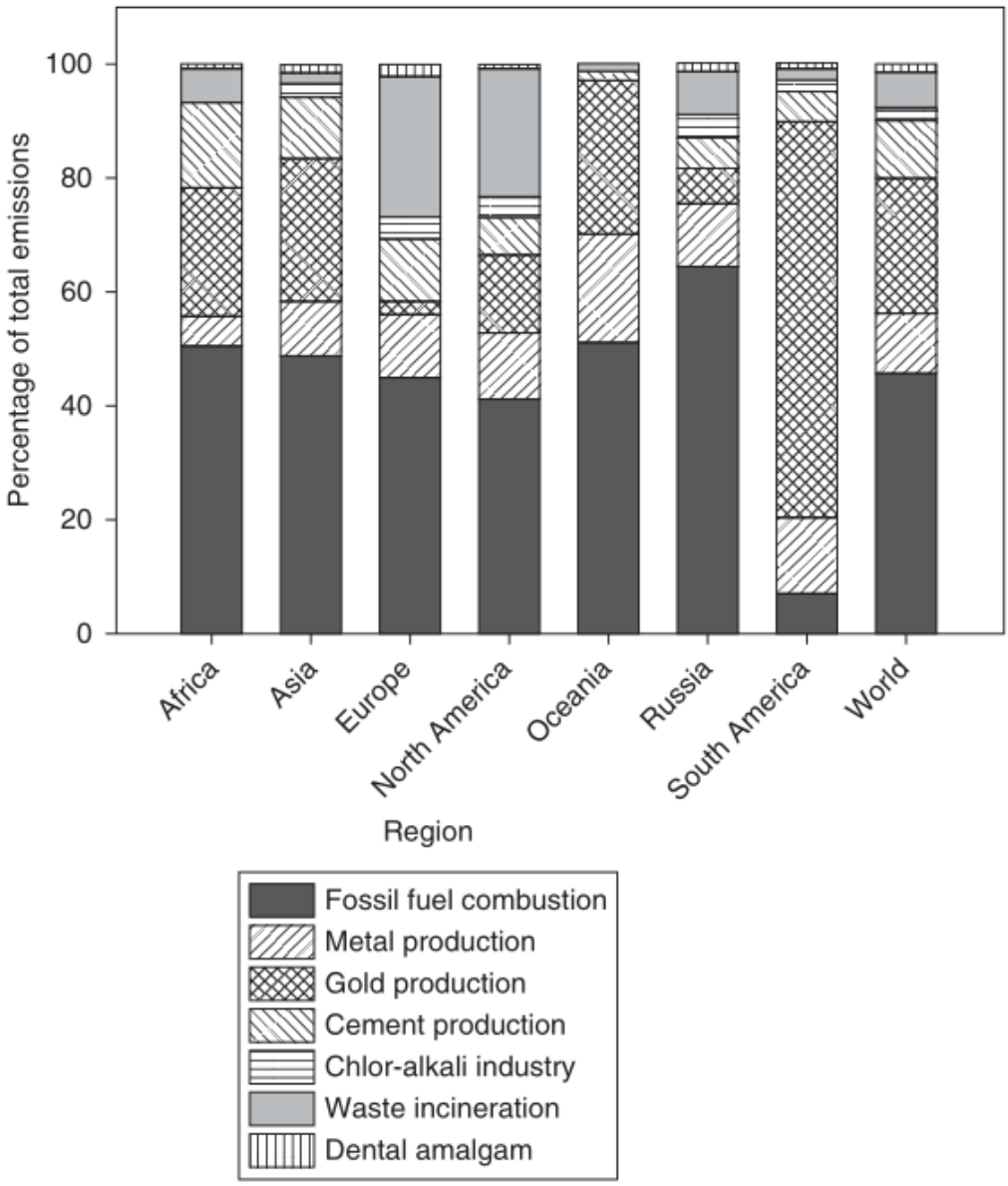

Figure 2.4 Relative percentage of mercury emissions from different anthropogenic activities around the world (AMAP/UNEP, 2008).

2.3 The Cycle of Mercury in the Environment

After mercury enters the environment, it undergoes a series of complex migration and transformation processes in the biogeochemical cycle. The natural biogeochemical cycle of mercury mainly includes the transport of mercury in the atmosphere, the deposition of mercury from the atmosphere to land and ocean, the volatilization of mercury from land and ocean, and the accumulation of mercury in organisms (**Fig. 2.5**) (Pavithra et al., 2022). Humans released mercury from long-term sediment storage into the environment through incineration, mining, and industrial activities. Due to the influence of biogeochemical cycles, mercury persists between the atmosphere, ocean, and land for hundreds to thousands of years. Finally, it will affect the environment and humans (**Fig. 2.6**) (Jitaru and Adams, 2004).

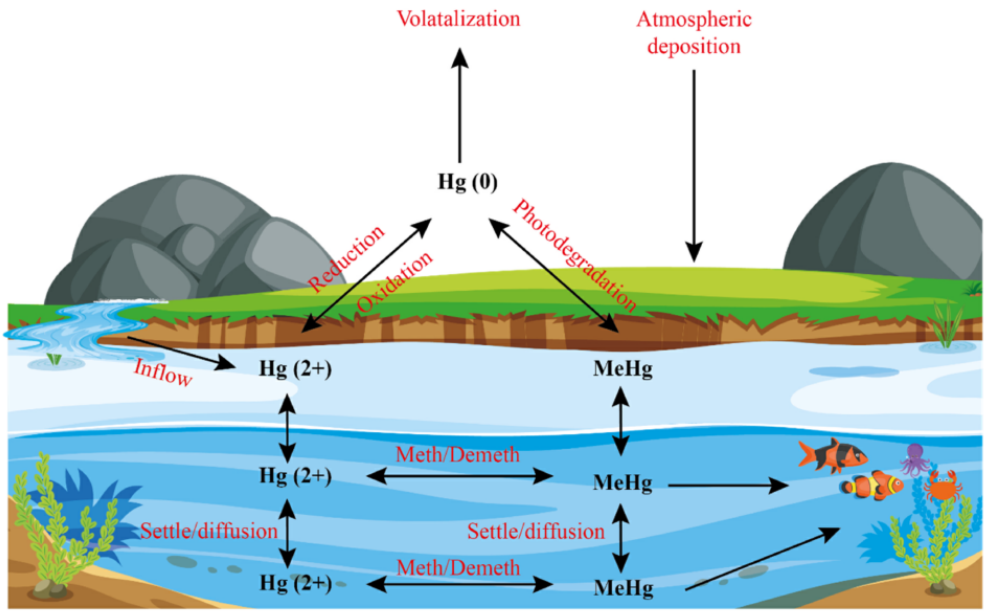

Figure 2.5 The natural biogeochemical cycle of mercury (Pavithra et al., 2022).

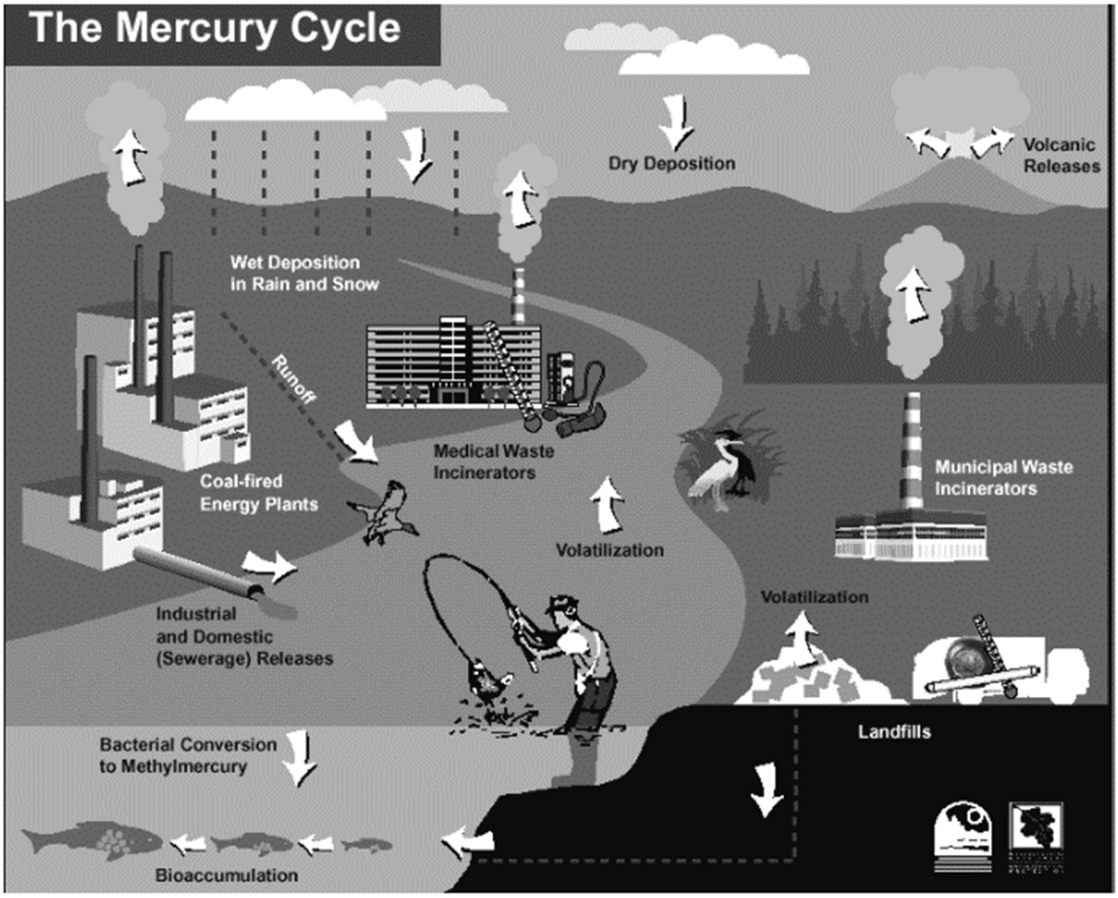

Figure 2.6 Mercury cycle with human activities (Jitaru and Adams, 2004).

2.3.1 Atmospheric cycle of mercury

Other metals migrate mainly through erosion and leaching processes. The migration of mercury is mainly carried out through the atmosphere. In addition, the atmosphere is not only a medium for mercury transport but also a medium for the chemical transformation of mercury (Sommar et al., 2001). In the atmosphere, elemental mercury (Hg^0) accounts for more than 90 percent of all Hg and is the dominant form in the gas phase, which facilitates the long-distance transport of Hg on a global scale (Ebinghaus et al., 1999; Pirrone and Mahaffey, 2005). Due to the relatively long lifetime of gaseous elemental mercury and its ability to be transported over long distances from source discharge areas, it may have impacts on soil, water, and vegetation in remote and pristine areas (Sprovieri et al., 2010; Slemr et al., 2011). The spatial distribution of annually averaged air concentrations of Hg^0 and Hg^{II} from a simulation by De Simone et al. (2014) is shown in **Fig. 2.7**. It can be seen that mercury is distributed throughout the atmosphere, and the mercury content in the atmosphere in some areas is very high.

Furthermore, Elemental mercury emitted into the atmosphere can be oxidized (Lam et al., 2019; Shah et al., 2016). Once elemental mercury is oxidized to oxidized mercury, the influence on the environment is more significant (Fu et al., 2015; Weiss-Penzias et al., 2011). Because they are more reactive, more soluble in water, and settle faster (Lin et al., 2006). In addition, the chemical and physical transformation of mercury in the atmosphere is usually reversible. Once elemental mercury is oxidized, mercury compounds are dynamically partitioned between the gas and aerosol phases (Cheng et al., 2014). Meanwhile, mercury compounds are readily reduced to elemental mercury from either stage (Landis et al., 2014; Saiz-Lopezet et al., 2018), and various other chemical transformations are possible, at least in cloud and fog water (Li et al., 2018; Lin and Pehkonen, 1999).

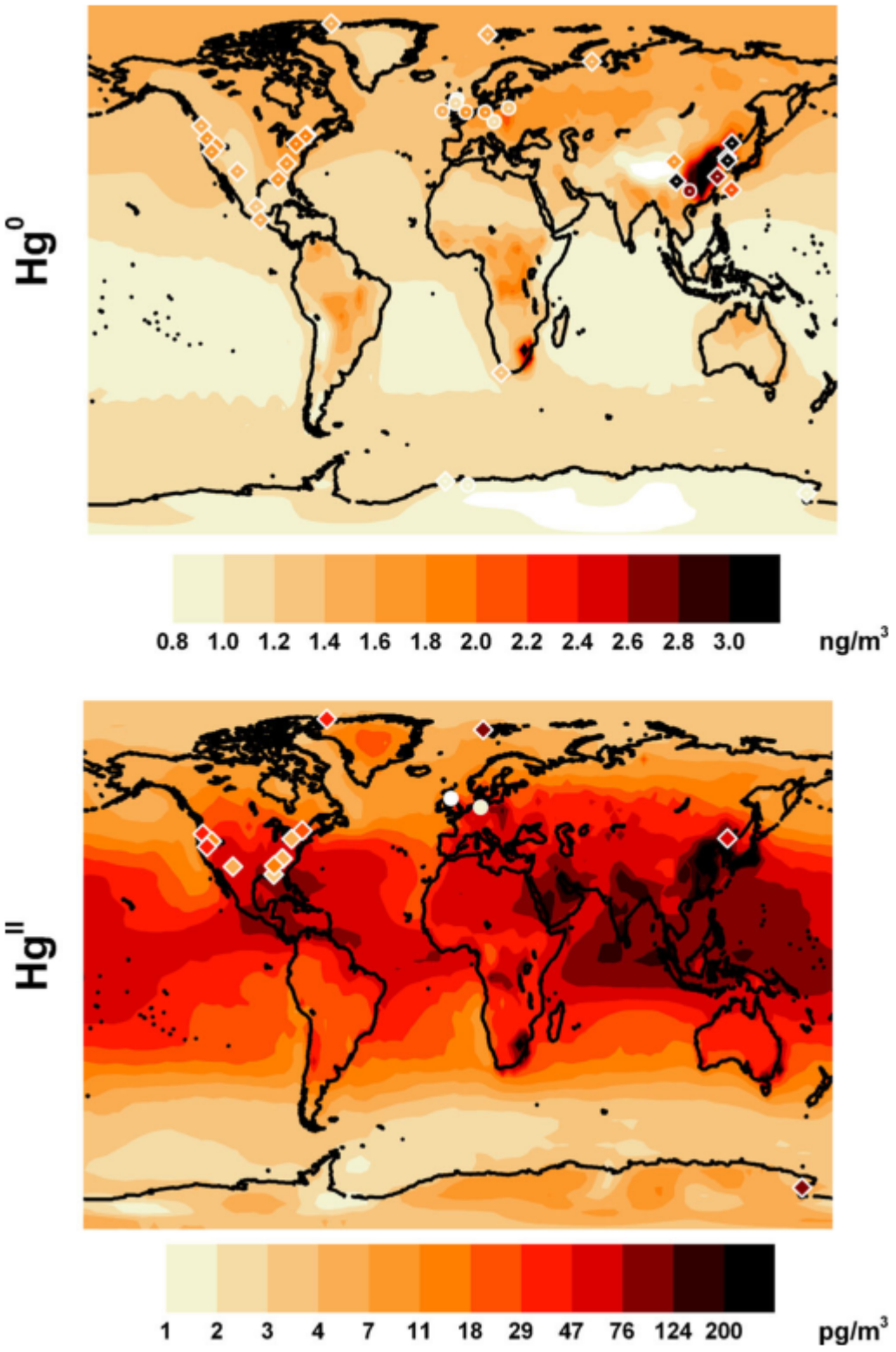

Figure 2.7 The spatial distribution of annually averaged air concentrations of Hg^0 and Hg^{II} (De Simone et al., 2014).

2.3.2 Terrestrial cycle of mercury

Most mercury on land surfaces globally is deposited from the atmosphere as Hg(II) through wet and dry deposition. After deposition, a portion of the mercury is released back into the atmosphere. The rest will be put into the soil and persist for a long time while being slowly released into the atmosphere (Selin, 2009). In addition to mercury from the atmosphere, some mercury is deposited by volcanism, geothermal activity, and near-surface mercury-bearing rocks. Another part of mercury is caused by human activities, such as industrial wastewater, mining, and biomedical waste (Bishop et al., 2020).

Most of the mercury in terrestrial systems is present in the soil, where it can be fixed for a long time due to the rich organic matter in the soil and the strong binding of mercury to it (Skyllberg, 2003). Smith-Downey et al.(2010) estimated that the Hg escape associated with the decomposition of soil organic carbon pools and the subsequent release of Hg(II) absorbed by soil organic matter exceeds 700 t/year, which indicates that there are large mercury pools stored in the global terrestrial ecosystem.

In terrestrial vegetation, Hg in above-ground biomass comes mainly from the atmosphere, while Hg in roots comes from the soil (Obrist, 2007). Hg(II) is deposited on the leaves by precipitation (wet deposition) and dry deposition, while Hg(0) enters the interior of the leaf through gas exchange through stomata (Seigneur e, 2004). On a seasonal scale, mercury deposited on vegetation enters the soil through rainfall and runoff (Grigal, 2002).

In addition, terrestrial systems receive mercury deposits from the atmosphere and re-release mercury from land to the atmosphere. These processes mainly include emissions from soil and vegetation surfaces, geological activities and biomass burning, and human activities. The research by Gworek et al. (2020) estimated that 56% of mercury deposited into terrestrial ecosystems is re-emitted. Similarly, Graydon et al. (2012) found that 45-70% of Hg(II), which was wet-deposited into forest watersheds, was re-emitted to the atmosphere.

Moreover, mercury in terrestrial ecosystems is not only released into the atmosphere but also enters aquatic systems through runoff, etc. In terrestrial systems, mercury

moves with the water along the hydraulic energy gradient to surface water "inlets" in particulate and dissolved form (Bishop et al., 2020). Mercury in the soil is tightly bound to organic matter, especially sulfur in the sulfur group (Skyllberg et al., 2003; Ravichandran, 2004). This also results in both particulate and dissolved mercury in terrestrial systems moving with water in association with organic matter (Mitchell et al., 2008). **Fig. 2.8** shows the basic concept of the terrestrial mercury cycle. Atmospheric mercury is deposited through precipitation and rainwater or absorbed by plant stomata and deposited with litter. In soil, Hg (II) is reduced by different pathways such as photochemistry, microorganisms, or natural organic matter and then released into the atmosphere. Meanwhile, mercury is leached from the soil into aquatic ecosystems due to surface or subsurface runoff (Jiskra et al., 2015).

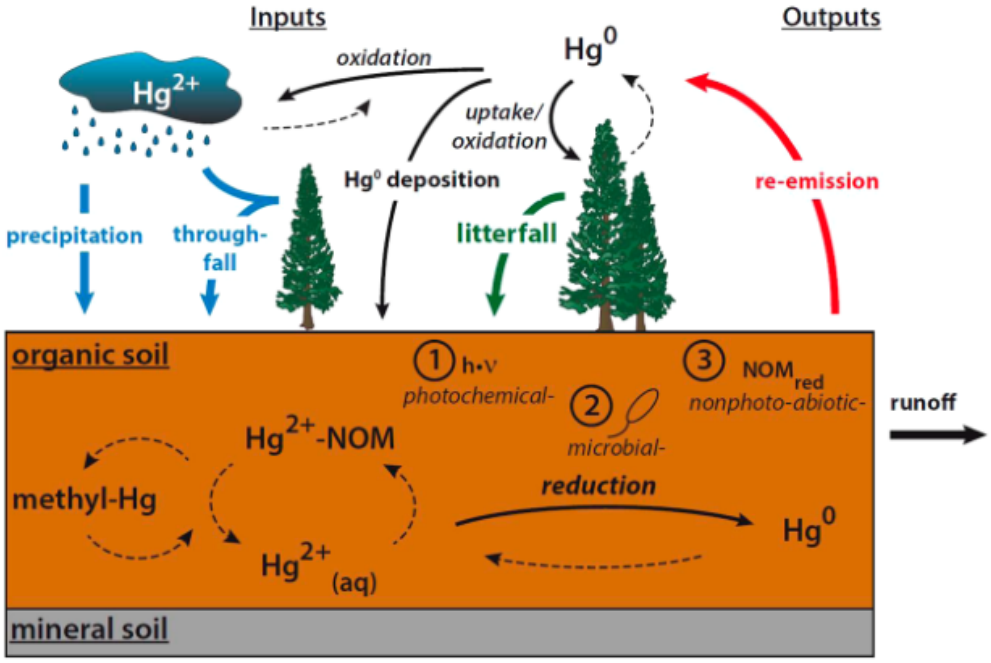

Figure 2.8 The basic concept of the terrestrial mercury cycle (Jiskra et al., 2015).

2.3.3 Aquatic mercury cycle

Atmospheric mercury reaches aquatic ecosystems through direct deposition onto water surfaces and through watershed runoff. This inorganic mercury (Hg^{II}) can be transported laterally and vertically by ocean circulation and suspended particulate matter deposition, or it can be reduced to dissolved gaseous elemental mercury (Hg^{0}) and escape into the atmosphere (Mason et al., 2012).

An amount of mercury (Hg^{II}) is converted to the more toxic methylmercury (MeHg). Methylmercury can bioconcentrate in living organisms and then pass through the food chain to further biomagnify (Selin, 2009). In coastal sediments, sulfate-reducing bacteria have been implicated as significant contributors to methylmercury production (King et al., 1999). These microorganisms can grow rapidly at both aerobic and anaerobic geochemical interfaces (Hintelmann et al., 2000).

In addition, factors affecting the production of MeHg include sulfur, sediment, organic carbon, composition and structure of the sediment layer, etc. (Achá et al., 2012). In aquatic systems, there is not only methylation of mercury but also demethylation of methylmercury. The photolytic degradation of MeHg is considered to be an important aspect of the MeHg cycle. Meanwhile, dissolved organic matter (DOM) also plays an essential role in the degradation of MeHg (Fleck et al., 2014). Demethylation and methylation coincide by both abiotic and biotic pathways, and the two processes are mutually reversible (Munson et al., 2018). The demethylation process of MeHg is also affected by biotic and abiotic factors. In addition, not all mercury compounds are affected by methylation and demethylation, which entirely depends on the bioavailability of mercury species in water (Klapstein et al., 2017).

The cycle of mercury in the aquatic environment is shown in **Fig. 2.9** (Zhu et al., 2018).

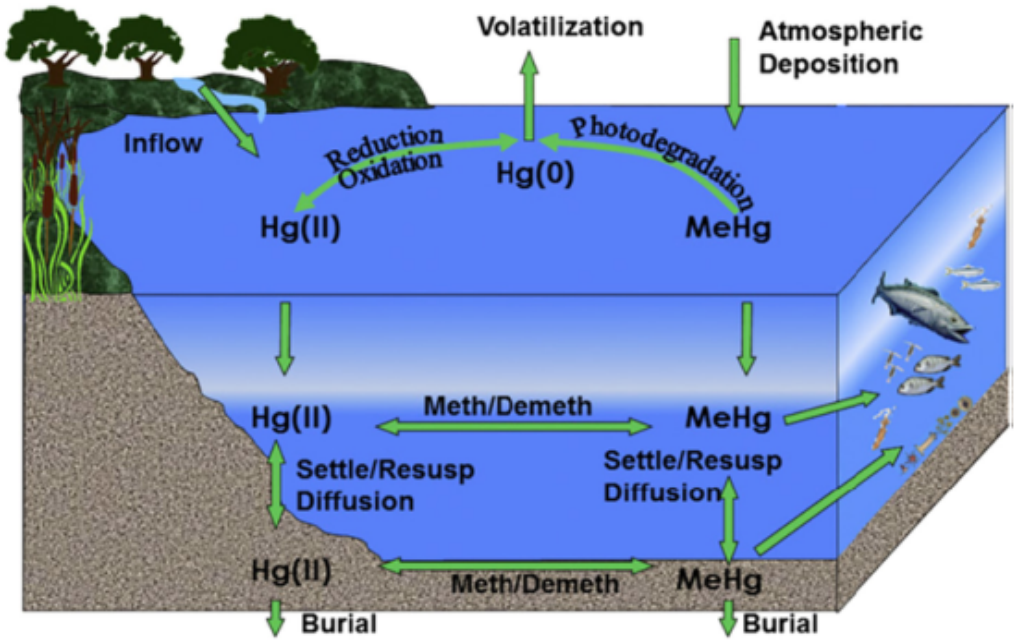

Figure 2.9 The basic concept of the terrestrial mercury cycle (Zhu et al., 2018).

2.4 Effects of Mercury on the Environment and Health

Mercury is used extensively in the economy. However, due to the use of mercury by humans, mercury is dispersed on the earth and pollutes the earth. Meanwhile, because mercury is not biodegradable, mercury pollution also threatens the environmental safety of future generations. Mercury is one of the most toxic elements and poses a serious threat to wildlife as it can accumulate in the food chain to unsafe levels in animals (Munthe et al., 2007). Mercury in the environment can be rapidly converted into organic compounds by microorganisms (such as methylmercury, etc.), allowing it to bioaccumulate and biomagnify in animals (Ronchetti et al., 2006). Humans at the top of the food chain are susceptible to the worst impacts due to the biomagnification effects of mercury. The effects on humans are not only harmful but also long-lasting (Azimi & Moghaddam, 2013).

2.4.1 Effects of mercury on the environment

Elemental mercury, which is liquid at room temperature, can evaporate into the air and be inhaled by humans. Even tiny amounts of mercury present in the air in enclosed spaces can easily reach levels that are harmful to health. Meanwhile, the longer people are exposed to mercury-polluted air, the greater the health risk. In addition, elemental mercury and its vapor are extremely difficult to remove from clothes, furniture, carpets, and other porous items, which results in that mercury can continue to pollute the air and other environments for a long time (Muhlendahl, 1990).

The severe pollution of water bodies by various pollutants has become a concern in the past few decades. Natural aquatic systems can be widely polluted by heavy metals released from households, industry, mining, and other anthropogenic activities (Domagalski et al., 2004). Due to the toxicity of mercury and its enrichment in aquatic organisms, once mercury enters the water body, it will cause severe pollution to the water body. Mercury is released into water systems from various sources through complex transport pathways (Driscoll et al., 2013). Mercury can enter rivers and lakes directly through atmospheric deposition. The discharge caused by human activities in the watershed, as well as the effects of surface runoff and soil leaching and erosion, also lead to the entry of mercury from land systems into water systems,

causing mercury pollution in water bodies. In addition, depending on soil properties, parts of mercury reservoirs can leach and contaminate groundwater (Bradley, 2013). Moreover, erosion of riverbanks and remobilization of previously deposited mercury with riverbed sediments during periods of high flow, especially in polluted systems, can also increase mercury levels in rivers, resulting in secondary mercury pollution (Horvat et al., 1999; Carroll et al., 2004).

In addition to air and water pollution, mercury pollution of the soil is also severe. Since the post-industrial era, there has been a significant increase in mercury levels in soils and sediments globally due to human industrial activities (Liu et al., 2021). In general, mining activities and industrial production are the main causes of soil mercury pollution (Zhang et al., 2011). Mercury in the soil can affect seed germination, plant disease incidence, and microbial activity. Mercury in soil not only affects plants and microorganisms but also enters the human body through exposure channels such as food chain, skin contact, and inhalation, endangering human health (Zhang et al., 2011). The study by Abeysinghe et al. (2017) found that after mercury enters the soil, it will continue to be absorbed by plants and undergo a series of transformations to form methylmercury. Methmercury in plants such as rice has more robust bioaccumulation characteristics and a more significant trophic level amplification factor, which increases the risk to human health.

2.4.2 Effects of mercury on health

In addition to its adverse environmental effects, mercury poses a serious health risk to people and other living things. The different forms of mercury affect the parts of the organism in different ways and to different degrees. In the blood, elemental mercury can be distributed in locations throughout the body because it readily crosses most cell membranes, including the blood-brain barrier and the placenta. Once high concentrations of elemental mercury are acutely inhaled, breathing difficulties may occur. Long-term exposure can induce central nervous system symptoms, including tremors, delusions, memory loss, and neurocognitive impairment, which can have lasting effects on brain function. In addition, long-term exposure may also cause damage to kidney function (Lohren et al., 2015).

Hg^0 is oxidized to inorganic forms (Hg^+ and Hg^{2+}) in the air and deposited in soil with rainfall or enters the water of rivers, lakes, and oceans. After entering the organism, inorganic mercury accumulates first in the kidneys and then in the liver. The most significant effect of mercury is to cause renal tubular necrosis and glomerulonephritis in the kidney.

At the same time, mercury may also cause autoimmune diseases (Stejskal, 2015). Methylmercury can accumulate to very high concentrations in shellfish, predatory fish, and marine mammals, so people whose diets consist primarily of fish and shellfish may be exposed to high levels of methylmercury. It is known that among the mercury flowing into the human body, methylmercury is the most toxic to the human body. At the same time, its residual rate in the human body is very high, and some studies have shown that it is as high as 95% (Hong et al., 2012).

Methylmercury is a potent toxin that affects enzymes, cell membrane function, and neuronal transmitters, causing oxidative stress, lipid peroxidation, and mitochondrial dysfunction, as well as affecting brain development (Sager et al., 1988). It is also reported that methylmercury can also cause movement disorders (such as trembling), sensory disturbances (such as impaired vision), and so on (Todd et al., 2003). In addition, exposure of pregnant women to methylmercury may increase the risk of malformations or severe neurologic disorders in infants even if the mother does not show any symptoms of toxicity (Fuyuta et al., 1978; Tsuchiya et al., 1984).

2.5 Mercury Pollution Problems Worldwide

Around the 1940s, a factory belonging to Chisso Co., Ltd. in Minamata City produced methylmercury during the production process, and the produced methylmercury was discharged into Minamata Bay without treatment, resulting in the pollution of Minamata Bay. Fish and shellfish are polluted by mercury, and people have a series of diseases after eating mercury-contaminated seafood, which has caused harmful effects.

Minamata disease was officially confirmed for the first time in Minamata City, Kumamoto Prefecture, Japan, in 1956, and this incident was also one of the worst pollution incidents in history (Ekino et al., 2007). Coincidentally, in 1965, the second Minamata disease (Niigata Minamata disease) occurred in Niigata Prefecture due to the release of methylmercury from the Showa Denko Kanose factory into the Agano Basin.

In addition to the Minamata incident, many serious incidents caused by mercury pollution have also occurred in other parts of the world. In Iraq in 1971, methylmercury poisoning was caused by using grains treated with methylmercury fungicides to make bread. The total number of hospitalizations reached more than 6,000, and more than 460 people died (Bakir et al., 1973).

The Amazon region is a major source of global mercury emissions and is also a region where human mercury exposure is high. Studies have shown that people in this region have relatively high blood mercury levels, with blood mercury levels in the range of 19.6-105.0 μg/L (de Araújo Mendes et al., 2021).

Mercury reserves in China rank third in the world, and 3000 years of long-term mercury mining activities have caused a large amount of mercury to be released into the environment through processing sites and distillation plants, causing serious mercury pollution (Li et al., 2009).

In India, due to the mercury discharge from the thermometer factory into Lake Kodai, the mercury content in the water body increased sharply. According to the measurement, it was found that the T-Hg content in Kodai Lake was 356-465 ng/L,

the MeHg content was 50 ng/L, the concentration range of total mercury in sediment was 276-350g/kg, and the total mercury content in fish is 120-290 g/kg (Karunasagar et al., 2006).

In France, untreated discharges from industrial chloralkali plants have resulted in significant releases of mercury into the local atmosphere and rivers, with ongoing impacts on the ecosystem of the River Thur (Hissler et al., 2006).

In south-central Spain, there is the world's largest mercury mining area (Almadén) which produced almost one-third of all mercury used by humans over a period of the past 2,000 years. Although mining and metallurgical activities had ceased at that time, mercury contamination in the area had affected all living organisms, including the soil and the plants that lived on it (Millán et al., 2006; Molina et al., 2006).

Moreover, in gold mining, due to the use of mercury to produce gold, mercury contamination in populations and ecological components has been observed in many gold mining sites in countries such as Brazil (Lebel et al. 1998), Indonesia (Bose-O'Reilly et al., 2010), Ghana (Basu et al. 2015) and so on.

In medicine, according to the United Nations Environment Programme, about 340 t of mercury is used in dentistry globally every year, of which about 100 tons of dental mercury enters the waste stream every year (UNEP, 2013).

2.6 Mercury Pollution in Minamata Bay, Japan

2.6.1 Overview of where mercury pollution occurred

In the early 1950s, massive methylmercury (MeHg) poisoning occurred among residents near Minamata Bay in Minamata City, on the southwestern coast of Kyushu Island, Japan, leading to the first awareness of the resulting severe neurological disorders (Kumamoto University, 1966).

Minamata City (**Fig. 2.10**) belongs to Kumamoto Prefecture. It was established as a village in 1889, transformed into a town in 1912, and established as a city in 1949. It is located in the southwestern part of Kyushu, at the southernmost tip of Kumamoto Prefecture. This city is adjacent to Izu City and Oguchi City in Kagoshima Prefecture. The city is surrounded by mountains on three sides, with hills all over, and the Minamata River across the sea. The city has a warm climate and covers an area of 163.29 square kilometers. Most of the city is surrounded by dense vegetation, and villages are scattered along the river, river bends, and fishing ports. National Highway 268 runs through the city from east to west, National Highway 3 and the JR Kagoshima Line run north and south, and the Kyushu Shinkansen also passes through the city (Minamata City, 2022). Seventy percent of the population lives in the urban area, where most shops and businesses are located. The principal inhabitants of Minamata city are mainly local fishermen and immigrants from other regions of Japan, who build huts along the coastline to catch fish, octopus, and shellfish (Aoyama, 2016; Noguchi, 2017).

Minamata Bay (**Fig. 2.10**) is a small bay with an area of 382 hectares on the south coast of Yatsushiro Sea in Kumamoto, Kyushu Island, Japan, with an average depth of 16.7 meters (Matsuyama et al., 2014). Compared with the tides in other places in Japan, the tidal range of the Yatsushiro Sea is relatively large, together with the influence of Koiji Island, resulting in a tidal range of nearly 4 meters in Minamata Bay (Kumamoto Prefecture, 2005). In addition, the diurnal tidal current is dominant rather than the semi-diurnal one in the sea area around the Minamata (Tai et al., 2007). In summer, a horizontal circulation flow occurred during ebb tide. During the winter circulation period, tidal currents were observed at the mouth of the western

bay (Tada et al., 2005).

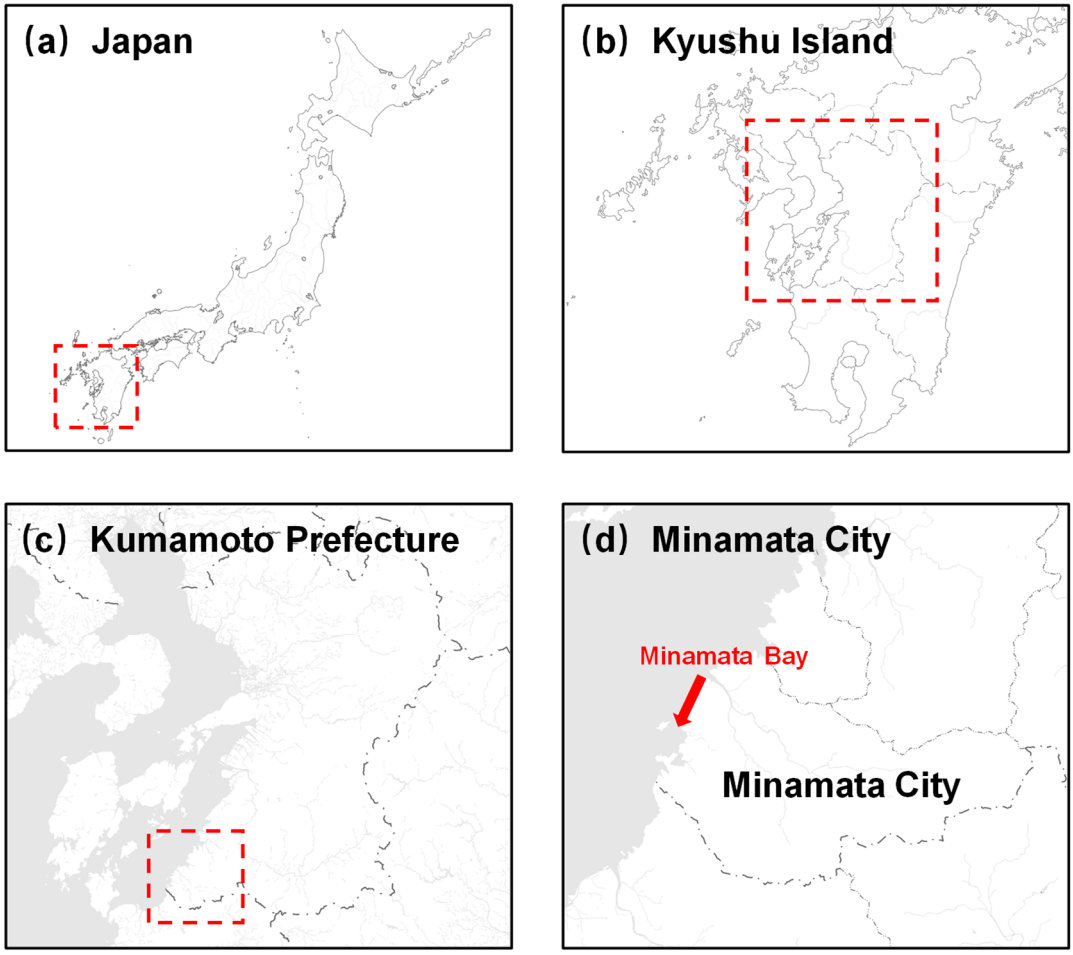

Figure 2.10 The map of Japan (a), Kyushu Island (b), Kumamoto Prefecture (c), and Minamata City (d)(Adapted from GSI Maps, Retrieved July 2023. Copyright by GSI Maps).

2.6.2 The outbreak of Minamata Disease

The Chisso plant in Minamata City uses mercury sulfate as a catalyst in the production of acetaldehyde. During this production process, part of the mercuric sulfate was converted to methylmercury (Fujiki and Tajima, 1992). The process of producing methylmercury during the production of acetaldehyde is shown in **Fig. 2.11** (Yokoyama, 2018). These methylmercuries contained in untreated sewage were discharged into Minamata Bay, polluted shellfish and fish in the sea, and continuously enriched in higher fish through the food chain. Finally, people have symptoms of mercury poisoning after eating this mercury-contaminated seafood (Minamata City, 2022). The mercury pollution mechanism in Minamata Bay is shown in **Fig. 2.12** (Nishimura and Okamoto, 2001). Since the investigation of the cause took a long time, the outbreak of Minamata disease continued and expanded along the coast of the Yatsushiro Sea (Also called the Shiranui Sea). **Fig. 2.13** shows the extent of the area affected by mercury pollution (Yokoyama, 2018).

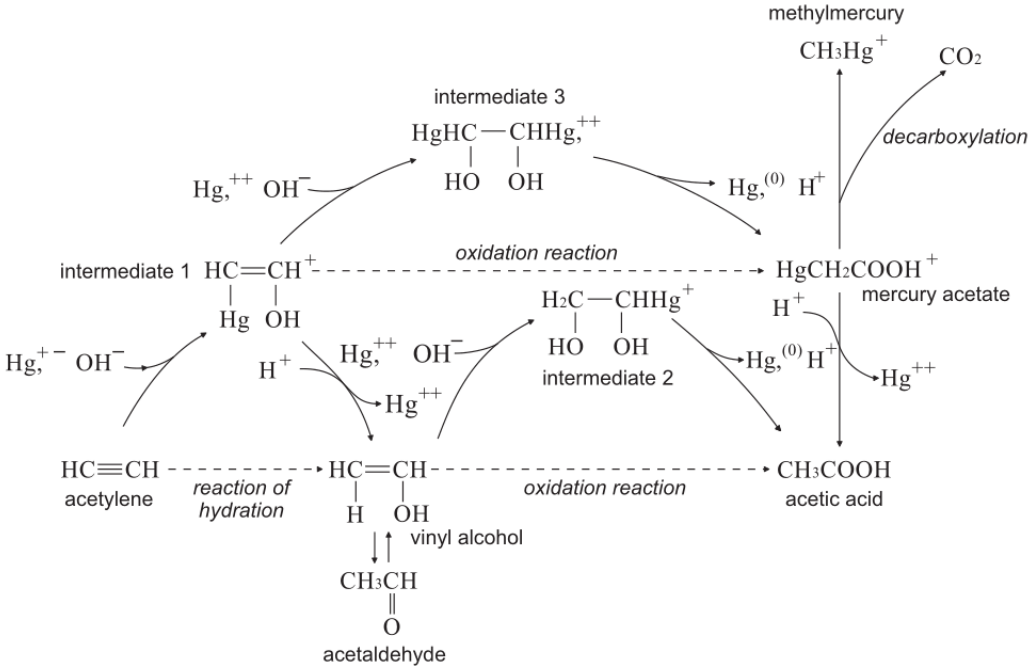

Figure 2.11 The process of producing methylmercury during the production of acetaldehyde (Yokoyama, 2018).

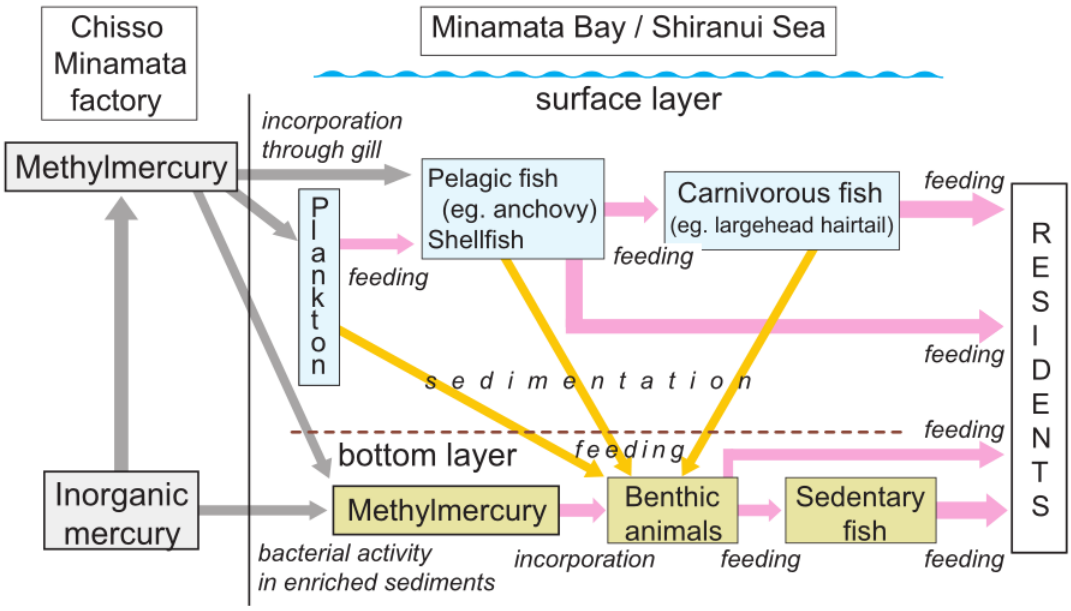

Figure 2.12 Mercury Pollution Mechanism in Minamata Bay (Nishimura and Okamoto, 2001).

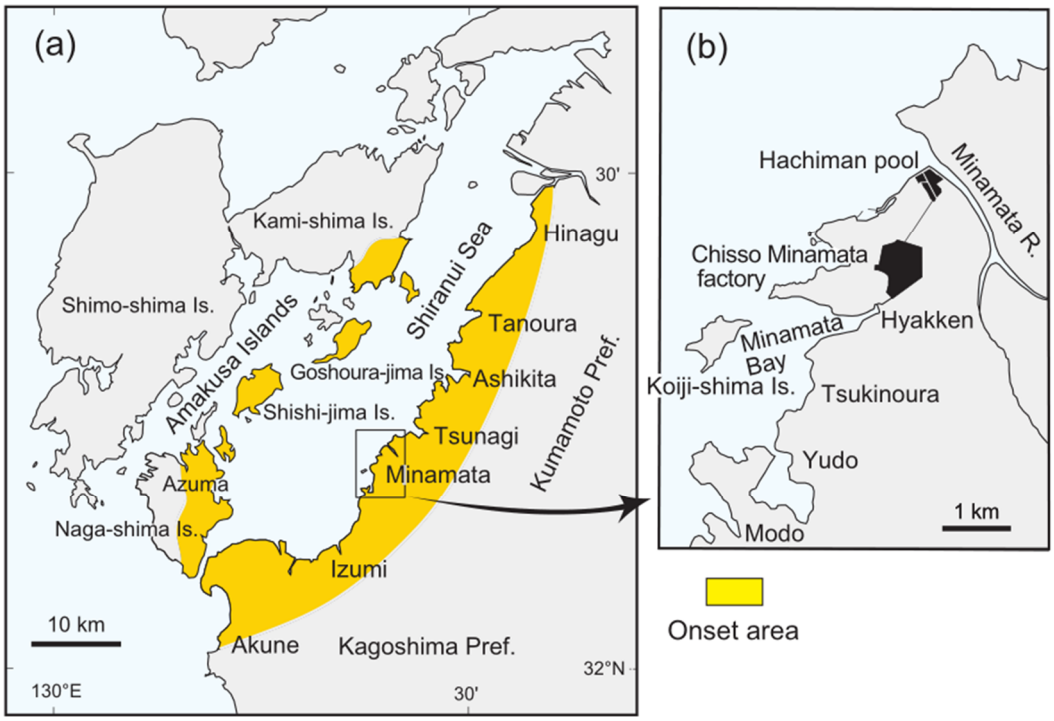

Figure 2.13 Map showing areas where methylmercury poisoning through environmental contamination occurred. (a) The Shiranui Sea (Yatsushiro Sea). (b) Minamata area (Yokoyama, 2018).

Minamata disease was recognized in 1956 when the Minamata Chisso Factory Hospital notified the Minamata Health Center of the first severe brain disease of unknown cause in Tsuno Ward (Minamata City, 2022). Patients with Minamata disease present with symptoms such as neurological disturbances, including sensory disorders, ataxia, dysarthria, narrowed vision, and hearing difficulties (Yorifuji et al., 2008; Eto et al., 2010). As of the end of April 2022, the total number of confirmed patients was 2,284, of which 1,791 were confirmed in Kumamoto Prefecture and 493 in Kagoshima Prefecture (**Fig. 2.14**) (Minamata City, 2022). In addition, more than 40,000 people showed some symptoms, such as sensory disturbances dominated by peripheral limbs (Hachiya, 2012). Moreover, a report indicated that from 1955 to 1959, more than 200 babies from 8,584 families were born with Minamata disease (Miyamoto, 2018).

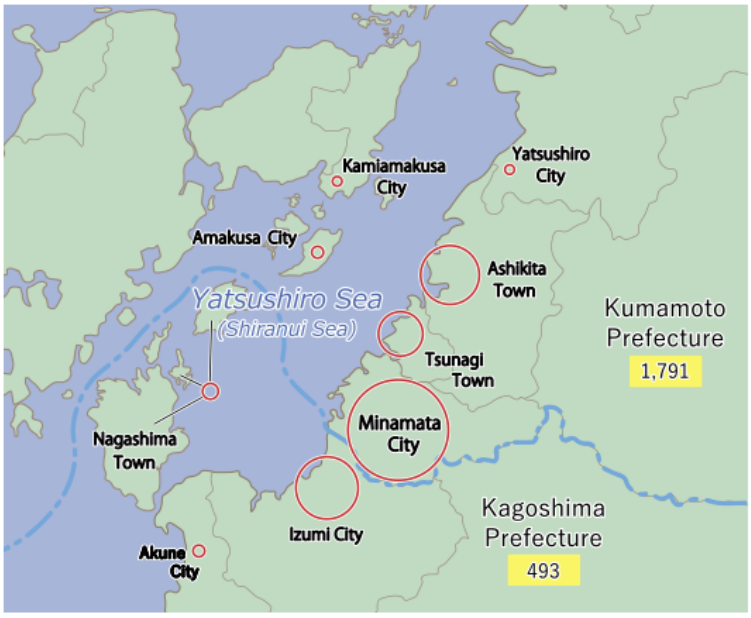

Figure 2.14 Distribution of certified patients (Minamata City, 2022).

2.6.3 Treatment after pollution occurs

Due to the increasing number of people suffering from Minamata disease, many of whom died from neurological complications, the Chisso plant finally ceased acetaldehyde production in 1968 (Harada，1978; Yorifuji et al., 2013). However, from 1932, it was reported that about 70-150 t or more of mercury was mixed with sewage from factories and discharged into Minamata Bay for 36 years (Premakumara et al., 2011). Mercury with a 25 ppm or more concentration exists in about 2.09 million square meters of seabed near Minamata Bay. In some areas inside the bay, the thickness of this sludge even reached a staggering 4 meters.

Therefore, it is essential to dispose of the contaminated sludge in the bay as soon as possible and properly and to create a strategy for restoring the environment. In October 1977, Kumamoto Prefecture launched the Minamata Bay Pollution Prevention Project to treat sediment sludge containing more than 25 ppm mercury (the criteria is computed based on the regulatory standards for sediment removal established by the Environmental Agency). Firstly, the interior of the bay, which has a high mercury content of about 580,000 square meters, was enclosed with metal plates to form a closed area. Then, the 1.51 million m^2 bay with low mercury content (including about 780,000 m^3 of deposited sludge) was dredged using a knifeless pump vessel and filled back to the closed area to form new land. The ground of reclamation was treated with synthetic sheets and covered with soil from nearby mountains to prevent secondary pollution of mercury (**Fig. 2.15**) (Minamata City, 2022).

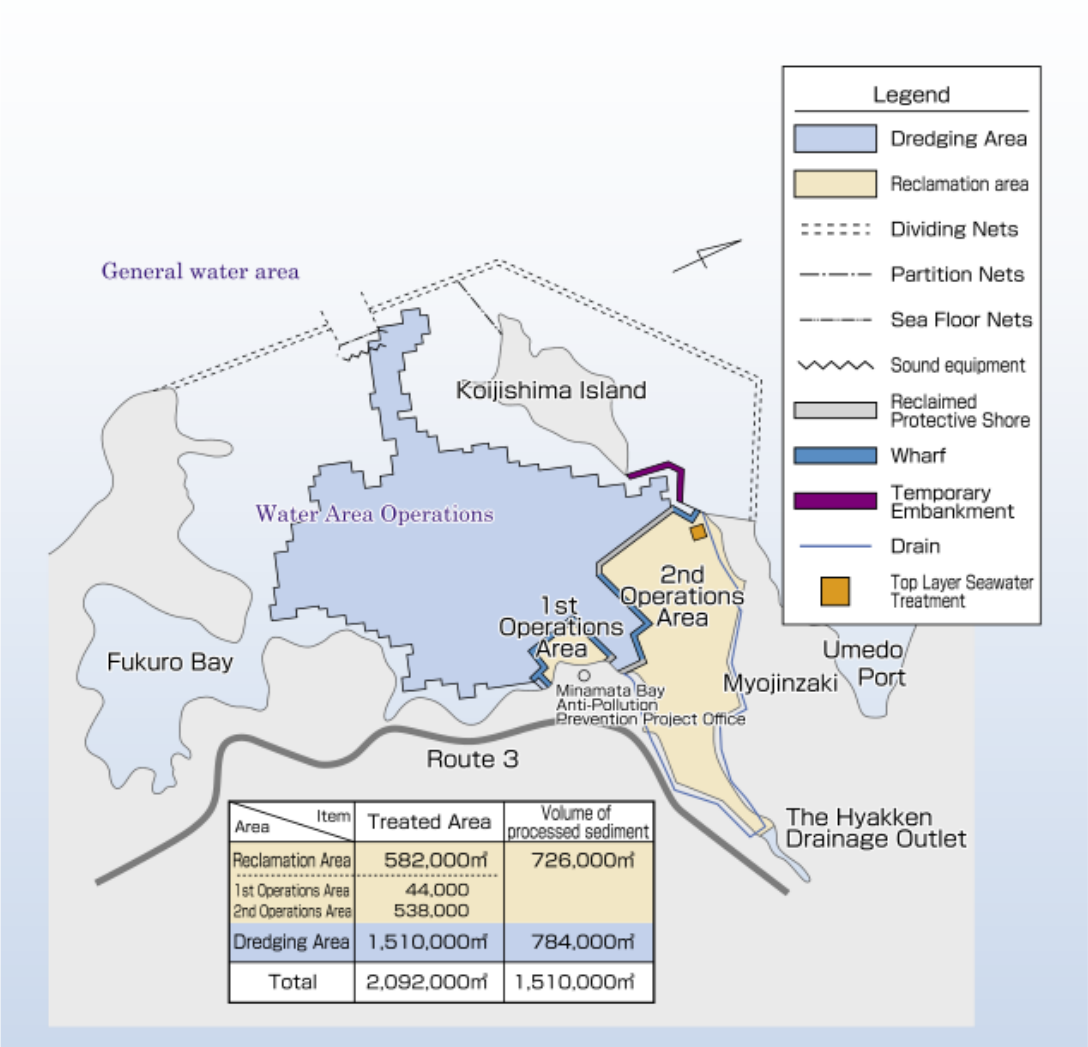

Figure 2.15 Map of Minamata Bay dredging operations (Minamata City, 2022).

2.6.4 Residual mercury pollution status after pollution treatment measures

Matsuyama et al. (2014) collected 691 sediment samples at 107 sampling points in Minamata Bay in 2012. The results showed that the weighted average of the total mercury concentration in the bottom sediment of Minamata Bay was 2.3 mg/kg, and the weighted average of the total mercury mass was 3.4 t. The distribution of total mercury in the surface layer of the sediments did not significantly differ from the findings reported after the dredging was finished, and the average concentration of total mercury in the sediment surface layer was 3.0 mg/kg dry weight. The distribution of total mercury concentration in the surface layer of Minamata Bay is shown in **Fig. 2.16**. Tomiyasu et al. (2014) studied the residual total mercury concentration and changes in sediments during 2002-2010. The results showed that the annual mean total mercury concentrations in the surface sediments of Minamata Bay and Fukuro Bay were 2.47-3.34 and 3.50-4.66 mg/kg, respectively.

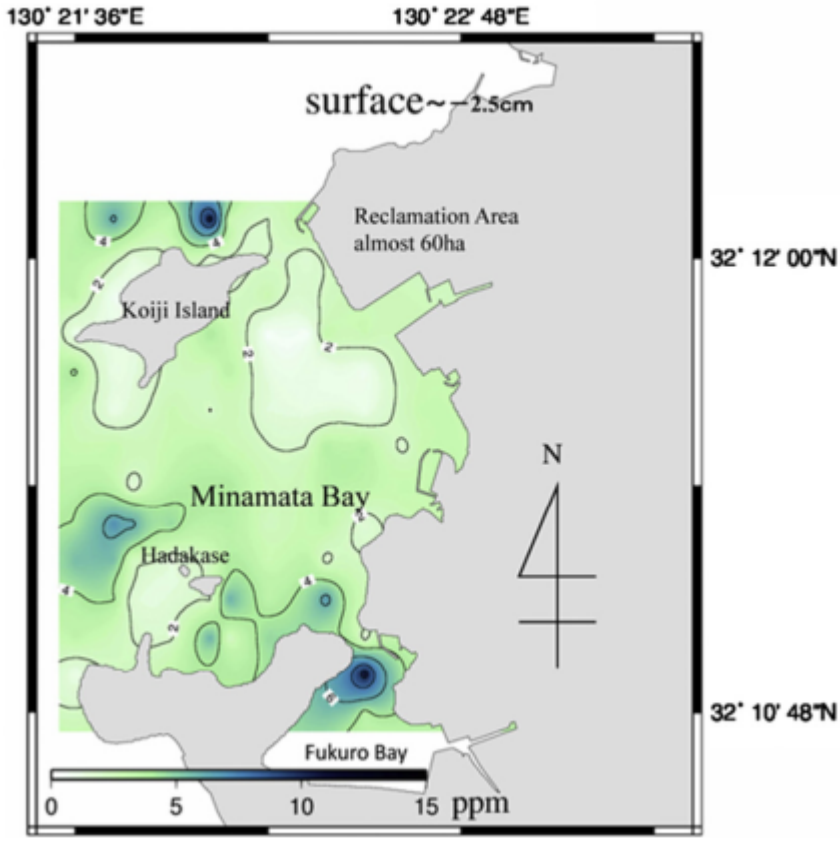

Figure 2.16 Distribution of T-Hg concentrations (ppm) in surface sediment (Matsuyama et al., 2014).

In addition, Yasuda et al. (2010) measured the methylmercury content in a small omnivorous crab (Gaetice depressus) and a carnivorous snail (Thais clavigera) near Minamata Bay. They found that the concentrations of methylmercury in these two benthic animals were 0.4 and 0.2 ppm. This result was higher than the methylmercury levels in benthic fauna from the western Japan region that was compared in this study. Matsuyama et al. (2013) conducted annual monitoring of mercury pollution in Japanese stickleback (Sebastiscus marmoratus) and bamboo wrasse (Pseudolabrus japonicas) in Minamata Bay from 2008 to 2010. The results showed that the average total concentrations of mercury in the muscles of these two fish species in Minamata Bay were 0.36 and 0.20 mg/kg wet weight, respectively. This concentration level is much higher than elsewhere in Japan (0.125 mg/kg and 0.038 mg/kg wet weight, respectively).

Rifard et al. (1998) collected some samples of seafloor sediments in the Yatsushiro Sea. The results indicated that the mercury-contaminated fine-grained sediments migrated northeast and south to the Yatsushiro Sea under weak shore currents. At the same time, it continued to spread northward and westward in the southern part of the Yatsushiro Sea (**Fig. 2.17**). Moreover, in 1996, sediments were sampled at 74 sites in the Yatsushiro Sea by Tomiyasu et al. (2000). The results showed that except for one sampling point located on the opposite coast of Minamata City, the total mercury concentration of other sampling points was higher than 0.1 mg/kg, indicating that mercury pollution in sediments had spread to a large area of the Yatsushiro Sea. In 2010, Yano (2013) conducted in-situ measurements of mercury transport in seawater from Minamata Bay, and the results showed that mercury migrated from Minamata Bay to Yatsushiro Sea, and the annual particle T-Hg and MeHg transport volumes from Minamata Bay to Yatsushiro Sea 6 kg and 0.05 kg, respectively. In addition, research by Matsuyama et al. (2019) showed that most of the mercury emitted from Chisso either stayed in Minamata Bay or near the exit of Minamata Bay, but some were transported from Minamata Bay to the Yatsushiro Sea. They estimated that about 51 tons and 6 tons of mercury accumulated in the Yatsushiro Sea and Amakusa Sea regions, respectively (**Fig. 2.18**).

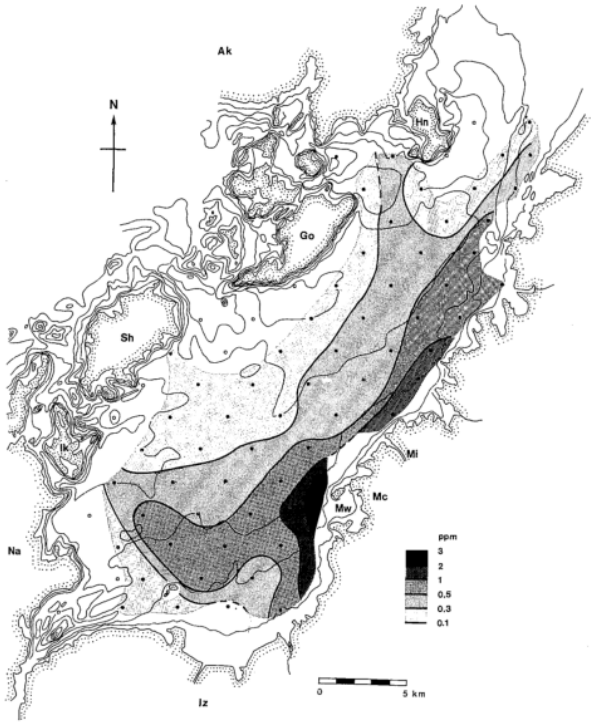

Figure 2.17 The distribution of the maximum mercury concentration (ppm) analyzed in specific horizons of each core (Rifard et al., 1998).

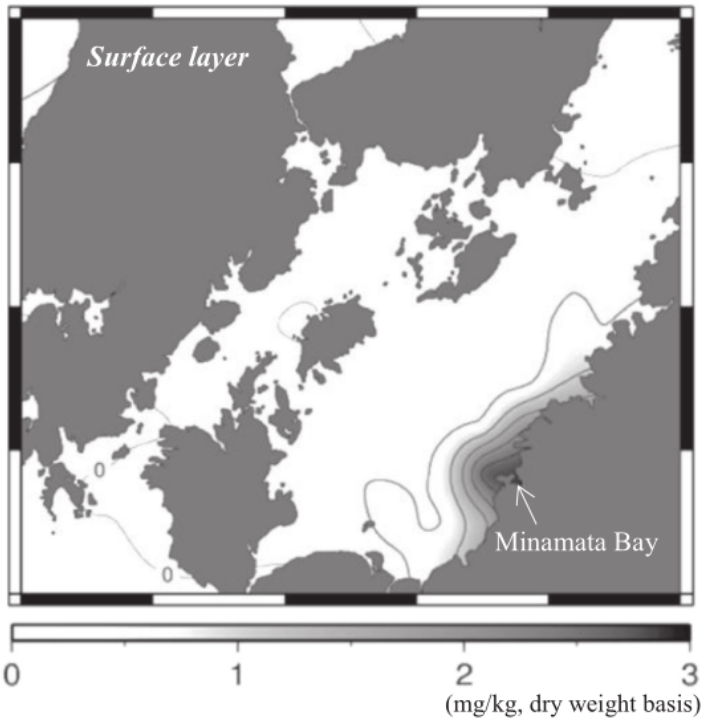

Figure 2.18 Spatial distribution characteristics of T-Hg concentration in surface sediments of the Yatsushiro Sea (Matsuyama et al., 2019).

According to the above studies, it can be seen that the mercury content in sediments in Minamata Bay and the mercury content in organisms in Minamata Bay are still high. At the same time, mercury in Minamata Bay migrated to the Yatsushiro Sea. In addition, mercury is highly toxic, bioaccumulative, persistent, and recyclable in the environment. Therefore, even if the mercury with high concentration has been dredged, it is essential to continue research on the residual mercury in Minamata Bay and the Yatsushiro Sea.

References

Abeysinghe, K. S., Qiu, G., Goodale, E., Anderson, C. W., Bishop, K., Evers, D. C., Goodale, M. W., Hintelmann, H., Liu, S., Mammides, C., Quan, R. Wang, J., Wu, P., Xu, X., Yang, X., & Feng, X. (2017). Mercury flow through an Asian rice-based food web. *Environmental Pollution*, 229, 219-228.

Achá, D., Hintelmann, H., & Pabón, C. A. (2012). Sulfate-reducing bacteria and mercury methylation in the water column of the lake 658 of the experimental lake area. *Geomicrobiology Journal*, 29(7), 667-674.

AMAP/UNEP. (2008). Technical Background Report to the Global Atmospheric Mercury Assessment. Arctic Monitoring and Assessment Programme / UNEP Chemicals Branch. 159 p.

Aoyama, M. (2016). Minamata: disability and the sea of sorrow. Occupying Disability: Critical Approaches to Community, Justice, and Decolonizing Disability, 31-45.

Azimi, S., & Moghaddam, M. S. (2013). Effect of mercury pollution on the urban environment and human health. *Environment and Ecology Research*, 1(1), 12-20.

Bailey, E., Clark, A., & Simith, R. (1973). United States mineral resources: mercury. *USGS Professional Paper 820*, 404-414.

Bakir, F., Damluji, S. F., Amin-Zaki, L., Murtadha, M., Khalidi, A., Al-Rawi, N. Y. Tikriti, S., Dhahir, H. I., Clarkson T. W., Smith, J.C., & Doherty, R. A. (1973). Methylmercury Poisoning in Iraq: An interuniversity report. *Science*, 181(4096), 230-241.

Basu, A., Phipps, S., Long, R., Essegbey, G., & Basu, N. (2015). Identification of response options to artisanal and small-scale gold mining (ASGM) in Ghana via the Delphi process. *International journal of Environmental research and public health*, 12(9), 11345-11363.

Bernhoft, R. A. (2012). Mercury toxicity and treatment: a review of the literature. *Journal of Environmental and Public Health*, 460508.

Biester, H., Kilian, R., Franzen, C., Woda, C., Mangini, A., & Schöler, H. F. (2002). Elevated mercury accumulation in a peat bog of the Magellanic Moorlands, Chile (53°S)–an anthropogenic signal from the Southern Hemisphere. *Earth and Planetary Science Letters*, 201(3-4), 609-620.

Bindler, R., Renberg, I., Appleby, P. G., Anderson, N. J., & Rose, N. L. (2001). Mercury accumulation rates and spatial patterns in lake sediments from west Greenland: a coast to ice margin transect. *Environmental Science & Technology*, 35(9), 1736-1741.

Bishop, K., Shanley, J. B., Riscassi, A., de Wit, H. A., Eklöf, K., Meng, B., Mitchell, C., Osterwalder, S., Schuster, P. F., Webster, J., & Zhu, W. (2020). Recent advances in understanding and measurement of mercury in the environment: Terrestrial Hg cycling. *Science of the Total Environment*, 721, 137647.

Bloom N.S. (1992). On the chemical form of mercury in edible fish and marine invertebrate tissue. *Canadian Journal of Fisheries and Aquatic Sciences*, 49(5), 1010-1017.

Bookman, R., Driscoll, C. T., Engstrom, D. R., & Effler, S. W. (2008). Local to regional emission sources affecting mercury fluxes to New York lakes. *Atmospheric Environment*, 42(24), 6088-6097.

Bose-O'Reilly, S., Drasch, G., Beinhoff, C., Rodrigues-Filho, S., Roider, G., Lettmeier, B. Maydl, A., Maydl, S., & Siebert, U. (2010). Health assessment of artisanal gold miners in Indonesia. *Science of the Total Environment*, 408(4), 713-725.

Bradley, P. (Ed.). (2013). Current perspectives in contaminant hydrology and water resources sustainability.

Brunke, E. G., Labuschagne, C., & Slemr, F. (2001). Gaseous mercury emissions from a fire in the Cape Peninsula, South Africa, during January 2000. *Geophysical Research Letters*, 28(8), 1483-1486.

Camargo, J. A. (2002). Contribution of Spanish–American silver mines (1570–1820) to the present high mercury concentrations in the global environment: a review. *Chemosphere*, 48(1), 51-57.

Carroll, R. W. H., Warwick, J. J., James, A. I., & Miller, J. R. (2004). Modeling erosion and overbank deposition during extreme flood conditions on the Carson River, Nevada. *Journal of Hydrology*, 297(1-4), 1-21.

Cheng, H., & Hu, Y. (2010). China needs to control mercury emissions from municipal solid waste (MSW) incineration. Environmental Science & Technology, 44, 7994-7995.

Cheng, I., Zhang, L., & Blanchard, P. (2014). Regression modeling of gas‐particle partitioning of atmospheric oxidized mercury from temperature data. *Journal of Geophysical Research: Atmospheres*, 119(20), 11864-11876.

Cohen, M., Artz, R., Draxler, R., Miller, P., Poissant, L.D., Ratte, D., Deslauries, M., Duval, R., Laurin, R., Slotnick, J., Nettesheim, T., & McDonald, J. (2004). Modeling the atmospheric transport and Deposition of Mercury to The Great Lakes, Environmental Research, 95, 247-265.

de Araújo Mendes, T. A., do Nascimento, R. S. C., da Silva Veras, R., Almeida, M. E., & Knauer, L. G. (2021). Geological knowledge advances on the Alto Rio Negro region, northwestern Amazonian Craton, Brazil: a review. *Journal of the Geological Survey of Brazil*, 4(3), 209-222.

De Simone, F., Gencarelli, C. N., Hedgecock, I. M., & Pirrone, N. (2014). Global atmospheric cycle of mercury: a model study on the impact of oxidation mechanisms. *Environmental Science and Pollution Research*, 21, 4110-4123.

Domagalski, J. L., Alpers, C. N., Slotton, D. G., Suchanek, T. H., & Ayers, S. M. (2004). Mercury and methylmercury concentrations and loads in the Cache

Creek watershed, California. *Science of the Total Environment*, 327(1-3), 215-237.

Driscoll, C. T., Mason, R. P., Chan, H. M., Jacob, D. J., & Pirrone, N. (2013). Mercury as a global pollutant: sources, pathways, and effects. *Environmental science & technology*, 47(10), 4967-4983.

Ebinghaus, R., Turner, R. R., de Lacerda, L. D., Vasiliev, O., & Salomons, W. (1999). Mercury contaminated sites: characterization, risk assessment and remediation. Springer Science & Business Media.

Ekino, S., Susa, M., Ninomiya, T., Imamura, K., & Kitamura, T. (2007). Minamata disease revisited: an update on the acute and chronic manifestations of methyl mercury poisoning. *Journal of the neurological sciences*, 262(1-2), 131-144.

Eto K., Marumoto M., & Takeya M. (2010). The pathology of methylmercury poisoning (Minamata disease). *Neuropathology*, 30(5), 471-479.

Ferrara, R., Mazzolai, B., Lanzillotta, E., Nucaro, E., & Pirrone, N. (2000). Volcanoes as emission sources of atmospheric mercury in the Mediterranean basin. *Science of the Total Environment*, 259(1-3), 115-121.

Fitzgerald, W. F., & Lamborg, C. H. (2007). Geochemistry of mercury in the environment. *Treatise on geochemistry*, 9, 1-47.

Fleck, J. A., Gill, G., Bergamaschi, B. A., Kraus, T. E., Downing, B. D., & Alpers, C. N. (2014). Concurrent photolytic degradation of aqueous methylmercury and dissolved organic matter. *Science of the Total Environment*, 484, 263-275.

Fu, X., Zhang, H., Yu, B., Wang, X., Lin, C., & Feng, X. (2015). Observations of atmospheric mercury in China: a critical review. *Atmospheric Chemistry and Physics*, 15, 9455-9476.

Fujiki, M., & Tajima, S. (1992). The pollution of Minamata Bay by mercury. *Water Science and Technology*, 25(11), 133-140.

Fuyuta, M., Fujimoto, T., & Hirata, S. (1978). Embryotoxic effects of methylmercuric chloride administered to mice and rats during organogenesis. *Teratology*, 18(3), 353-365.

Gill, G.A. & Bruland, K.W.(1990). Mercury speciation in surface freshwater systems in California and other areas. *Environmental Science and Technology*, 24, 1392-1400.

Gray, J. E., & Hines, M. E. (2006). Mercury: distribution, transport, and geochemical and microbial transformations from natural and anthropogenic sources. *Applied Geochemistry*, 21(11), 1819-1820.

Graydon, J. A., St. Louis, V. L., Lindberg, S. E., Sandilands, K. A., Rudd, J. W., Kelly, C. A., Harris, R., Tate, M.T., Krabbenhoft, D. P., Emmerton, C. A., Asmath, H., & Richardson, M. (2012). The role of terrestrial vegetation in atmospheric Hg deposition: Pools and fluxes of spike and ambient Hg from the METAALICUS experiment. *Global Biogeochemical Cycles*, 26(1), GB1022.

Grigal, D. F. (2002). Inputs and outputs of mercury from terrestrial watersheds: a review. *Environmental Reviews*, 10(1), 1-39.

Gustin, M. S. (2003). Are mercury emissions from geologic sources significant? A status report. *Science of the Total Environment*, 304(1-3), 153-167.

Gworek, B., Dmuchowski, W., & Baczewska-Dąbrowska, A. H. (2020). Mercury in the terrestrial environment: a review. *Environmental Sciences Europe*, 32(1), 1-19.

Hachiya, N. (2012). Epidemiological update of methylmercury and Minamata disease. *Methylmercury and Neurotoxicity*, 1-11.

Harada, M. (1978). Congenital Minamata disease: intrauterine methylmercury poisoning. *Teratology*, 18(2), 285-288.

Harris, H.H., Pickering, I.J., & George, G.N. (2003). The chemical form of mercury in fish. *Science*, 301(5637), 1203-1203.

Hintelmann, H., Keppel-Jones, K., & Evans, R. D. (2000). Constants of mercury methylation and demethylation rates in sediments and comparison of tracer and ambient mercury availability. *Environmental Toxicology and Chemistry*, 19(9), 2204-2211.

Hissler, C., & Probst, J. L. (2006). Impact of mercury atmospheric deposition on soils and streams in a mountainous catchment (Vosges, France) polluted by chlor-alkali industrial activity: the important trapping role of the organic matter. *Science of the Total Environment*, 361(1-3), 163-178.

Hong, Y. S., Kim, Y. M., & Lee, K. E. (2012). Methylmercury exposure and health effects. *Journal of preventive medicine and public health*, 45(6), 353.

Horvat, M., Covelli, S., Faganeli, J., Logar, M., Mandić, V., Rajar, R., Širca, A., & Žagar D. (1999). Mercury in contaminated coastal environments; a case study: the Gulf of Trieste. *Science of the Total Environment*, 237, 43-56.

Jiang, G. B., Shi, J. B., & Feng, X. B. (2006). Mercury pollution in China. *Environmental science & technology*, 40(12), 3672-3678.

Jiskra, M., Wiederhold, J. G., Skyllberg, U., Kronberg, R. M., Hajdas, I., & Kretzschmar, R. (2015). Mercury deposition and re-emission pathways in boreal forest soils investigated with Hg isotope signatures. *Environmental Science & Technology*, 49(12), 7188-7196.

Jitaru, P., & Adams, F. (2004). Toxicity, sources and biogeochemical cycle of mercury. *Journal de Physique IV (Proceedings)*, EDP sciences, 121, 185-193.

Kabata-Pendias A. (2010). Trace elements in soils and plants. CRC Press, 548p.

Karunasagar, D., Krishna, M. B., Anjaneyulu, Y. A., & Arunachalam, J. (2006). Studies of mercury pollution in a lake due to a thermometer factory situated in a tourist resort: Kodaikkanal, India. *Environmental pollution*, 143(1), 153-158.

King, J. K., Saunders, F. M., Lee, R. F., & Jahnke, R.A. (1999). Coupling mercury methylation rates to sulfate reduction rates in marine sediments. *Environmental Toxicology and Chemistry*, 18(7), 1362-1369.

Klapstein, S. J., Ziegler, S. E., Risk, D. A., & O'Driscoll, N. J. (2017). Quantifying the effects of photoreactive dissolved organic matter on methylmercury photodemethylation rates in freshwaters. *Environmental Toxicology and Chemistry*, 36(6), 1493-1502.

Kumamoto Prefecture. (1997). An Outline of the Enviromental Restoration of Minamata Bay.

Kumamoto Prefecture. (2005). Basic Plan for Coastal Preservation of Yatsushiro Sea (in Japanese).

Kumamoto University. Kumamoto University Medical School Minamata Disease Study Group. (1966). Minamata Disease: Study on the Organic Mercury Poisoning.

Lam, K.T., Wilhelmsen, C.J., Schwid, A.C., Jiao, Y., & Dibble, T.S. (2019). Computational study on the photolysis of BrHgONO and the reactions of BrHgO·with CH_4, C_2H_6, NO, and NO_2: implications for formation of Hg (II) compounds in the atmosphere. *The Journal of Physical Chemistry A*, 123, 1637-1647.

Lamborg, C. H., Fitzgerald, W. F., O'Donnell, J., & Torgersen, T. (2002a). A non-steady-state compartmental model of global-scale mercury biogeochemistry with interhemispheric atmospheric gradients. *Geochimica et Cosmochimica Acta*, 66(7), 1105-1118.

Lamborg, C. H., Fitzgerald, W. F., Damman, A. W. H., Benoit, J. M., Balcom, P. H., & Engstrom, D. R. (2002b). Modern and historic atmospheric mercury fluxes in both hemispheres: global and regional mercury cycling implications. *Global Biogeochemical Cycles*, 16(4), 51-1-51-11.

Landis, M. S., Ryan, J. V., ter Schure, A. F., & Laudal, D. (2014). Behavior of mercury emissions from a commercial coal-fired power plant: The relationship between stack speciation and near-field plume measurements. *Environmental science & technology*, 48(22), 13540-13548.

Lebel, J., Mergler, D., Branches, F., Lucotte, M., Amorim, M., Larribe, F., & Dolbec, J. (1998). Neurotoxic effects of low-level methylmercury contamination in the Amazonian Basin. *Environmental Research*, 79(1), 20-32.

Li, P., Feng, X. B., Qiu, G. L., Shang, L. H., & Li, Z. G. (2009). Mercury pollution in Asia: a review of the contaminated sites. *Journal of hazardous materials*, 168(2-3), 591-601.

Li, T., Wang, Y., Mao, H., Wang, S., Talbot, R. W., Zhou, Y., Wang, Z., Nie, X., & Qie, G. (2018). Insights on chemistry of mercury species in clouds over Northern China: Complexation and adsorption. *Environmental Science & Technology*, 52(9), 5125-5134.

Lin, C. J., & Pehkonen, S. O. (1999). The chemistry of atmospheric mercury: a review. *Atmospheric Environment*, 33(13), 2067-2079.

Lin, C.J., Pongprueksa, P., Lindberg, S.E., Pehkonen, S.O., Byun, D., & Jang, C. (2006). Scientific uncertainties in atmospheric mercury models I: model science evaluation. *Atmospheric Environment*, 40, 2911-2928.

Lindberg, S. E., Hanson, P. J., Meyers, T. A., & Kim, K. H. (1998). Air/surface exchange of mercury vapor over forests—the need for a reassessment of continental biogenic emissions. *Atmospheric Environment*, 32(5), 895-908.

Lindqvist, O., Johansson, K., Bringmark, L., Timm, B., Aastrup, M., Andersson, A., Hovsenius, G., Håkanson, L., Iverfeldt, Å. & Meili, M. (1991). Mercury in the Swedish environment—recent research on causes, consequences and corrective methods. *Water, Air, & Soil Pollution*, 55(1-2): xi-261.

Liu, S., Wang, X., Guo, G., & Yan, Z. (2021). Status and environmental management of soil mercury pollution in China: A review. *Journal of Environmental Management*, 277, 111442.

Lohren, H., Bornhorst, J., Galla, H. J., & Schwerdtle, T. (2015). The blood–cerebrospinal fluid barrier–first evidence for an active transport of organic mercury compounds out of the brain. *Metallomics*, 7(10), 1420-1430.

Loux, N.T. (1998). An assessment of mercury-species-dependent binding with natural organic carbon. *Chemical Speciation and Bioavailability*, 10, 127-136.

Mason, R. P., Fitzgerald, W. F., & Morel, F. M. (1994). The biogeochemical cycling of elemental mercury: anthropogenic influences. *Geochimica et Cosmochimica Acta*, 58(15), 3191-3198.

Mason, R. P., & Sheu, G. R. (2002). Role of the ocean in the global mercury cycle. *Global biogeochemical cycles*, 16(4), 40-1-40-14.

Mason, R. P., Choi, A. L., Fitzgerald, W. F., Hammerschmidt, C. R., Lamborg, C. H., Soerensen, A. L., & Sunderland, E. M. (2012). Mercury biogeochemical cycling in the ocean and policy implications. *Environmental Research*, 119, 101-117.

Matsuyama, A., Yokoyama, S., Kindaichi, M., Sonoda, I., & Koyama, J. (2013). Effect of seasonal variation in seawater dissolved mercury concentrations on mercury accumulation in the muscle of red sea bream (Pagrus major) held in Minamata Bay, Japan. *Environmental Monitoring and Assessment*, 185, 7215-7224.

Matsuyama, A., Yano, S., Hisano, A., Kindaichi, M., Sonoda, I., Tada, A., & Akagi, H. (2014). Reevaluation of Minamata Bay, 25 years after the dredging of mercury-polluted sediments, *Marine Pollution Bulletin*, 89, 112-120.

Matsuyama, A., Yano, S., Matsunoshita, K., Kindaichi, M., Tada, A., & Akagi, H. (2019). The spatial distribution of total mercury in sediments in the Yatsushiro Sea, Japan. *Marine Pollution Bulletin*, 149, 110539.

Meili, M. (1997). Mercury in lakes and rivers. *Metal Ions in Biological Systems*, 34, 21-51.

Millán, R., Gamarra, R., Schmid, T., Sierra, M. J., Quejido, A. J., Sánchez, D. M., Cardona, A.I., Fernández, M., & Vera, R. (2006). Mercury content in vegetation and soils of the Almadén mining area (Spain). *Science of the Total Environment*, 368(1), 79-87.

Minamata City. (2022). Minamata Disease -Its History and Lessons -2022, 66p.

Mitchell, C. P., Branfireun, B. A., & Kolka, R. K. (2008). Total mercury and methylmercury dynamics in upland–peatland watersheds during snowmelt. *Biogeochemistry*, 90, 225-241.

Miyamoto, Y. (2018). Environmental violence in Minamata: responsibility, resistance, and religiosity in the case of Ogata Masato and Hongan no Kai. *Religions*, 9(5), 166.

Molina, J. A., Oyarzun, R., Esbrí, J. M., & Higueras, P. (2006). Mercury accumulation in soils and plants in the Almadén mining district, Spain: one of the most contaminated sites on Earth. *Environmental Geochemistry and Health*, 28, 487-498.

Muhlendahl, K. (1990). Intoxication from mercury spilled on carpets. *The Lancet*, 336(8730-8731), 1578.

Munson, K. M., Lamborg, C. H., Boiteau, R. M., & Saito, M. A. (2018). Dynamic mercury methylation and demethylation in oligotrophic marine water. *Biogeosciences*, 15(21), 6451-6460.

Munthe, J., Bodaly, R. D., Branfireun, B. A., Driscoll, C. T., Gilmour, C. C., Harris, R. Horvat M., Lucotte M., & Malm O. (2007). Recovery of mercury-contaminated fisheries. *AMBIO: A Journal of the Human Environment*, 36(1), 33-44.

Nishimura H., & Okamoto T. (2001). Science of Minamata disease. Nippon Hyoron Sha, Tokyo (in Japanese).

Noguchi, F. (2017). Within and Beyond: Towards a praxis framework for socially-critical Education for Sustainable Development (ESD) in a community development context. Doctoral dissertation, RMIT University.

Nriagu, J. O. (1989). A global assessment of natural sources of atmospheric trace metals. *Nature*, 338, 47-49.

Nriagu, J. O. (1994). Mechanistic steps in the photoreduction of mercury in natural waters. *Science of the Total Environment*, 154(1), 1-8.

Nriagu, J., & Becker, C. (2003). Volcanic emissions of mercury to the atmosphere: global and regional inventories. *Science of the Total Environment*, 304(1-3), 3-12.

Obrist, D. (2007). Atmospheric mercury pollution due to losses of terrestrial carbon pools?. *Biogeochemistry*, 85, 119-123.

Padmavathiamma, P..K, & Li, L.Y. (2007). Phytoremediation technology: hyper-accumulation metals in plants. *Water, Air, & Soil Pollution*, 184(1-4), 105-26.

Pai, P., Niemi, D., & Powers, B. (2000). A North American inventory of anthropogenic mercury emissions. *Fuel Processing Technology*, 65, 101-115.

Pavithra, K. G., SundarRajan, P., Kumar, P. S., & Rangasamy, G. (2022). Mercury sources, contaminations, mercury cycle, detection and treatment techniques: A review. *Chemosphere*, 137314.

Pirrone, N., Keeler, G. J., & Nriagu, J. O. (1996). Regional differences in worldwide emissions of mercury to the atmosphere. *Atmospheric Environment*, 30(17), 2981-2987.

Pirrone, N., Costa, P., Pacyna, J. M., & Ferrara, R. (2001). Mercury emissions to the atmosphere from natural and anthropogenic sources in the Mediterranean region. *Atmospheric Environment*, 35(17), 2997-3006.

Pirrone, N., & Mahaffey, K. R. (2005). Dynamics of mercury pollution on regional and global scales: atmospheric processes and human exposures around the world. Springer Science & Business Media.

Premakumara, D. G. J., Yoshimura, T., & Clatterbuck, A. (2011). Local Governance and Environmental Sustainability in Minamata City: Beyond Deadlock and Conflict to Multi-Stakeholder Collaboration. *APSA congress 2011*, 1063-1074.

Pyle, D. M., & Mather, T. A. (2003). The importance of volcanic emissions for the global atmospheric mercury cycle. *Atmospheric Environment*, 37(36), 5115-5124.

Ravichandran, M. (2004). Interactions between mercury and dissolved organic matter—a review. *Chemosphere*, 55(3), 319-331.

Rifardi, Oki, K., & Tomiyasu, T. (1998). Sedimentary environments based on textures of surface sediments and sedimentation rates in the South Yatsushiro Kai (Sea), southwest Kyushu, Japan. *Journal of the Sedimentological Society of Japan*, 48, 67-84.

Ronchetti, R., Zuurbier, M., Jesenak, M., Koppe, J. G., Ahmed, U. F., Ceccatelli, S., & Villa, M. P. (2006). Children's health and mercury exposure. *Acta Paediatrica*, 95, 36-44.

Rytuba, J. J. (2003). Mercury from mineral deposits and potential environmental impact. *Environmental Geology*, 43, 326-338.

Sager, P. R., & Matheson, D. W. (1988). Mechanisms of neurotoxicity related to selective disruption of microtubules and intermediate filaments. *Toxicology*, 49(2-3), 479-492.

Saiz-Lopez, A., Sitkiewicz, S. P., Roca-Sanjuán, D., Oliva-Enrich, J. M., Dávalos, J. Z., Notario, R., Jiskra, M., Xu, Y., Wang, F., Thackray, C. P., Sunderland, E. M., Jacob, D. J., Travnikov, O., Cuevas, C. A., Acuña, A. U., Rivero, D., Plane, J. M. C., Kinnison, D. E. & Sonke, J. E. (2018). Photoreduction of gaseous oxidized mercury changes global atmospheric mercury speciation, transport and deposition. *Nature Communications*, 9(1), 4796.

Schroeder, W. H., & Munthe, J. (1998). Atmospheric mercury—an overview. *Atmospheric Environment*, 32(5), 809-822.

Seigneur, C., Vijayaraghavan, K., Lohman, K., Karamchandani, P., & Scott, C. (2004). Global source attribution for mercury deposition in the United States. *Environmental Science & Technology*, 38(2), 555-569.

Selin, N. E., Jacob, D. J., Park, R. J., Yantosca, R. M., Strode, S., Jaeglé, L., & Jaffe, D. (2007). Chemical cycling and deposition of atmospheric mercury: Global

constraints from observations. *Journal of Geophysical Research: Atmospheres*, 112, D02308.

Selin, N. E. (2009). Global biogeochemical cycling of mercury: a review. *Annual review of environment and resources*, 34, 43-63.

Shah, V., Jaeglé, L., Gratz, L., Ambrose, J., Jaffe, D., Selin, N., Song, S., Campos, T., Flocke, F.,Reeves, M., Stechman, D., Stell, M., Festa, J., Stutz, J., Weinheimer, A., Knapp, D.J.,Montzka, D.D., Tyndall, G., Apel, E.C., Hornbrook, R.S., Hills, A.J., Riemer, D.D., Blake,N., Cantrell, C.A., & Mauldin, R.L. (2016). Origin of oxidized mercury in the summertime free troposphere over the southeastern US. *Atmospheric Chemistry and Physics*, 16, 1511-1530.

Shi, J. B., Liang, L. N., Jiang, G. B., & Jin, X. L. (2005). The speciation and bioavailability of mercury in sediments of Haihe River, China. *Environment International*, 31(3), 357-365.

Skyllberg, U. L. F., Qian, J. I. N., Frech, W., Xia, K., & Bleam, W. F. (2003). Distribution of mercury, methyl mercury and organic sulphur species in soil, soil solution and stream of a boreal forest catchment. *Biogeochemistry*, 64, 53-76.

Slemr F., Brunke E.G., Ebinghaus R., & Kuss J. (2011). Worldwide trend of atmospheric mercury since 1995. *Atmospheric Chemistry and Physics*, 11(10), 4779-4787.

Smith-Downey, N. V., Sunderland, E. M., & Jacob, D. J. (2010). Anthropogenic impacts on global storage and emissions of mercury from terrestrial soils: Insights from a new global model. *Journal of Geophysical Research: Biogeosciences*, 115(G3).

Sommar J., Gardfeldt K., Stromberg D., & Feng X. (2001). A kinetic study of the gas-phase reaction between the hydroxyl radical and atomic mercury, *Atmospheric Environment*, 35, 3049-3054.

Sprovieri, F., Pirrone, N., Ebinghaus, R., Kock, H., & Dommergue, A. (2010). A review of worldwide atmospheric mercury measurements. *Atmospheric Chemistry and Physics*, 10(17), 8245-8265.

Stejskal, V. (2015). Allergy and autoimmunity caused by metals: a unifying concept. *Vaccines and Autoimmunity*, 57-64.

Streets, D. G., Zhang, Q., & Wu, Y. (2009). Projections of global mercury emissions in 2050. *Environmental Science & Technology*, 43(8), 2983-2988.

Tada, A., Yanase, N., Yano, S., Nakamura, T., Oshikawa, H., & Akagi, H. (2005). Seasonal behavior on tidal current by using in situ measurement data in the Minamata Bay. *Proceedings of hydraulic engineering*, 49, 1285-1290 (in Japanese).

Tai, A., & Yano, S. (2007). Numerical analysis of characteristics of tide and tidal current in the Yatsushiro Sea. *Proceedings of civil engineering in the ocean, Japan Society of Civil Engineers*, 23, 603-608 (in Japanese).

Tangahu, B.V., Sheikh Abdullah, S.R., Basri, H., Idris, M., Anuar, N., & Mukhlisin, M. (2011). A review on heavy metals (As, Pb, and Hg) uptake by plants through phytoremediation. *International Journal of Chemical Engineering*, 939161.

Todd, D. G., Wohlers, D., & Citra, M. (2003). Agency for Toxic Stubstances and Disease Registry: Toxicological Profile for Pyrethrins and Pyrethroids. Agency for Toxic Substances and Disease Registry: Atlanta, GA, USA.

Tomiyasu, T., Nagano, A., Yonehara, N., Sakamoto, H., Ōki, K., & Akagi, H. (2000). Mercury contamination in the Yatsushiro Sea, south-western Japan: spatial variations of mercury in sediment. *Science of the Total Environment*, 257(2-3), 121-132.

Tomiyasu, T., Takenaka, S., Noguchi, Y., Kodamatani, H., Matsuyamab, A., Oki, K., Kono, Y., Kanzaki, R., & Akagi, H. (2014). Estimation of the residual total mercury in marine sediments of Minamata Bay after a pollution prevention project. *Marine Chemistry*, 159, 19-24.

Tsuchiya, H., Mitani, K., Kodama, K., & Nakata, T. (1984). Placental transfer of heavy metals in normal pregnant Japanese women. *Archives of Environmental Health: An International Journal*, 39(1), 11-17.

Ullrich, S.M., Tanton, T.W., & Abdrashitova, S.A. (2001). Mercury in the aquatic environment: a review of factors affecting methylation. *Critical Reviews in Environmental Science and Technology*, 31(3), 241-293.

UNEP studies show rising mercury emissions in developing countries. (2013). Nairobi, Kenya: United Nations Environment Programme. Available from: https:// www.unenvironment.org/es/node/6317.

USEPA (1997). EPA Mercury Study Report to Congress. Washington (DC): Office of Air Quality and Standards and Office of Research and Development, U.S. Environmental Protection Agency. EPA-452/R-97-009.

Wang, Q., Kim, D., Dionysiou, D. D., Sorial, G. A., & Timberlake, D. (2004). Sources and remediation for mercury contamination in aquatic systems—a literature review. *Environmental pollution*, 131(2), 323-336.

Weiss-Penzias, P.S., Gustin, M.S., & Lyman, S.N. (2011). Sources of gaseous oxidized mercury and mercury dry deposition at two southeastern US sites. *Atmospheric Environment*, 45, 4569-4579.

Yano, S. (2013). In-situ measurement of mercury transport in the sea water of Minamata Bay. *Procedia Earth and Planetary Science*, 6, 448-456.

Yasuda, Y., & Mori, K. (2010). Mercury deposit distribution in Minamata Bay. *Coastal marine science*, 34(1), 223-229.

Yokoyama, H. (2018). Mercury pollution in Minamata. Springer Nature.

Yorifuji, T., Tsuda, T., Takao, S., & Harada, M. (2008). Long-term exposure to methylmercury and neurologic signs in Minamata and neighboring communities. *Epidemiology*, 19(1), 3-9.

Yorifuji, T., Tsuda, T., & Harada, M. (2013). Minamata disease: a challenge for democracy and justice. Late Lessons from Early Warnings: Science, Precaution, Innovation. Copenhagen, Denmark: European Environment Agency.

Zhang, L., Zhang, X. Q., & Sun, M. (2011). Study on the Characteristics of Adsorption and Enrichment of Mercury by the Mosses in Mining Districts in Wanshan Guizhou. *Environmental Science*, 32(6), 1734-1739.

Zhu, S., Zhang, Z., & Žagar, D. (2018). Mercury transport and fate models in aquatic systems: A review and synthesis. *Science of the Total Environment*, 639, 538-549.

Chapter 3

Numerical Modeling of Mercury Contaminated Sediment Transport in the Yatsushiro Sea Based on In-situ Measurement of Sediment Erosion

3.1 Introduction

Minamata Disease is a serious neurological disease caused by mercury poisoning. Mercury contaminated effluent discharged from the Minamata plants including Shin-Nippon Chisso Hiryo K.K. did harm to humans through the food chain (Ministry of the Environment, 2013). The Minamata Bay Pollution Prevention Project was carried out and initiated to dispose of sedimentary sludge containing over 25 ppm of total mercury (Minamata City, 2022). Meanwhile, mercury (Hg) was considered to be deposited in bed sediments in Minamata Bay but not transported to the Yatsushiro Sea (Kudo and Miyahara, 1984).

On the other hand, Tomiyasu et al. (2000) measured the total mercury concentration of sediments collected at 62 locations in the south of the Yatsushiro Sea. They suggested that the mercury had spread over a wide area of the Yatsushiro Sea. A study by Tomiyasu et al. (2014) has shown that the content of total mercury in sediments of undredged areas was still almost up to 10 ppm. The level was much higher than the background concentration in the natural environment (about 0.2 ppm). The concern about Hg in aquatic environments arises from its toxicity and the fact that it will threaten human health due to human consumption of primarily fish or fish predators due to bioaccumulation and biomagnification, particularly in the aquatic environment (Lavoie et al., 2013; Nakamura, 2014). Therefore, efficient remediation procedures must be implemented in substantially Hg-polluted aquatic systems to reduce Hg levels (Wang et al., 2004). The geographical and temporal distribution of Hg within aquatic systems should be characterized as completely as possible to evaluate the potential for bioaccumulation and appropriate remediation procedures adequately. Since field data are sometimes not abundant and sufficient for regional

and temporal extrapolation, mathematical models have become an important tool that may provide more information and improve the precision of the analysis (Knightes et al., 2009).

To research mercury transports and transformations in aquatic systems, a variety of models have been developed, ranging from simple mass balance models to complex biogeochemical models that account for hydrodynamics, water quality, and sediment transport as well as Hg biogeochemical processes (Zhu et al., 2018). Since mercury transport is a complicated process affected by many factors such as terrain, climate, seawater salinity, and electrical condition, a novel model with taking more experimental data into account is urgently required.

3.2 Establishment of Numerical Model

3.2.1 Calculation domain

The numerical model was established in Delft3D-Flow, which is a hydrodynamic model in a coastal region, to simulate mercury migration from Minamata Bay to the Yatsushiro Sea. In this model, the combination of the Yatsushiro Sea and the Ariake Sea was set as the calculation domain (**Fig. 3.1**).

The Ariake Sea and the Yatsushiro Sea are more closed than other sea areas, with large tidal water level differences, vast tidal flats and brackish waters, turbid sea water, high biodiversity, and rich biological productivity, forming a unique ecosystem.

The Ariake Sea is an inner bay that enters a stomach-shaped depth from the Amakusa Sea in western Kyushu. The sea area is about 1,700 square kilometers, surrounded by the four prefectures of Fukuoka, Saga, Nagasaki, and Kumamoto. In the Ariake Sea, the tidal range during spring tide is 3 to 4 m at the mouth of the bay, Hayasaki Seto, and exceeds 5 m at the inner part of the bay (Suminoe Port).

The Yatsushiro Sea, also known as the Shiranui Sea, is an inner bay that enters the northeast side of the Amakusa Sea. The sea area is about 1,200 square kilometers and is surrounded by Kumamoto Prefecture and Kagoshima Prefecture. The tidal range at the time of spring tide reaches approximately 4 m in Yatsushiro Port. Meanwhile, in the northern part of the Yatsushiro Sea (from the mouth of the Kuma River to the east coast in the bay), there is a vast tidal flat adjacent to the Ariake Sea.

The characteristics of the Ariake Sea and the Yatsushiro Sea are shown in **Table 3.1** (Ministry of the Environment, 2017).

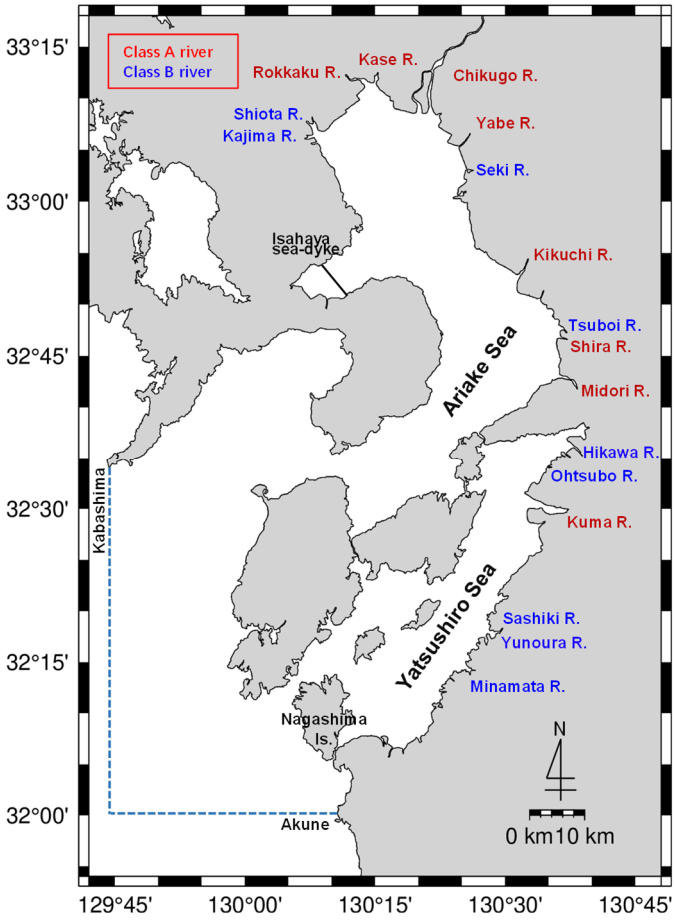

Figure 3.1 Calculation domain.

Table 3.1 The characteristics of the Ariake Sea and the Yatsushiro Sea (Ministry of the Environment, 2017).

Item	Ariake Sea	Yatsushiro Sea
Water area (km^2)	1,700	1,200
Volume (km^3)	34	22
Average water depth (m)	20	22
Tidal flat area (ha)	18,841	4,085
Segrass bed area (ha)	1,599	1,141
Average tide difference [Spring tide] (m)	5.4	3.7
Geographical enclosed index	12.9	32.5
Inflow of first-class rivers (10^6 m^3/year)	10,049	4,992
Basin area	8,420	3,409
Population in the basin(in thousands)	3,293	453

3.2.2 Calculation grid

The horizontal variable grid determined by Fathya et al. (2016) was used, where Minamata Bay and its adjacent area were with highest grid accuracy, equal to 62.5 m, and the other two grid accuracies were respectively 125 m and 250 m according to the distance from Minamata Bay. The vertical grid uses a σ-coordinate system, which is defined as five layers as well as each layer with 20%.

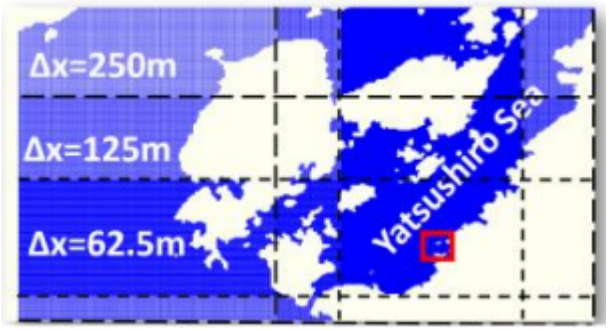

Figure 3.2 The horizontal variable grid (Fathya et al., 2016).

3.2.3 Governing equations

(1) Fundamental equations for pure 3D models

Motion equation (3D Reynolds-Averaged Navier-Stokes Equation)：

$$\frac{\partial U}{\partial t}+U\frac{\partial U}{\partial x}+V\frac{\partial U}{\partial y}+W\frac{\partial U}{\partial z}-fV=-\frac{1}{\rho}\frac{\partial p}{\partial x}+\frac{1}{\rho}\left(\frac{\partial}{\partial x}\tau_{xx}+\frac{\partial}{\partial y}\tau_{yx}+\frac{\partial}{\partial z}\tau_{zx}\right) \tag{3-1}$$

$$\frac{\partial V}{\partial t}+U\frac{\partial V}{\partial x}+V\frac{\partial V}{\partial y}+W\frac{\partial V}{\partial z}+fU=-\frac{1}{\rho}\frac{\partial p}{\partial y}+\frac{1}{\rho}\left(\frac{\partial}{\partial x}\tau_{xy}+\frac{\partial}{\partial y}\tau_{yy}+\frac{\partial}{\partial z}\tau_{zy}\right) \tag{3-2}$$

$$\frac{\partial W}{\partial t}+U\frac{\partial W}{\partial x}+V\frac{\partial W}{\partial y}+W\frac{\partial W}{\partial z}=-g-\frac{1}{\rho}\frac{\partial p}{\partial z}+\frac{1}{\rho}\left(\frac{\partial}{\partial x}\tau_{xz}+\frac{\partial}{\partial y}\tau_{yz}+\frac{\partial}{\partial z}\tau_{zz}\right) \tag{3-3}$$

Continuity equation：

$$\frac{\partial \rho}{\partial t}+\frac{\partial(\rho U)}{\partial x}+\frac{\partial(\rho V)}{\partial y}+\frac{\partial(\rho W)}{\partial z}=0 \tag{3-4}$$

State equation for density：

$$\rho=\rho(S,T) \tag{3-5}$$

where U denotes velocity in the x-direction (m/s), V is the velocity in the y-direction (m/s), W respects velocity in the z-direction (m/s), τ_{nx} is shear stress at the surface in the x-direction (kg/ms^2), τ_{ny} denotes shear stress at the surface in the y-direction (kg/ms^2), τ_{nz} is shear stress at the surface in the z-direction (kg/ms^2), f is Coriolis parameter (inertial frequency) (1/s), p respects hydrostatic water pressure (kg/ms^2), ρ is the density of water (kg/m^3), S is salinity (ppt), T respects temperature (°C), g denotes acceleration due to gravity (m/s^2), x,y,z is Cartesian coordinates (m), t is time (s).

(2) Equations for turbulence closure modeling

Assuming the x, y, and z directions as I, j=1, 2, and 3, respectively, and introducing the Boussinesq eddy viscosity assumption, the following equation holds:

$$\frac{\tau_{ij}}{\rho_0}=-\overline{u_i u_j}=\nu_t\left(\frac{\partial U_i}{\partial x_j}+\frac{\partial U_j}{\partial x_i}\right)-\frac{2}{3}k\delta_{ij} \tag{3-6}$$

where u_i is the velocity turbulence component, ν_t denotes eddy viscosity，k respects

turbulent energy (=1/2$\overline{u_i u_j}$)， δ_{ij} is Kronecker product (when $i = j$, δ_{ij} =1; when $i \neq j$, δ_{ij} =0)． k that appears in the case of $i = j$ acts as a normal stress, so it is included in the pressure and not explicitly considered, and is described only by the gradient diffusion type of the first term on the right side (Rodi, 1993). On the other hand, i in this paper, the spatial scales are different in the horizontal and vertical directions, and the turbulence in the vertical direction is damped due to density stratification. Therefore, if the eddy viscosity coefficients in the horizontal and vertical directions are ν_{tH} and ν_{tV}, respectively, the following equation is assumed to hold:

$$\frac{\tau_{xx}}{\rho_0} = 2\nu_{tH}\frac{\partial U}{\partial x}, \quad \frac{\tau_{yx}}{\rho_0} = \frac{\tau_{xy}}{\rho_0} = \nu_{tH}\left(\frac{\partial U}{\partial y} + \frac{\partial U}{\partial x}\right), \quad \frac{\tau_{yy}}{\rho_0} = 2\nu_{tH}\frac{\partial V}{\partial y} \tag{3-7}$$

$$\frac{\tau_{zx}}{\rho_0} = \nu_{tV}\frac{\partial U}{\partial z}, \quad \frac{\tau_{zy}}{\rho_0} = \nu_{tV}\frac{\partial V}{\partial z} \tag{3-8}$$

The SGS (Sub-Grid Scale) model was applied for the evaluation of the horizontal eddy dynamic viscosity coefficient ν_{tH}. In the SGS model, eddies larger than the computational grid interval (Grid Scale component) are directly calculated in LES (Large Eddy Simulation), eddies smaller than the computational grid interval (sub-grid scale components) are modeled by the Kolmogoroff similarity law of turbulent flow and reflected in the eddy dynamic viscosity coefficient.

The vertical coefficient ν_{tV} is described by the k-ε turbulence closure model as follows:

$$\frac{\partial k}{\partial t} + U_i\frac{\partial k}{\partial x_i} = \frac{\partial}{\partial x_i}\left(\frac{\nu_t}{\sigma_{tk}}\frac{\partial k}{\partial x_i}\right) + \nu_t\left(\frac{\partial U_i}{\partial x_j} + \frac{\partial U_j}{\partial x_i}\right)\frac{\partial U_i}{\partial x_j} - C_D\frac{k^{3/2}}{L} + \frac{\mathrm{g}}{\rho}\frac{\nu_t}{\sigma_{tp}}\frac{\partial \rho}{\partial x_3} \tag{3-9}$$

$$\frac{\partial \varepsilon}{\partial t} + U_i\frac{\partial \varepsilon}{\partial x_i} = \frac{\partial}{\partial x_i}\left(\frac{\nu_t}{\sigma_{t\varepsilon}}\frac{\partial \varepsilon}{\partial x_i}\right) + c_{1\varepsilon}\frac{\varepsilon}{k}\left\{\nu_t\left(\frac{\partial U_i}{\partial x_j} + \frac{\partial U_j}{\partial x_i}\right)\frac{\partial U_i}{\partial x_j} + \frac{\mathrm{g}}{\rho}\frac{\nu_t}{\sigma_{t\rho}}\frac{\partial \rho}{\partial x_3}(1 - c_{3\varepsilon})\right\} - c_{2\varepsilon}\frac{\varepsilon^2}{k} \tag{3-10}$$

where k denotes turbulent kinetic energy (m^2/s^2), C_D respects constant relating mixing length, L is mixing length (m), ε denotes dissipation in transport equation for turbulent kinetic energy (m^2/s^3), σ_{tp} is turbulent Prandtl/Schmidt number (= 0.7) and $c_{1\varepsilon}$, $c_{2\varepsilon}$, σ_{tk}, $\sigma_{t\varepsilon}$ are constants, the values are 1.44, 1.92, 1.0, 1.3, respectively. In addition, $c_{3\varepsilon}$ is equal to 1.0 when it is stable stratification, while $c_{3\varepsilon}$ is equal to 0.0 when it is unstable stratification.

3.2.4 Open boundary condition

Open boundaries are located on the line connecting Kabashima Suido and Akune (**Fig. 3.1**). According to the existing harmonic constants at both ends, only the main four tidal components (M2, S2, K1, O1) were tuned in amplitude and phase. Meanwhile, a total of 40 tidal components were obtained. The harmonic constants were calibrated from the result of the tide measured by Yano et al. (2010). The amplitudes and phases of the open boundary are shown in **Table 3.2.** The amplitudes and phases were linearly interpolated between the ends.

Table 3.2 The amplitudes and phases of the open boundary.

Location	Tidal components	Amplitude (m)	Phase (°)
Kabashima Suido	M_2	0.86	219
	S_2	0.36	240
	K_1	0.25	205
	O_1	0.19	186
Akune	M_2	0.72	211
	S_2	0.31	229
	K_1	0.23	209
	O_1	0.18	185

3.2.5 Freshwater inflows

Freshwater inputs were considered from eight Class A rivers (Chikugo River, Yabe River, Kase River, Rokkaku River, Kikuchi River, Shirakawa River, Midori River, Kuma River), nine large Class B rivers (Shiota River, Kashima River, Seki River, Tsuboi River, Hikawa River, Otsubo River, Sashiki River, Yunoura River, Minamata River), and the north and south drainage gates of the Isahaya Sea Dyke.

Hourly flow measurement data at observation stations obtained from the Hydrology and Water Quality Database of the Ministry of Land, Infrastructure, Transport and Tourism were used to calculate the flow of each Class A river. The calculation formula is as follows:

$$Q_{(A-class)} = Q_0 \times \frac{A_1}{A_0} \tag{3-11}$$

where $Q_{(A\text{-}class)}$ is the discharge of Class A rivers, Q_0 is the discharge from the observation stations, A_1 and A_0 are the catchment area of the entire rivers and the upstream catchment area of the observation stations, respectively. The calculation schematic diagram of river flow is shown in **Fig. 3.3**.

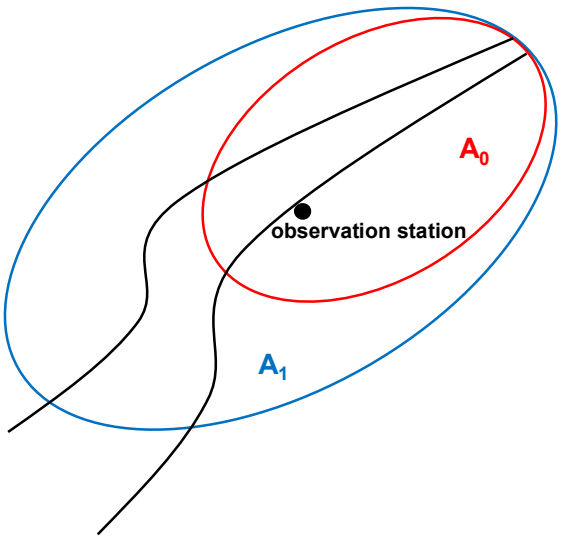

Figure 3.3 Schematic diagram of the calculation of river flow.

Discharge of each Class B river was estimated from a ratio of the river basin area in comparison with the neighboring Class A river by the following equation:

$$Q_{(B-class)} = Q_{(A-class)} \times \frac{A_2}{A_1} \quad (3\text{-}11)$$

where $Q_{(B\text{-}class)}$ is the discharge of Class B rivers, $Q_{(A\text{-}class)}$ is the discharge of Class A rivers, A_1 and A_2 are the catchment area of Class A rivers and Class B rivers, respectively.

The relevant data of Class A rivers and Class B rivers are shown in **Table 3.3** and **Table 3.4**.

Table 3.3 The relevant data of Class A rivers.

Name of Class A river	Total catchment area (km^2)	Observation station	Maximum flow (m^3/s)
Chikugo River	2, 863	Senoshita	3,319
Yabe River	647	Funagoya	2,752
Kase River	368	Ikemori Bridge	1,039
Rokkaku River	341	Myoken Bridge	1,094
Kikuchi River	996	Tamana	4,274
Shirakawa River	480	Yotsugi Bridge	1,761
Midori River	1,100	Jyona	2,686
Kuma River	1,880	Yokoishi	6,953

Table 3.4 The relevant data of Class B rivers.

Name of Class B river	Total catchment area (km^2)	Class A river used for estimation	Maximum flow (m^3/s)
Shiota River	60.4	Rokkaku River	194
Kashima River	125.7	Rokkaku River	403
Seki River	47.8	Yabe River	203
Tsuboi River	141.7	Shirakawa River	520
Hikawa River	148.6	Kuma River	550
Otsubo River	34.6	Kuma River	128
Sashiki River	67	Kuma River	248
Yunoura River	42.5	Kuma River	157
Minamata River	132.5	Kuma River	490

3.2.6 Initial conditions

Based on the previous study, mercury was considered only from Minamata Bay. And it was assumed that mercury adheres to the surface of soil particles in the sediments and is transported by the tidal current in the process of being rolled up and resuspended (Yano et al., 2014). Therefore, initial sediment distribution assumed there was one-meter-thick sediment only inside Minamata Bay while no sediments in other areas (**Fig. 3.4**). This means the sediments, which were in Minamata Bay initially, were contaminated by mercury when high mercury pollution occurred only in Minamata Bay area in the era of Minamata Disease.

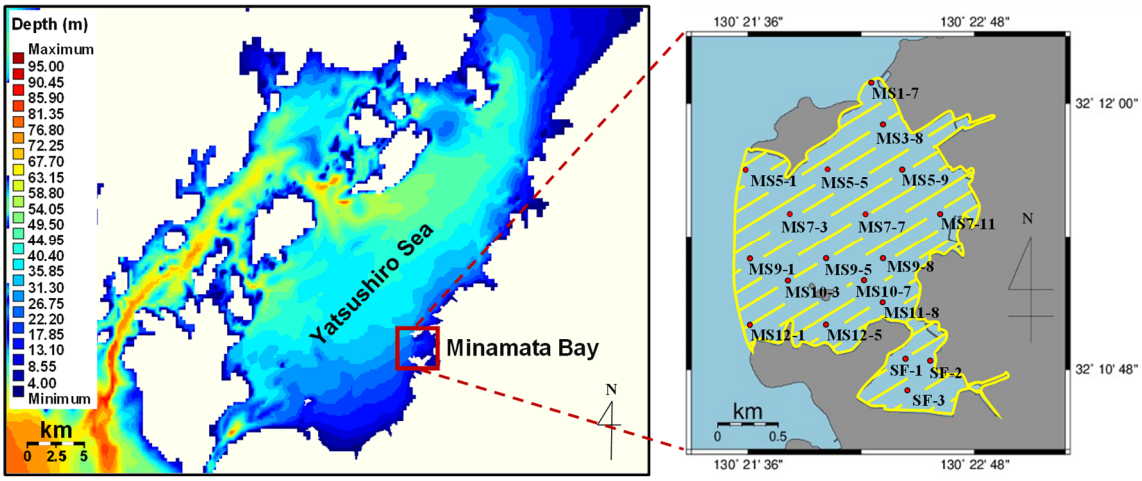

Figure 3.4 Bathymetry distribution, initial sediment distribution assuming there is 1 m thick sediment in Minamata Bay (inside from dot line) and measurement sites in **Table 3.5**.

3.2.7 Application of in-situ measurement result

Instead of the traditional presumed constant, the result of *in-situ* measurement proposed by Yano et al. (2020) was used for the critical shear stress and erosion rate parameters, which were coupled with the internal diffusion technique and then applied in the model.

The critical shear stresses τ_{cr}, erosion rate parameters M, and D_{50} were respectively measured at 19 different positions by using a new *in-situ* measurement device (Yano et al., 2020). Those values are shown in **Table 3.5**.

Table 3.5 *In-situ* measurement results in Minamata Bay after the correction (Yano et al., 2020).

Location	τ_{cr} (Pa)	M (kg/m^2/s)	D_{50} (μm)
MS1-7	5.25×10^{-2}	5.00×10^{-4}	eliminated
MS3-8	1.03×10^{-2}	5.00×10^{-4}	19.68
MS5-1	5.16×10^{-3}	2.03×10^{-4}	50.35
MS5-5	3.29×10^{-3}	2.31×10^{-4}	27.88
MS5-9	4.13×10^{-3}	5.00×10^{-4}	26.44
MS7-3	4.70×10^{-4}	8.70×10^{-5}	17.59
MS7-7	4.61×10^{-3}	3.69×10^{-4}	24.57
MS7-11	5.61×10^{-3}	2.00×10^{-4}	25.91
MS9-1	5.70×10^{-3}	5.00×10^{-4}	17.64
MS9-5	5.56×10^{-3}	5.00×10^{-4}	19.20
MS9-8	9.72×10^{-3}	5.00×10^{-4}	23.17
MS10-3	6.27×10^{-4}	5.00×10^{-4}	15.68
MS10-7	5.61×10^{-3}	5.00×10^{-4}	19.99
MS11-8	3.47×10^{-2}	5.00×10^{-4}	22.39
MS12-1	2.58×10^{-3}	3.39×10^{-4}	19.18
MS12-5	7.71×10^{-4}	8.10×10^{-5}	22.94
SF-1	2.73×10^{-3}	5.00×10^{-4}	26.93
SF-2	7.17×10^{-3}	5.00×10^{-4}	23.16
SF-3	4.84×10^{-2}	5.00×10^{-4}	21.68

It should be noted that M was assumed to be 0.0005 kg/m^2/s for stations where the measured ones exceeded 0.0005 kg/m^2/s due to numerical instability in the established model. The horizontal distributions of critical shear stresses and erosion rate parameters (**Fig. 3.5** and **Fig. 3.6**) were obtained by coupling the values with the internal diffusion process for interpolation and extrapolation in the model. The

critical shear stress is primarily determined by flow velocity, which results in unobvious changes in its grid distribution after internal diffusion due to the similar small flow velocity around Minamata Bay. While it is the opposite for the grid distribution of erosion rate parameters after internal diffusion, indicating the erosion rate parameters are significantly affected by measurement position.

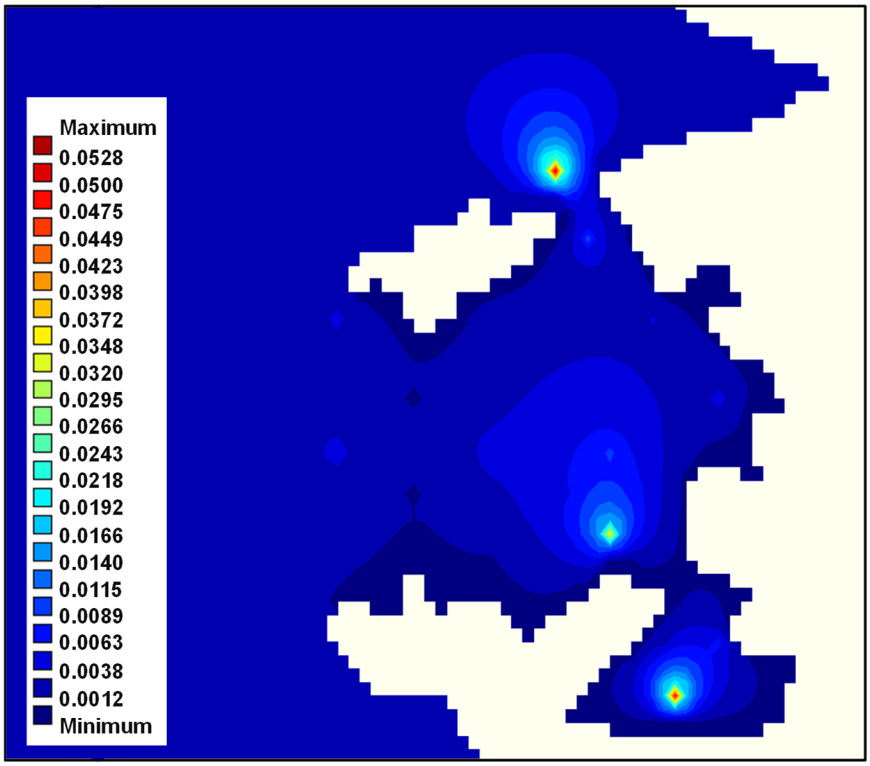

Figure 3.5 Horizontal distribution of the critical shear stress after internal diffusion around Minamata Bay.

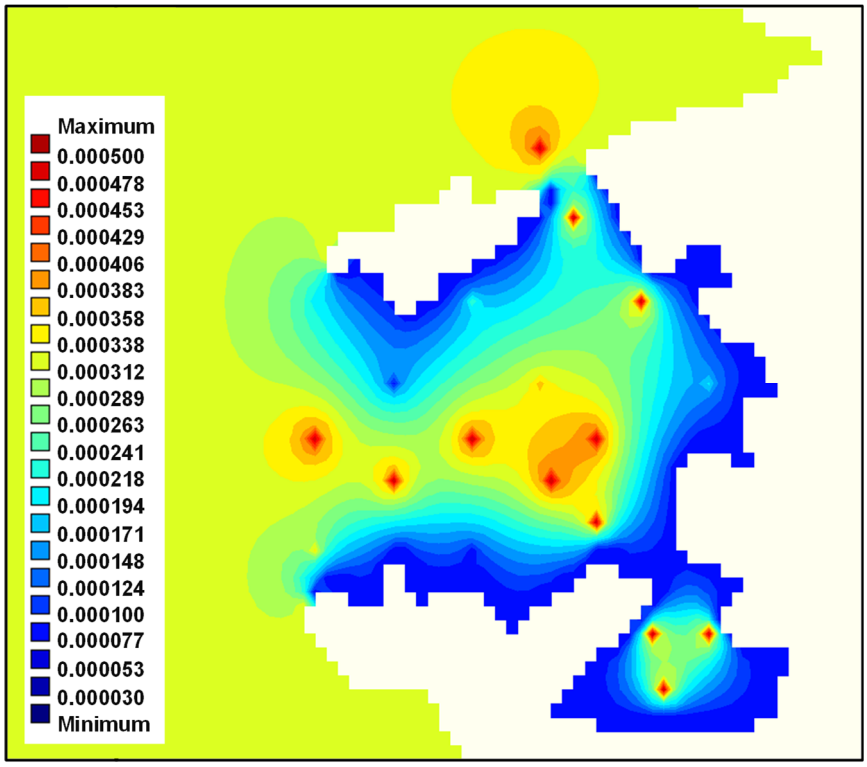

Figure 3.6 Horizontal distribution of the erosion rate parameters after internal diffusion around Minamata Bay.

The sedimentation rate of suspended particles dependent on the median grain size of the sediment can be calculated according to the formula proposed by Rubey as follows:

$$\frac{w_0}{\sqrt{(\sigma_s - 1)gD}} = \sqrt{\frac{2}{3} + \frac{36}{d_*}} - \sqrt{\frac{36}{d_*}} \tag{3-12}$$

$$d_* = \frac{(\sigma_s - 1)gD^3}{\nu^2} \tag{3-13}$$

where w_0 is the sedimentation velocity (cm/s); σ_s respects particle density equal to 2.65 g/cm^3; D denotes the average median grain size (cm); g is gravity acceleration which is 981.0 cm/s^2, and ν is the kinematic viscosity coefficient calculated as 0.01 cm^2/s.

D is calculated by taking the average of each point's median grain size except for MS1-7 (**Table 3.5**). The sediment at MS1-7 is considered as sandy soil, and its grain size is around 20 times larger than that of other points because the location of MS1-7 is close to the entrance of the north bay, and the waves are relatively strong as well. It greatly affects the

estimation of the total median grain size of 19 measurement points. Therefore, D_{50} measured at MS1-7 was ignored in the model.

3.3 Results and Discussions

3.3.1 Model validation

Fig. 3.7 shows that the mercury-containing sediment transport was mainly divided into two patterns, that is, southwest migration and northeast one. The migration to the southwest has reached the sea region around Nagashima Island and continued to spread widely with a greater amount of deposition. The migration to the northeast has reached the sea region around Amakusa. It agreed with the measured total mercury concentration distribution of surface sediment shown in **Fig. 3.8** (Matsunoshita et al., 2018). While the migration to the northeast is dispersed, the amount of diffusion is relatively tiny. Although diffusion occurs in both the northeast and southwest directions, there are significant variances in the degree of diffusion. The diffusion to the northeast is wider, but the volume of sediment deposition is smaller, while the diffusion to the southwest is more concentrated, and the volume of sediment deposition is larger. The difference in the extent and amount of diffusion to the northwest and southeast is also consistent with the result in **Fig. 3.8**. Meanwhile, the northeast direction is greatly affected by the baroclinic flow, which is unstable. It may be the reason for the deviation of the measurement and simulation results in the northeast direction. Furthermore, it could be found that the diffusion near Minamata Bay is more prominent. It is easy to form an arc-shaped sedimentary accumulation phenomenon surrounding the bay. This phenomenon of simulation also agreed fairly well with the measured one. And compared with previous research results (Matsunoshita et al., 2018), this model reflects more prominently in terms of details. Thus, the simulation results indicate the applicability of the model.

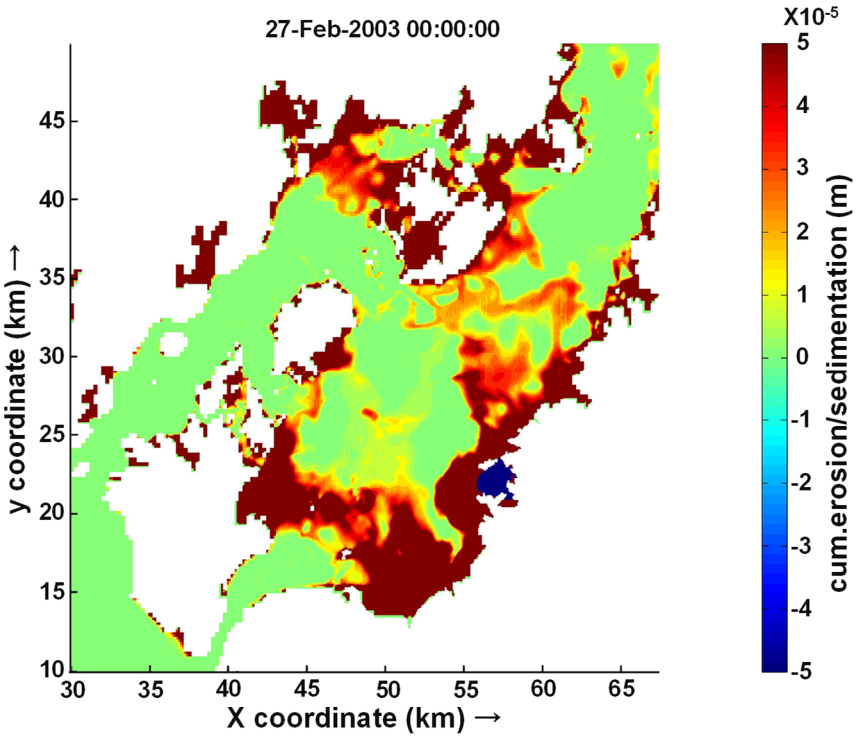

Figure 3.7 Distribution of cumulative deposition/erosion thickness.

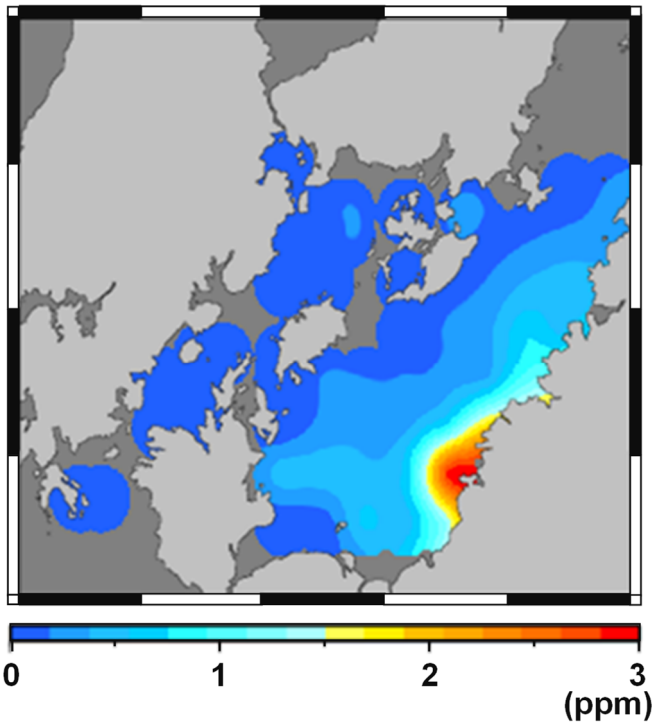

Figure 3.8 T-Hg concentration distribution of surface sediment from in-situ measurement (Matsunoshita et al., 2018).

3.3.2 Temporary sediment migration in the Yatsushiro Sea

Fig. 3.9 describes the distribution changes of cumulative deposition and erosion thickness with time. During the first three months, mercury migration was shifting on the whole bay scale, while mercury gradually deposited to the southwest Yatsushiro Sea and the area near the coastline. Since then, the deposition scope of sediments in the area of the Yatsushiro Sea was slowly reduced. After eight months, the mercury migration did not show significant changes except for the transport around the southwest and northeast Yatsushiro Sea which was close to Minamata Bay.

Initially, the mercury-containing sediments from Minamata Bay were considered to transport to the Yatsushiro Sea on the whole scale due to the residual currents by the freshwater inflow from the rivers. In the process of sediment migration, the deposition happened when the sediments reached the coast because of insurmountable geographical obstacles. Also, the effect of tides plays an important role in the migration from Minamata Bay to the Yatsushiro Sea. After a certain time, the mercury-containing sediments were mainly regarded to deposit along the coastline.

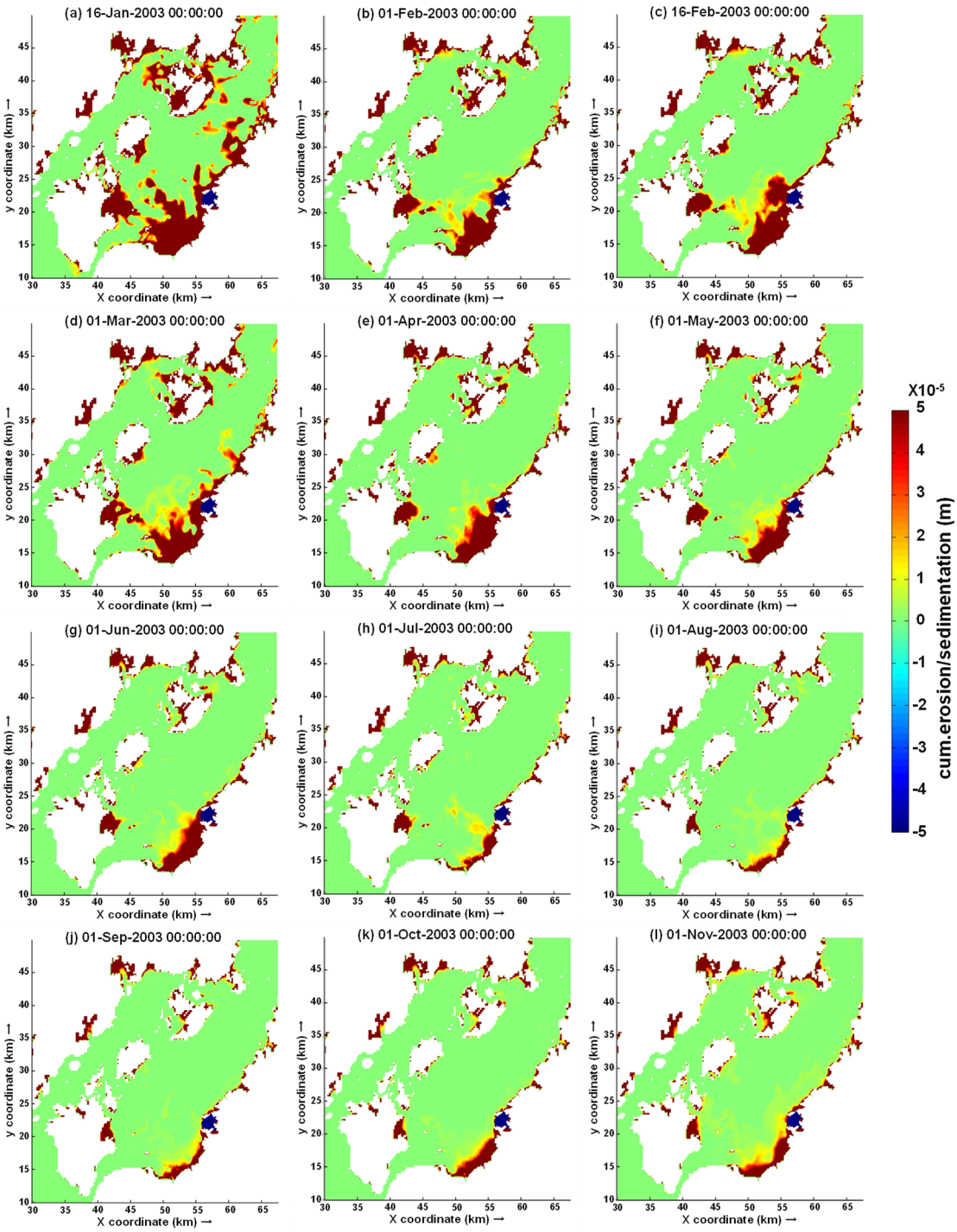

Figure 3.9 Distribution of cumulative deposition/erosion thickness in (a)0.5, (b)1, (c)1.5, (d)2, (e)3, (f)4, (g)5, (h)6, (i)7, (j)8, (k)9 and (l)10 months after the initial condition, respectively.

3.3.3 Analysis of sediments deposition at observation points

The locations of observation points are shown in **Fig. 3.10**, including three positions along the coastline as well as six positions in the sea. The cumulative depositions at the observation points in the areas along the coastline are shown in **Fig. 3.11**. Deposition in the sea area near the coast increased rapidly at the start of the simulation, then steadily slowed as the accumulation efficiency decreased, eventually reaching equilibrium after eight months. Furthermore, the amount of deposition in the sea region near the coast in the northeast direction was greater than the amount in the southwest direction. C1 and C2 were near the shoreline, so sediments could be trapped more easily than C6 in the main body of the Yatsushiro Sea, as shown in **Fig. 3.12.** In addition, mercury distribution (**Fig. 3.8**) has a low resolution with limited measurement sites. Therefore, this result is also compatible with the measured result in **Fig. 3.8**.

As shown in **Fig. 3.12**, the deposition in the middle of the Yatsushiro Sea was rather substantial at the start of the simulation and fluctuated periodically. Then the deposition gradually declined over time and was eventually maintained at a low level. The highest deposition volume in the area can reach around 0.002 m, whereas the maximum deposition volume in the sea area near the coast is about 0.26 m, shown in **Fig. 3.11**. The deposition volume in the area was still quite tiny when compared to the area near the shore. Furthermore, the deposition volume in the southern Yatsushiro Sea region is clearly greater than that in the northern area.

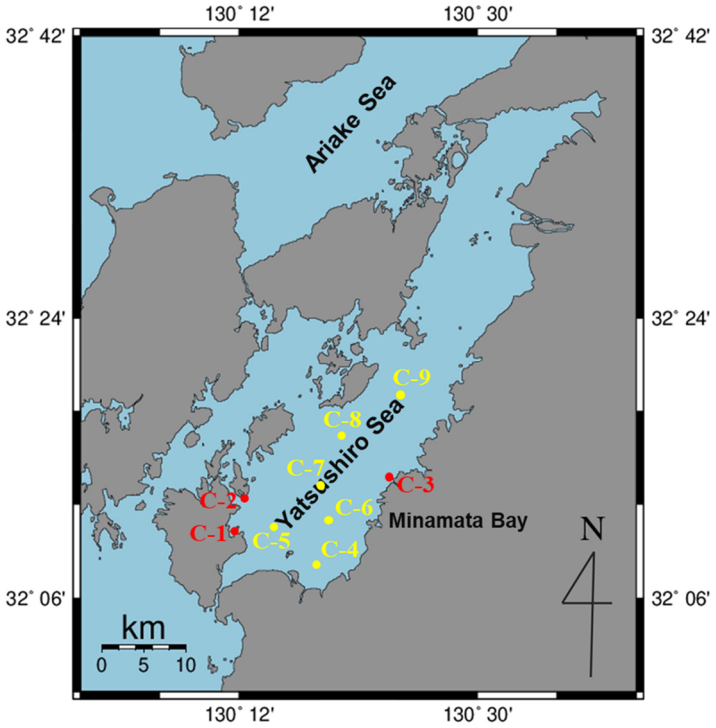

Figure 3.10 The location of observation points.

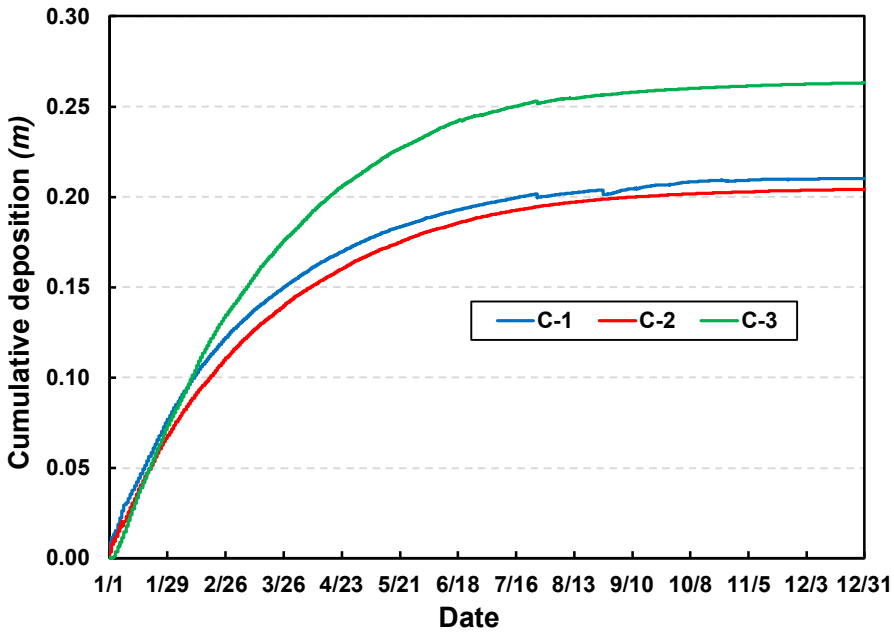

Figure 3.11 Cumulative deposition of the observation points along the coastline of the Yatsushiro Sea.

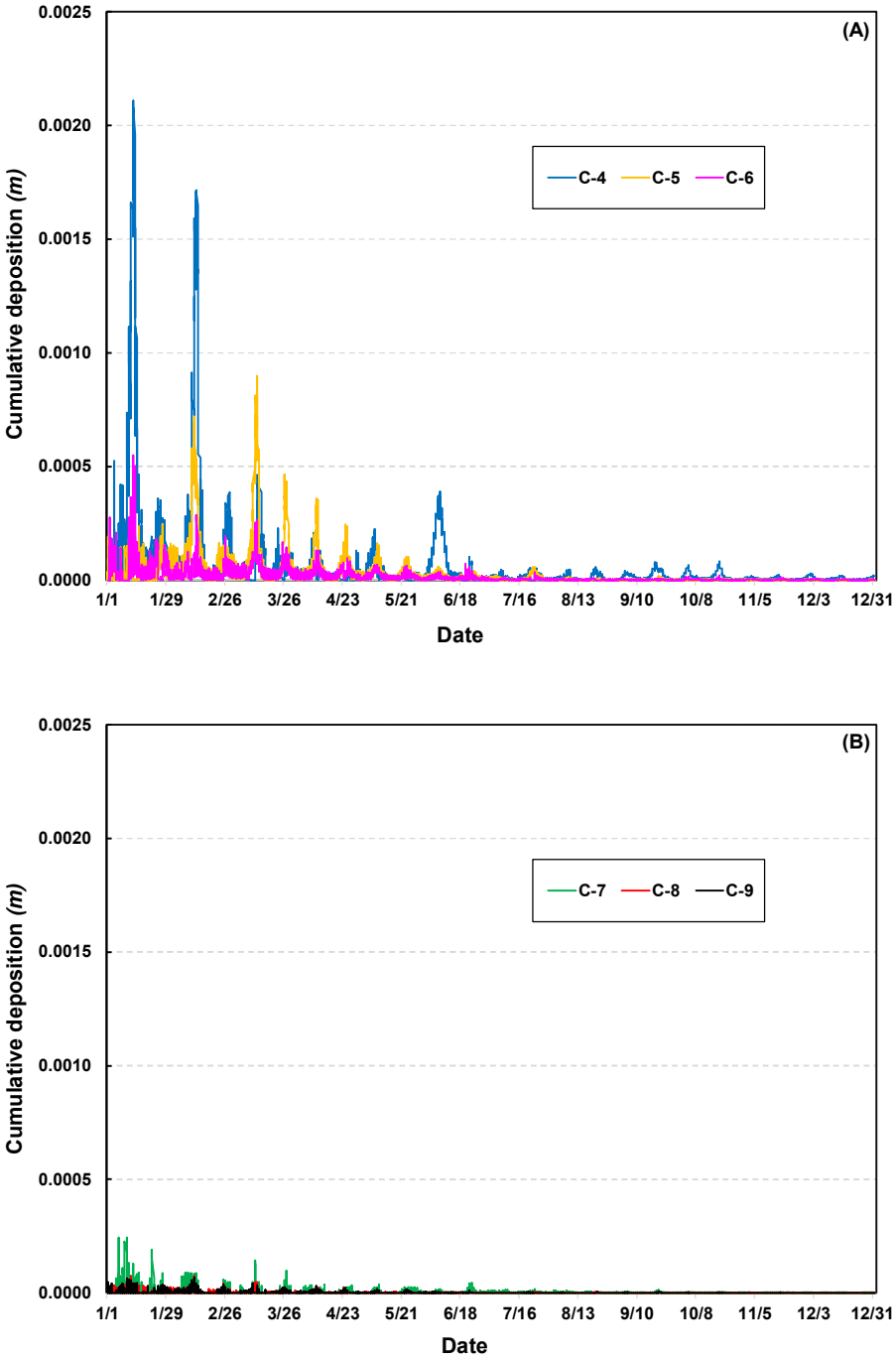

Figure 3.12 Cumulative deposition of the observation points in the middle of the Yatsushiro Sea.

3.4 Conclusions

In this study, a numerical model to simulate the transport of bottom sediments from Minamata Bay to the Yatsushiro Sea was established in Delft3D based on *in-situ* measurement results adapting internal diffusion. According to the simulation results, we can conclude the following conclusions:

1. The sediments transported from Minamata Bay to the Yatsushiro Sea significantly. The sediment migration was pre-dominantly divided into two patterns, which are southwest migration and northeast migration, as same as the mercury migrated primarily from *in-situ* measurements. The results of simulation and measurement are nearly identical.

2. Mercury-containing sediments migrated from Minamata Bay to the seas around Minamata Bay and gradually spread to the entire Yatsushiro Sea. The migration is not a static process. The sediments were mainly deposited in the coastal seas of the southwest and northeast Yatsushiro Sea and the seas surrounding Nagashima Island and Amakusa over time.

3. The mercury-containing sediments trended to deposit along the seacoast, which was mainly considered due to the terrain effect. In addition, the deposition gradually declined over time and finally stabilized at a low level in the middle of the Yatsushiro Sea.

References

Fathya, E.N., Yano, S., Matsuyama, A., Tada, A. & Riogilang, H. (2016). Impact of reclamation project on mercury contaminated sediment transport from Minamata Bay into the Yatsushiro Sea. *Journal of Japan Society of Civil Engineers, Ser. B2 (Coastal Engineering)*, 72(2), I_1285-I_1290.

Kudo, A., & Miyahara, S. (1984). Mercury dispersion from Minamata Bay to the Yatsushiro Sea during 1975–1980. *Ecotoxicology and environmental safety*, 8(6), 507-510.

Knightes, C. D., Sunderland, E. M., Barber, M. C., Johnston, J. M., & Ambrose Jr, R. B. (2009). Application of ecosystem‐scale fate and bioaccumulation models to predict fish mercury response times to changes in atmospheric deposition. *Environmental Toxicology and Chemistry*, 28(4), 881-893.

Lavoie, R. A., Jardine, T. D., Chumchal, M. M., Kidd, K. A., & Campbell, L. M. (2013). Biomagnification of mercury in aquatic food webs: a worldwide meta-analysis. *Environmental Science & Technology*, 47(23), 13385-13394.

Matsunoshita, K., Yano, S., Matsuyama, A., Kitaoka, T. & Tada, A. (2018). Analysis on dispersion of mercury in bottom sediments in Minamata Bay by long-term numerical simulation of sediment transport using particle size classification model. *Journal of Japan Society of Civil Engineers, Ser. B2 (Coastal Engineering)*, 74(2), I_1153-I_1158 (in Japanese).

Minamata City. (2022). Minamata Disease -Its History and Lessons-2022, 66p.

Ministry of the Environment, Japan. (2013). Lessons from Minamata Disease and Mercury Management in Japan, 58p.

Ministry of the Environment, Japan. (2017). Report of the Ariake Sea and Yatsushiro Sea Comprehensive Survey and Evaluation Committee (in Japanese).

Nakamura, M., Hachiya, N., Murata, K. Y., Nakanishi, I., Kondo, T., Yasutake, A., Miyamoto, K., Ser, P. H., Omi, S., Furusawa, H., Watanabe, C., Usuki, F. &

Sakamoto, M. (2014). Methylmercury exposure and neurological outcomes in Taiji residents accustomed to consuming whale meat. *Environment International*, 68, 25-32.

Rodi, W. (1993). On the simulation of turbulent flow past bluff bodies. *Journal of Wind Engineering and Industrial Aerodynamics*, 46, 3-19.

Tomiyasu, T., Nagano, A., Yonehara, N., Sakamoto, H., Ōki, K., & Akagi, H. (2000). Mercury contamination in the Yatsushiro Sea, south-western Japan: spatial variations of mercury in sediment. *Science of the Total Environment*, 257(2-3), 121-132.

Tomiyasu, T., Takenaka, S., Noguchi, Y., Kodamatani, H., Matsuyamab, A., Oki, K., Kono, Y., Kanzaki, R. & Akagi, H. (2014). Estimation of the residual total mercury in marine sediments of Minamata Bay after a pollution prevention project. *Marine Chemistry*, 159, 19-24.

Wang, Q., Kim, D., Dionysiou, D. D., Sorial, G. A., & Timberlake, D. (2004). Sources and remediation for mercury contamination in aquatic systems—a literature review. *Environmental pollution*, 131(2), 323-336.

Yano, S., Winterwerp, J. C., Tai, A., & Saita, T. (2010). Numerical experiments on features of nonlinear tide and its influences on sediment transport in the Ariake Sea and the Yatsushiro Sea. *Journal of Japan Society of Civil Engineers, Ser. B2 (Coastal Engineering)*, 66(1), 341-345 (in Japanese).

Yano, S., Kawase, H., Hisano, A. Riogilang, H., Matsuyama, A., & Tada, A. (2014). Examination on the Relationship between Bottom Sediment Transport and Baroclinic Structure by Numerical Model in Minamata Bay. *Journal of Japan Society of Civil Engineers, Ser. B2 (Coastal Engineering)*, 70(2), I_461-I_420 (in Japanese).

Yano, S., Abe, T., Matsuyama, A. & Ide, T. (2020). Development of in-situ measurement device for model parameters of mud resuspension on seabed. *Journal of Japan Society of Civil Engineers, Ser. B3 (Ocean Engineering)*, 76(2), I_798-I_803.

Zhu, S., Zhang, Z., & Žagar, D. (2018). Mercury transport and fate models in aquatic systems: A review and synthesis. *Science of the Total Environment*, 639, 538-549.

Chapter 4
A Novel Particle Size Classification-based Method for Analyzing T-Hg Concentration Distribution of Sediment in the Yatsushiro Sea

4.1 Introduction

From 1932, effluent containing methylmercury, produced in the acetaldehyde manufacturing process of the Chisso Minamata factory, was discharged into Minamata Bay (Minamata City, 2022). In 1956, the first well-documented case of Minamata disease occurred and was reported (Hachiya, 2006). In 1968, the company stopped producing acetaldehyde and producing vinyl chloride, representing the end of acetylene mercury discharge (Kumamoto Prefecture, 1998). From 1977 to 1990, 1.5 million m^3 of bottom sediments with the mercury concentration above 25 ppm was removed. Then, the sediments were reclaimed to 58 ha of land (sealed filling) (Ministry of the Environment, 2013). After dredging, the average total mercury (T-Hg) concentration in the sediments was still up to 2.3 mg/kg dry weight (Matsuyama et al., 2014). Moreover, the study by Yano et al. (2013) has shown that the mercury from Minamata Bay has been gradually dispersed into the Yatsushiro Sea by ocean currents.

In the previous study, Matsunoshita et al. (2018) studied the migration of sediment from Minamata Bay using a computer simulation with a three-dimensional topographical model of the Yatsushiro Sea and basic monitoring data for sea currents. In addition, Matsuyama et al. (2019) measured the plane distribution of sediments with a T-Hg concentration of > 0.5 mg/kg dry weight in the Yatsushiro Sea. By comparing the results of the two studies, it can be seen that there is a good correlation between the deposition of sediment particles in the Yatsushiro Sea by simulation and the measured T-Hg concentration of > 0.5 mg/kg dry weight for sediments in the horizontal direction. It suggests that the mercury migrated from Minamata Bay to the Yatsushiro Sea with the movement of sediment particles in seawater.

Mercury was considered to adsorb on sediment particles and realized the transport. Therefore, the particle size of the sediment may affect the mercury content in the sediments and the migration of mercury with the sediments. However, the influence of particle size as a crucial factor is barely considered in previous studies. Therefore, we aim to develop a novel method based on particle size classification to comprehend the horizontal and vertical distribution of the T-Hg concentration in sediment fractions in the Yatsushiro Sea.

4.2 Experimental Method

4.2.1 Collection and pre-processing for sediment samples

The sediment samples used in our experiments were collected from the Yatsushiro Sea along two sampling lines A and B using a gravity core sampler. The location of the sediment sampling points is shown in **Fig. 4.1**. The core sediment samples were cut into 1 cm sections from top to bottom, which were then kept in an ultra-low freezer (lower than −80 °C) for storage. Two 1 cm sediment sections (equal to 2 cm thick) were combined to create a suitable sample volume in order to investigate changes in the sediments in the vertical direction accurately.

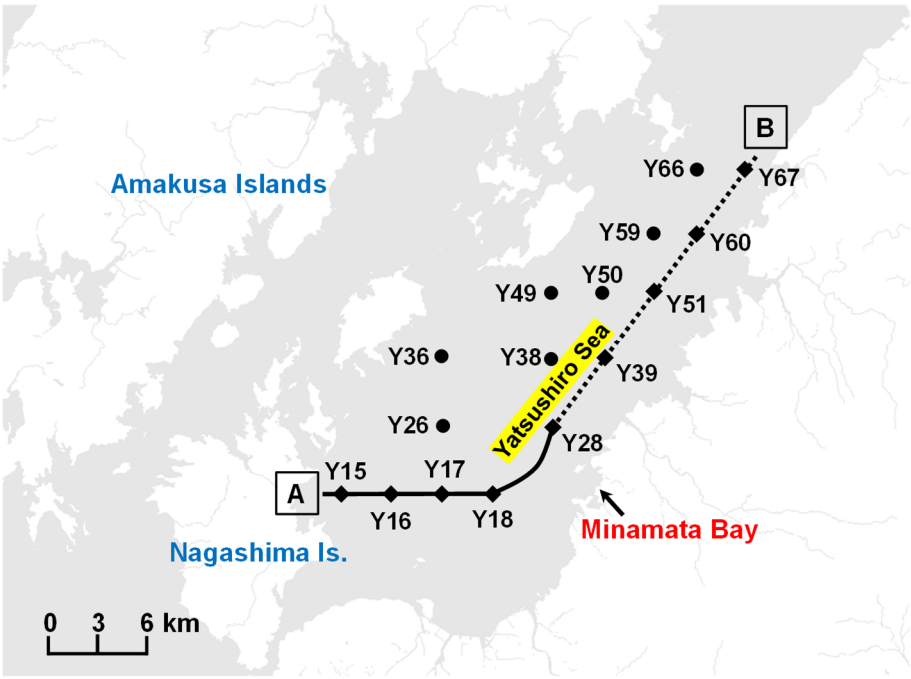

Figure 4.1 Locations for collection of core sediment samples (Diamond-shaped marks denoting the sampling points for classification experiments; solid dots respecting the sampling points used for the background T-Hg concentration determination).

4.2.2 Particle size classification

Organic compounds, adsorbed on the particles, are often removed by chemical method firstly in order to classify sediment particles accurately and effectively (Yoshinaga et al., 1984). However, mercury that has been adsorbed on the organic molecules is also removed in this process. Therefore, the procedure of removing organic compounds was not carried out for remaining the mercury adsorbed on sediment particles. To facilitate this classification, the published settling method was selected (Japanese Standards Association, 2016), where a suitable dispersion and sedimentation time for the sediment particles in the dispersion solvent was needed. In addition, turbidimetric analysis of sulfate ions (SO_4^{2-}) using an established method [EPA 375.4] (EPA, 1978) was used, which provided suitable dispersion conditions for the sediment particles as well. Moreover, when performing the classification process, to reduce the absorption of sediment particles and organic material to the inner wall as much as possible, the material and quality of the dispersion tube were considered.

Specific operations (**Fig. 4.2**) are as follows: On a hot plate heated to 110°C, heat-shrink tubing (50 cm) was slowly rolled to form a tube with a diameter of 14 mm. One end of the tube was plugged with a rubber stopper. The prepared sediment sample was put in the tube. Thereafter, the dispersion solvent (glycerin/ethanol, 1:2 v/v) was poured into the tube until the liquid level was 10 cm near the tube top, meaning that the height of the liquid level from the tube bottom was 40 mm. After the addition of the dispersion solvent to the tube, the other top of the tube was also plugged with a rubber stopper. By handshaking for one minute, the sediments and dispersion solvent were mixed thoroughly in the tube. The well-mixed sample was allowed to rest in a refrigerator (4°C) for two weeks (**Fig. 4.3**). The last step was freezing the sample with liquid nitrogen (**Fig. 4.4**) and cutting it into 5 mm sections, where the particle-classified sample was obtained.

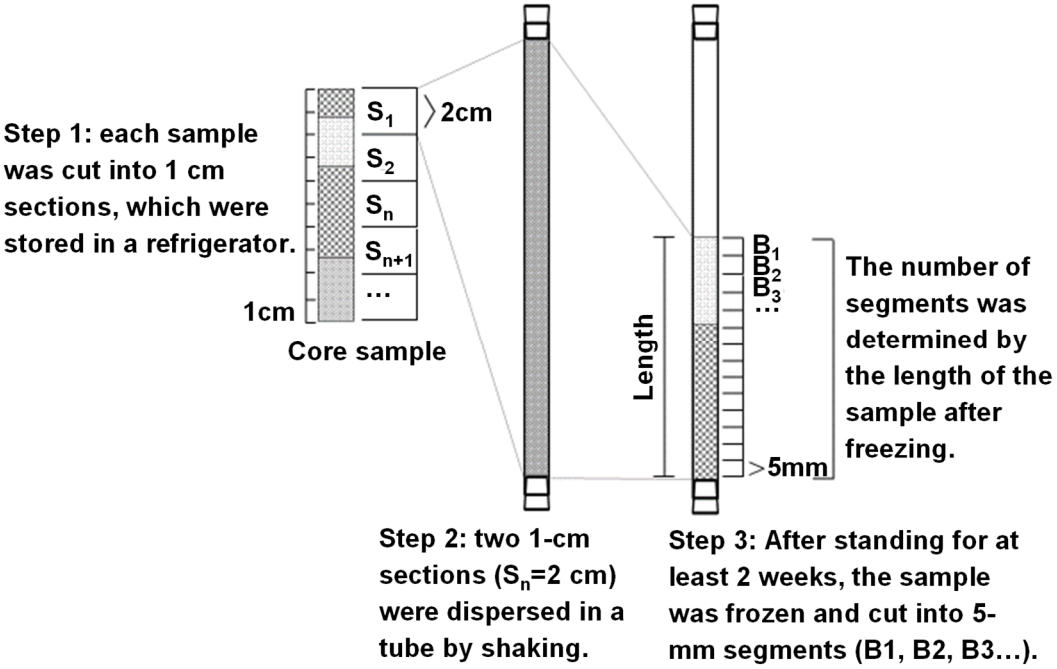

Figure 4.2 Classification process for the sediment samples.

Figure 4.3 The sample was placed in a refrigerator (4°C) for two weeks.

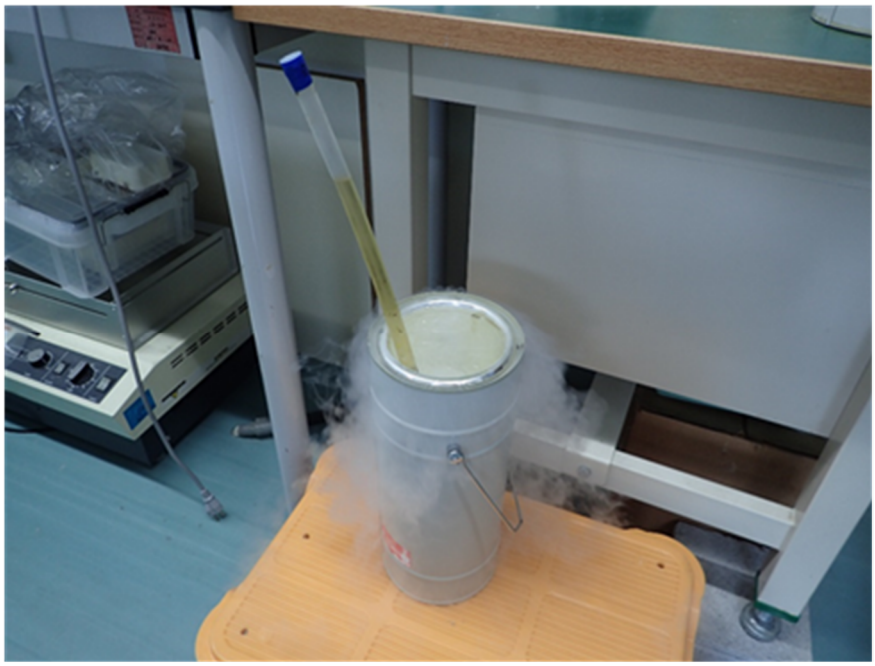

Figure 4.4 The sample was frozen with liquid nitrogen.

4.2.3 Analysis of particle size

Prior to measuring the particle size, water should be taken out of the sediment samples. After being defrosted at room temperature, the frozen sediment samples from the ultra-low-temperature freezer (−80 °C) were dried by a circulation dryer (105 °C, overnight). The sediments were mixed after drying, and any impurities were manually taken out. Then, the particle size analysis of the sediments was performed on the samples using a laser diffraction particle size analyzer (SALD-3100, Shimadzu Corporation, Kyoto, Japan) (**Fig. 4.5**). The following equation was used to calculate the abundance ratio of each particle size in the sediment:

$$\text{Abundance ratio (\%)} = B/A \times 100 \quad (4\text{-}1)$$

where B is the number of sections of the sediment sample for the particle size, and A is the total number of sections of the sediment sample.

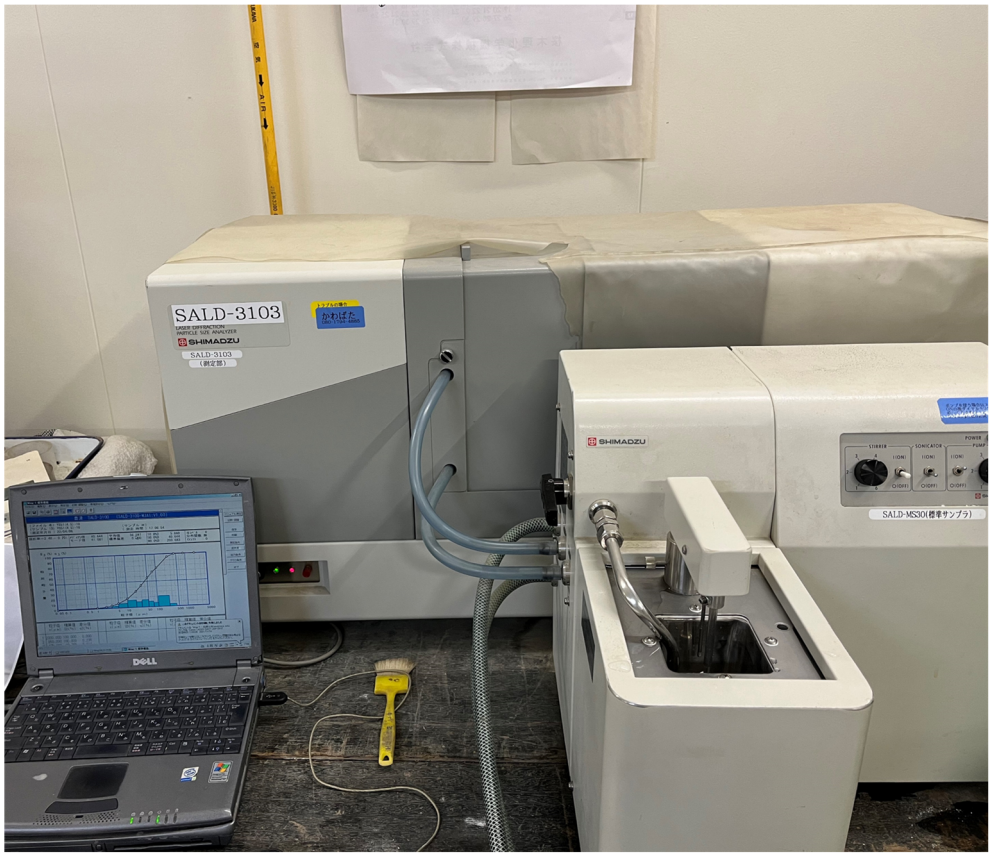

Figure 4.5 The laser diffraction particle size analyzer.

4.2.4 Analysis of the total mercury (T-Hg) concentration

The T-Hg concentration of each classified particle size section was measured according to the method developed by Akagi and Nishimura (1991) and improved by Akagi et al. (1995). The accuracy and precision of this method have been repeatedly verified in interlaboratory calibrations (Malm et al., 1995) and through the analysis of the IAEA-158 reference standards (Campbell et al., 2008). Based on six repeat measurements, the average T-Hg concentration of the reference material was 0.136 ± 0.060 mg/kg dry weight, consistent with the reference material's certified value of 0.132 ± 0.014 mg/kg dry weight. The sediments were mixed by hand after removing any impurities in the sample. Each sample of the sediments (<0.5 g) was put in a 50 mL volumetric flask together with 1 mL of distilled water, 2 mL of nitric acid/perchloric acid (1:1 v/v), and 5 mL of concentrated sulfuric acid. The volumetric flask was heated for 20 minutes at a temperature of over 200 °C on a hot plate after 5 minutes. After cooling, the flask was filled with purified water to make up the volume to 50 mL (deionized water filtered through activated carbon). Cold vapor atomic absorption spectrometry (Hg-201, Sanso Seisakusho Co., Tokyo, Japan) (**Fig. 4.6**) was used to evaluate an aliquot of the final solution (< 20 mL) by $SnCl_2$ as a reducing agent. In addition, the water content of the samples was obtained by calculating the difference in sediment mass before and after the samples dried in a convection oven at 105°C for 24 hours.

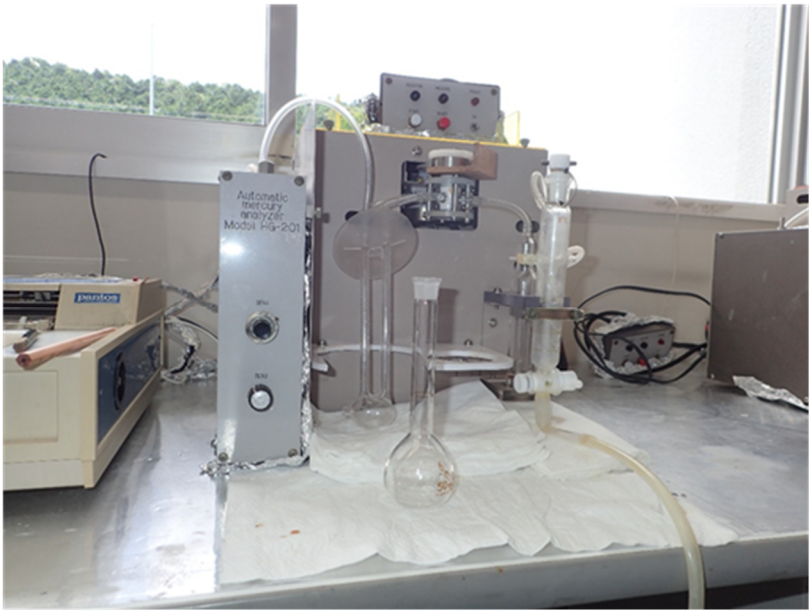

Figure 4.6 Model Hg-201 Semi-automated Mercury Analyzer.

4.3 Results and Discussions

4.3.1 Distribution of sediment particle sizes in the Yatsushiro Sea

In this study, the method modified based on the approach described by Wentworth (1922) was used (**Table 4.1**). For samples obtained along the A and B sampling lines, particle size distribution ratios were calculated for each vertical depth (**Table 4.2, Table 4.3**). The particle fractions were classified as follows: very fine silt to fine silt (79.38 ± 21.77%), medium silt to coarse silt (16.76 ± 16.57%), very fine sand to fine sand (21.89 ± 9.87%), and medium sand to very coarse sand (17.27 ± 7.76%). According to the classification results, it comes to be concluded that silt that ranged in size from very fine to fine was the predominant sediment type.

Table 4.1 Classification of the sediment particles (modified from Wentworth, 1922).

Particle name	**clay**	**very fine silt-fine silt**	**medium silt-coarse silt**	**very fine sand-fine sand**	**medium sand-coarse sand**	**coarse sand-very coarse sand**
Particle size (mm)	0.004>	0.004-0.016	0.016-0.062	0.062-0.250	0.250-0.500	0.500-1.000

Table 4.2 Classification of sediments in the Yatsushiro Sea (A line).

A line	Vertical depth(cm)	A number of cut sample	Particle size classification (%)			
			4-16 (μm)	16-62 (μm)	62-250 (μm)	250-1,000 (μm)
Y28	0-2	7	100.0			
	3-5	14	100.0			
	5-7	7	85.7	14.3		
	8-10	20	95.0	5.0		
	10-12	18	100.0			
	12-14	16	87.5	12.5		
Y18	0-2	6	33.3	66.7		
	3-5	16	87.5	6.3		6.3
	6-8	15	93.3	6.7		
	8-10	15	100.0			
	10-12	16	68.8	18.8	12.5	
	12-14	23	87.0	4.3	8.7	
	15-17	23	95.7	4.3		
Y17	0-2	8	75.0	12.5		12.5
	3-5	16	62.5	12.5	12.5	12.5
	6-8	16	62.5	12.5	12.5	12.5
	8-10	19	52.6	10.5	10.5	26.3
	10-12	17	64.7	5.9	17.6	11.8
	12-14	20	60.0	5.0	15.0	20.0
	14-16	25	56.0	8.0	16.0	20.0
Y16	0-2	11	63.6	18.2	18.2	
	3-5	12	66.7	25.0	8.3	
	6-8	15	60.0	13.3	26.7	
	8-10	17	58.8	17.6	23.5	
	10-12	15	53.3	13.3	33.3	
	12-14	21	52.4	19.0	28.6	
Y15	0-2	5	60.0	20.0	20.0	
	3-5	9	44.4	33.3	22.2	
	6-8	17	47.1	5.9	41.2	5.9
	sample (n)	cut (n)	Average (%) ± SD			
A line	29	439	71.50 ±19.43	14.86 ±12.80	19.26 ±8.96	14.19 ±6.52

Table 4.3 Classification of sediments in the Yatsushiro Sea (B line).

B line	Vertical depth (cm)	A number of cut sample	Particle size classification （%）			
			4-16 (μm)	16-62 (μm)	62-250 (μm)	250-1,000 (μm)
Y28	0-2	7	100.0			
	3-5	14	100.0			
	5-7	7	85.7	14.3		
	8-10	20	95.0	5.0		
	10-12	18	100.0			
	12-14	16	87.5	12.5		
Y39	0-2	6	16.7	66.7	16.7	
	3-5	10	80.0		20.0	
	6-8	8	50.0		37.5	12.5
	8-10	15	53.3	6.7	26.7	13.3
	10-12	12	8.3	50.0	41.7	
	12-14	18	55.6	5.6	16.7	22.2
	17-19	24	50.0	4.2	12.5	33.3
Y51	0-2	8	75.0	25.0		
	3-5	16	93.8	6.3		
	6-8	15	100.0			
	8-10	19	100.0			
	10-12	11	90.9	9.1		
	13-15	19	100.0			
	16-18	15	100.0			
	19-21	19	100.0			
Y60	0-2	19	100.0			
	3-5	14	100.0			
	6-8	15	100.0			
	8-10	16	100.0			
	10-12	25	100.0			
	12-14	22	100.0			
	15-17	25	100.0			
	18-20	42	100.0			
Y67	0-2	7	100.0			
	3-5	12	100.0			
	6-8	15	100.0			
	8-10	18	100.0			
	10-12	23	100.0			
	13-15	25	100.0			
	15-17	32	100.0			
	sample (n)	cut (n)	Average (%) ± SD			
B line	36	607	87.27 ±24.10	18.65 ±20.34	24.52 ±10.78	20.35 ±8.99

4.3.2 The background concentrations of T-Hg in sediment

For effectively evaluating the migration of mercury from Minamata Bay to the Yatsushiro Sea, the background concentrations of T-Hg in sediments should be measured. In this study, the T-Hg concentrations in the upper 3 cm of the deepest layer in seven core sediment samples (The sampling points marked as solid dots in **Fig. 4.1**) that had stable T-Hg concentrations were investigated. The results are shown in **Table 4.4**. The average background T-Hg concentration in sediments in the Yatsushiro Sea was 0.08 ± 0.01 mg/kg dry weight. In 2000, Tomiyasu et al. (2000) reported that the background T-Hg concentration in sediment in the Yatsushiro Sea was almost 0.068 ± 0.012 mg/kg dry weight. According to the study that Nakata et al. (2008) proposed in 2008, the background level of T-Hg in the Yatsushiro Sea sediments was close to 0.10 mg/kg dry weight. While the study of Matsuyama et al. (2014) performed in 2014 showed that the average background concentration of T-Hg was 0.10 ± 0.05 mg/kg dry weight. Therefore, the value of the background concentration determined is reliable.

Table 4.4 T-Hg concentrations of sediment in the upper 3 cm of the deepest layer in the Yatsushiro Sea.

		T-Hg concentration(mg/kg.dry basis)						
Sediment sample No.		Y66	Y59	Y50	Y49	Y38	Y36	Y26
Vertical depth	-17cm		0.07	0.09		0.06	0.07	
	-18cm	0.10	0.09	0.07	0.06	0.07	0.07	0.13
	-19cm	0.09	0.09	0.07	0.05			0.14
	-20cm	0.09			0.06			0.06
Average		0.09	0.08	0.08	0.06	0.07	0.07	0.11
SD		0.01	0.01	0.01	0.01	0.01	0.00	0.04
Total avergae ±SD		0.08±0.01						

4.3.3 The total mercury concentrations of different particle size fractions and the vertical distribution

As is shown in **Fig. 4.7**, the T-Hg concentrations in different particle size fractions were measured, and the distribution in the vertical direction was evaluated. At point Y28, which was near Minamata Bay, the T-Hg concentration in the sediments gradually increased from the surface to the layer of 9 cm. Then the T-Hg concentration in the sediments gradually decreased with depth. The maximum T-Hg concentration at 9 cm below the surface was 1.23 mg/kg dry weight. According to a sedimentation rate of 13.0 ± 2.8 g/m^2/day that was recorded in Minamata Bay by Matsuyama et al. (2019), the sediment age at 9 cm below the surface can be calculated, equal to around 50 years old (i.e., deposition in the 1960s to 1970s). The physicochemical properties of the sea have an impact on the rate of sedimentation of dispersed particulate matter. This indicates that the real age of sediment may be different from its calculated age. However, the estimated age in the present study is consistent with the acetaldehyde production history of the Chisso Corporation and discharge into Minamata Bay, which peaked between 1960 and 1963 (Matsuyama et al., 2019). On the other hand, even if the background total mercury concentration in the Yatsushiro Sea is subtracted, the T-Hg concentration in the sediments is still high. All these prove that the mercury in Minamata Bay has migrated to the Yatsushiro Sea. Moreover, compared with other points, the sampling point Y28 in the Yatsushiro Sea is closest to Minamata Bay, which is greatly affected by mercury migrating from Minamata Bay. It implied that more attention and continuous monitoring should be paid and carried out for sea areas near Minamata Bay. At point Y18, the total mercury concentration in the sediments in the vertical direction gradually increased from the surface layer to the depth of 4 cm and remained basically stable from the depth of 4 cm to 14 cm, and then gradually decreased when the depth was higher than 14 cm. There are two reasons considered to cause the results above: One is that the sediments at that depth lower than 14 cm may be migrated from Minamata Bay; The other is that the particle size distribution of the sediments at each vertical distance (**Table 4.2, Table 4.3**) is relatively stable because the mercury adsorption on sediments is affected by sediment particle size. Therefore, the mercury migration from Minamata Bay has a significant effect on the sediments at point Y18. At point Y17, the total mercury concentration in the sediment increased and maintained at a

certain level from the surface layer to the depth of 7 cm, and then decreased rapidly, indicating that the sediments adsorbing mercury migrating from Minamata Bay had a greater impact on the seven cm-deep sediments. In comparison, it has less impact on the sediments ultra to 7 cm deep. At points Y16 and Y15, although the total mercury concentration in the sediment also increased first and then decreased, the trend was not obvious. The concentration of total mercury at different depths was relatively stable, indicating that the amount of mercury migrating to this sea area was relatively stable.

At point Y39, the total mercury concentration in the sediment is higher from the surface layer to the depth of 10 cm, and the concentration fluctuates greatly at the same time. According to Kumamoto Prefecture (1998)， the Chisso Corporation temporarily switched the drainage location from the Hyakken drain to the Minamata River in 1958. As a result, mercury pollution moved in the direction of Ashikita, which is situated between the city of Yatsushiro and Minamata. The vertical distribution of the T-Hg content in the sediments at point Y39 may have been impacted by the mercury emitted during this period. On the other hand, different from point Y18, the particle size distribution of the sediments at each vertical distance varied for point Y39 (**Table 4.2, Table 4.3**), which is considered to contribute to the result. At points Y51 and Y60, the total mercury concentration in the sediment both increases first and then decreases with depth. While their total mercury concentrations in the sediments at the two points are quite different, and their changes are also distinct. This difference in mercury concentration is mainly due to the different distances of the two points from Minamata Bay. The T-Hg concentration at Y67 was approximately 0.25 mg/kg dry weight and almost constant between the surface sediment and the lower layer. Using the anthropogenic mass fraction and considering the background T-Hg concentration, the analysis revealed that about 65% of the T-Hg concentration was obtained from an anthropogenic source. Although the T-Hg concentration is relatively low, it is possible that mercury from Minamata Bay has gradually migrated widely.

Overall, in the horizontal direction, the T-Hg concentration became smaller and smaller along A and B lines from the sampling point Y28, indicating the mercury transport from Minamata Bay to the Yatsushiro Sea. The sediment migration along line A is considered to be mainly affected by barotropic current, while the sediment

migration along line B is mainly influenced by baroclinic current, consistent with the findings by Yano et al. (2014). In the vertical direction, the T-Hg concentration increased first and then decreased overall. From the surface layer to a certain depth, the total mercury concentration in the sediment is relatively large and increases gradually. After reaching a certain depth, the total mercury concentration in the sediment decreases rapidly until it approaches the background value. To some extent, the T-Hg concentrations of sediments at different vertical depths reflect the mercury migration from Minamata Bay to the Yatsushiro Sea in the corresponding periods. After stopping discharging effluent containing mercury, the mercury concentration in Minamata Bay sediments should be reduced with its transport. Therefore, the surface sediments at most points did not show the highest adsorbing mercury concentration. In addition, the presence of the sediments is not considered to be caused by migration when greater than a certain vertical depth, and its T-Hg concentration is close to the background. It is suggested that the migrated mercury was mainly deposited in the upper sediments (ex. 0-16 cm for point Y60). Furthermore, the average mercury contents for different particle size fractions except for YS60 and YS67 sampling points (only one category of particle size distribution) were calculated. The concentrations of very fine silt to fine silt, medium silt to coarse silt, very fine sand to fine sand, and medium sand to very coarse sand are 620 ppb, 547 ppb, 360 ppb, and 214 ppb, respectively. Comparing the total mercury concentration in sediments with different classified particle sizes indicated that the sediments with smaller particle sizes had higher T-Hg concentrations.

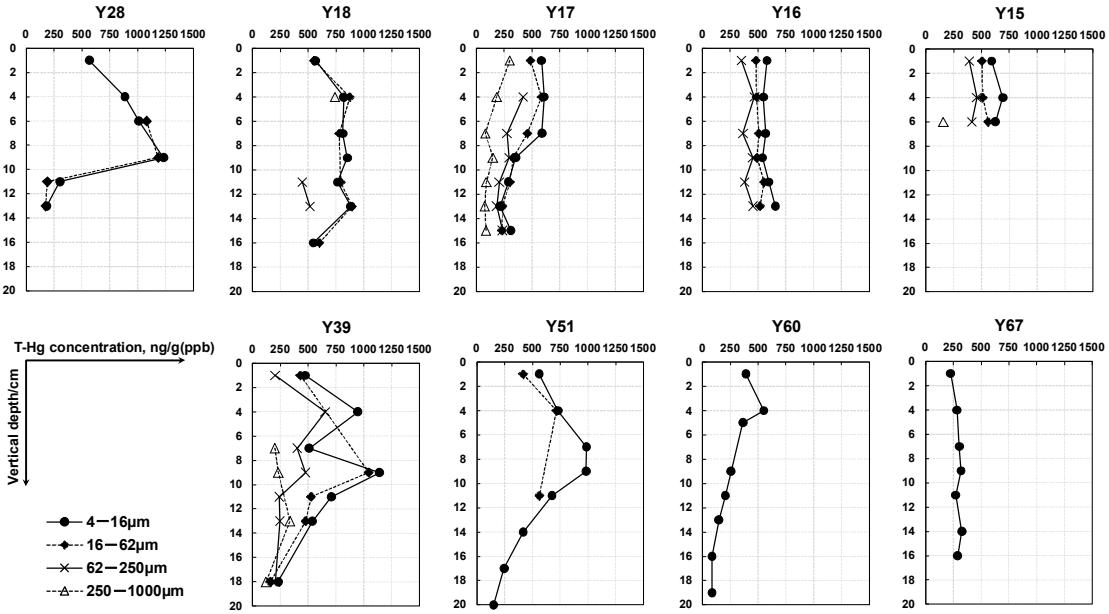

Figure 4.7 The T-Hg concentrations of different particle size fractions and the vertical distribution.

4.4 Conclusions

We develop a novel method based on particle size classification to comprehend both horizontal and vertical distribution of the total-Hg (T-Hg) concentration in sediment fractions in the Yatsushiro Sea.

In the horizontal direction, the T-Hg concentration became smaller and smaller along A and B lines from the sampling point Y28, indicating the mercury transport from Minamata Bay to the Yatsushiro Sea. Moreover, it suggested that the migrated mercury was mainly deposited in the upper sediments by analyzing the vertical distribution of total mercury in sediment.

In addition, according to the classification experiment results, it can be concluded that overall, the smaller the particle size, the higher the T-Hg concentration.

Furthermore, very fine silt to fine silt particles are the main particles that are transferred.

References

Akagi, H., & Nishimura, H. (1991). Speciation of mercury in the environment. *Advances in mercury toxicology*, 53-76.

Akagi, H., Malm, O., Branches, F., Kinjo, Y., Kashima, Y., Guimaraes, J.R.D., Oliveira, R.B., Haraguchi, K., Pfeiffer, W.C., Takizawa, Y., & Kato, H. (1995). Human exposure to mercury due to goldmining in the Tapajos river basin, Amazon, Brazil: speciation of mercury in human hair, blood and urine. *Water, Air, & Soil Pollution*, 80(1-4), 85-94.

Campbell, M. J., Oh, J., & Azemard, S. (2008). World-wide Intercomparison Exercise for the Determination of Trace Elements in IAEA-158 Marine Sediment. International Atomic Energy Agency, Marine Environment Laboratories.

EPA. (1978). METHOD #: 375.4. Approved for NPDES (Editorial Revision).

Hachiya, N. (2006). The history and the present of Minamata disease. *Japan Medical Association Journal*, 49, 112-118.

Japanese Standards Association. (2016). Determination of particle size distribution by gravitational liquid sedimentation methods—Part 1: General principles and guidelines, JIS Z8820, 1.

Kumamoto Prefecture. (1998). An Outline of the Environmental Restoration of Minamata Bay.

Malm, O., Branches, F. J., Akagi, H., Castro, M. B., Pfeiffer, W. C., Harada, M., Bastos, W.R., & Kato, H. (1995). Mercury and methylmercury in fish and human hair from the Tapajos river basin, Brazil. *Science of the Total Environment*, 175 (2), 141-150.

Minamata City. (2022). Minamata Disease -Its History and Lessons-2022, 66p.

Ministry of the Environment, Japan. (2013). Lessons from Minamata Disease and Mercury Management in Japan, 58p.

Matsunoshita, K., Yano, S., Matsuyama, A., Kitaoka, T. & Tada, A. (2018). Analysis on dispersion of mercury in bottom sediments in Minamata Bay by long-term numerical simulation of sediment transport using particle size classification model. *Journal of Japan Society of Civil Engineers, Ser. B2 (Coastal Engineering)*, 74(2), I_1153-I_1158.

Matsuyama, A., Yano, S., Hisano, A., Kindaichi, M., Sonoda, I., Tada, A., & Akagi, H. (2014). Reevaluation of Minamata Bay, 25 years after the dredging of mercury-polluted sediments. *Marine pollution bulletin*, 89(1-2), 112-120.

Matsuyama, A., Yano, S., Matsunoshita, K., Kindaichi, M., Tada, A., & Akagi, H. (2019). The spatial distribution of total mercury in sediments in the Yatsushiro Sea, Japan. *Marine Pollution Bulletin*, 149, 110539.

Nakata, H., Shimada, H., Yoshimoto, M., Narumi, R., Akimoto, K., Yamashita, T., Matsunaga, T., Nishimura, K., Tanaka, M., Hiraki, K., Shimasaki, H., & Takikawa, K. (2008). Concentrations and distribution of mercury and other heavy metals in surface sediments of the Yatsushiro Sea including Minamata Bay, Japan. *Bulletin of Environmental Contamination and Toxicology*, 80, 78-84.

Tomiyasu, T., Nagano, A., Yonehara, N., Sakamoto, H., Ōki, K., & Akagi, H. (2000). Mercury contamination in the Yatsushiro Sea, south-western Japan: spatial variations of mercury in sediment. *Science of the Total Environment*, 257(2-3), 121-132.

Wentworth, C.K. (1922). A scale of grade and class terms for clastic sediments. *Journal of Geology*, 30(5), 377-392.

Yano, S. (2013). In-situ measurement of mercury transport in the sea water of Minamata Bay. *Procedia Earth and Planetary Science*, 6, 448-456.

Yano, S., Kawase, H., Hisano, A. Riogilang, H., Matsuyama, A., & Tada, A. (2014). Examination on the Relationship between Bottom Sediment Transport and Baroclinic Structure by Numerical Model in Minamata Bay. *Journal of Japan Society of Civil Engineers, Ser. B2 (Coastal Engineering)*, 70(2), I_461-I_420 (in Japanese).

Yoshinaga, O., Eto, K., & Nakai, S. (1984). Classification process of Kuroboku soil. *Journal of Soil Science and Plant Nutrition*, 55(3), 248-256.

Chapter 5
Analysis of the Relationship Between T-Hg Concentration and Particle Size as well as Specific Surface Area

5.1 Introduction

An acetaldehyde-producing factory released mercury-contaminated sewage into Minamata Bay from 1932 and continued for more than 30 years until 1968 (Minamata City, 2022). The mercury accumulated in the sediment, bioaccumulated in fish and shellfish, and led to the Minamata Disease (Harada, 1995; Hachiya, 2006). To get rid of sedimentary sludge with over 25 ppm of mercury, the Minamata Bay Pollution Prevention Project was started on October 1st, 1977 (Li et al., 2009). After the remediation project, the mercury concentration was significantly decreased. However, the residual mercury concentrations remained ten times higher than the background level of the natural environment (Tomiyasu et al., 2006). The total mercury content in the sediments of the Minamata Bay area was measured from 2002 to 2010 (Tomiyasu et al., 2014). It was found that the amount of discharged mercury remaining in the contaminated layer was estimated to be 750 ± 290 kg. In 2012, a detailed survey of mercury concentrations in sediments at the bottom of Minamata Bay was conducted (Matsuyama et al., 2014). The total quantity of mercury was calculated to be 3.4 t and 2.3 mg/kg dry weight basis in the bottom sediments of Minamata Bay, respectively. Moreover, it was suggested that the mercury that remained in Minamata Bay migrated from Minamata Bay to the Yatsushiro Sea (Matsuyama et al., 2019). Therefore, the pollution of residual mercury in the Minamata Bay area still arouses widespread concern.

Tomiyasu et al. (2008) measured the concentrations of total mercury (T-Hg) and methylmercury (MeHg) in the bottom water, suspended solids, and surface sediments of Minamata Bay. The results showed that the sediments were an essential source of mercury in the water of the bay. In addition, MeHg concentrations in the bottom water were also much higher in the upper and middle layers of the water column,

suggesting that methylmercury may be mainly released into water from sediments. Therefore, it is essential to grasp the content and distribution of mercury in the sediment. In the past, there were some studies on the distribution of mercury in the sediments of the sea around the bay. However, sediments are composed of various particles, and there are few studies on whether the composition of sediments affects the content of mercury in sediments.

The different particle sizes of sediments may influence gravity-induced sedimentation and cause various specific surface areas that result in different amounts of absorbed mercury. Hence, in this study, dependent on sedimentation classification, the relationships between the T-Hg concentration and sediment particle size as well as particle specific surface area were investigated.

5.2 Methodology

5.2.1 Investigate location and sample collection

The area investigated in this study is located in the Yatsushiro Sea. As a closed water system, the Yatsushiro Sea is surrounded by the prefectures of Kagoshima and Kumamoto, whose area is 1200 km^2 and 22.2 m deep on average (Ministry of the Environment, 2006). Minamata Bay is located in the southeastern region of the Yatsushiro Sea. In an earlier study, Matsunoshita et al. (2018) measured the plane distribution of surface sediment in the Yatsushiro Sea. The result indicated that mercury was more distributed in the northeast and southwest regions of the Yatsushiro Sea near Minamata Bay (**Fig. 5.1**). Therefore, sediment sampling was carried out in the northeast and southwest regions of the Yatsushiro Sea in this study. **Fig. 5.2** depicts the location of the sampling points. The process of core sampling of the sediment is as follows: using a core sampler to fall freely at a certain height and then biting the sediments with the sampler (**Fig. 5.3**). Additionally, a GPS system was used in order to reach the sampling points accurately.

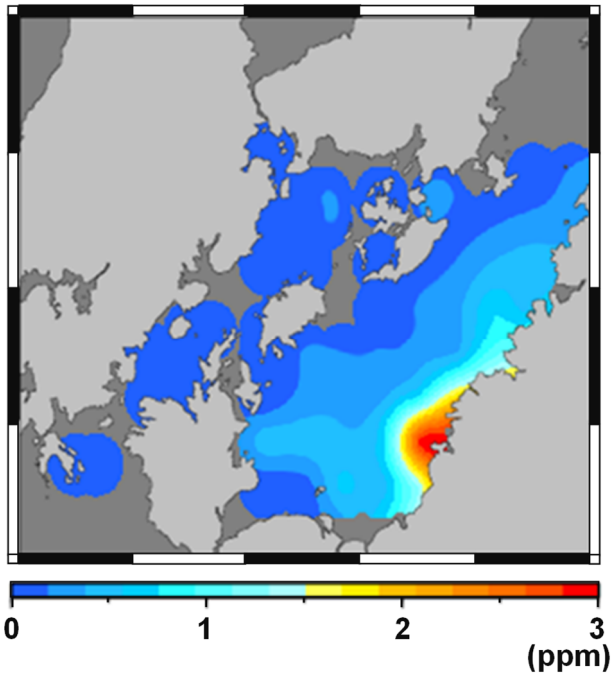

Figure 5.1 A T-Hg concentration distribution of surface sediment (Matsunoshita et al., 2018).

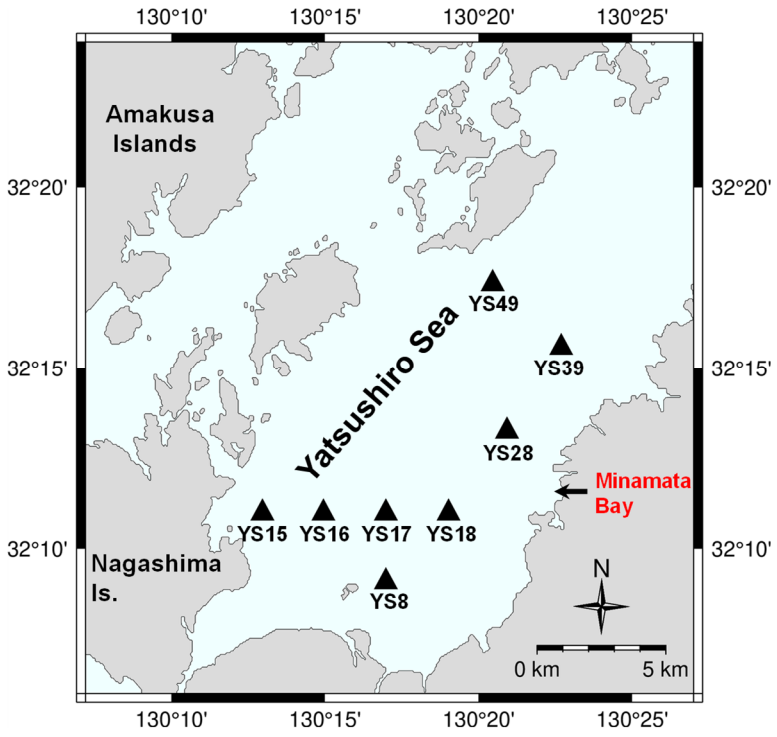

Figure 5.2 The location of the sampling points.

Figure 5.3 The core sampler (Rigo Co. Ltd., Saitama, Japan).

5.2.2 Classification process of samples

Generally, sediments in marine areas have a particle size distribution but do not being with uniform particle sizes. In order to classify sediment samples dependent on particle size, sedimentation classification was conducted using the difference in sedimentation velocity due to the difference in particle weight, as detailed below. The core sediment samples were cut into 1 cm slices from top to bottom and stored in an ultra-low temperature freezer (< -80 °C). In order to obtain a suitable sample volume, each adjacent two 1 cm sediment slices were mixed. The pre-prepared sediment sample was put into a 14 mm heat-shrinkable tube that had been plugged at one end with a rubber stopper. After adding the dispersion solvent (glycerol/ethanol, 1:2 v/v) to the tube, the top of the tube was plugged with another rubber stopper. The sample and dispersion solvent in the tube were thoroughly mixed by hand shaking for 1 minute, and then stored in a refrigerator. After two weeks, samples were frozen in liquid nitrogen and cut into 5 mm sections. This process is the same as in **Chapter 4**.

5.2.3 Measurement of particle size distribution and calculation of specific surface area

Water needs to be removed from the sediment prior to particle size analysis. Frozen sediment samples from an ultra-low temperature freezer (<-80°C) were thawed at room temperature and placed in a circulating dryer for drying. Thereafter, the sediment samples were thoroughly mixed while impurities in the sediment were manually removed. A laser diffraction particle size analyzer (SALD-3100, Shimadzu Corporation, Kyoto, Japan) was used to analyze the particle size distribution of the samples.

In reality, sediments are not just composed of particles of uniform size, but there is a distribution of particle sizes. For example, the distribution proportion of each particle size in the measured sediment sample of YS28(1,2)-1 is shown in **Fig. 5.4**.

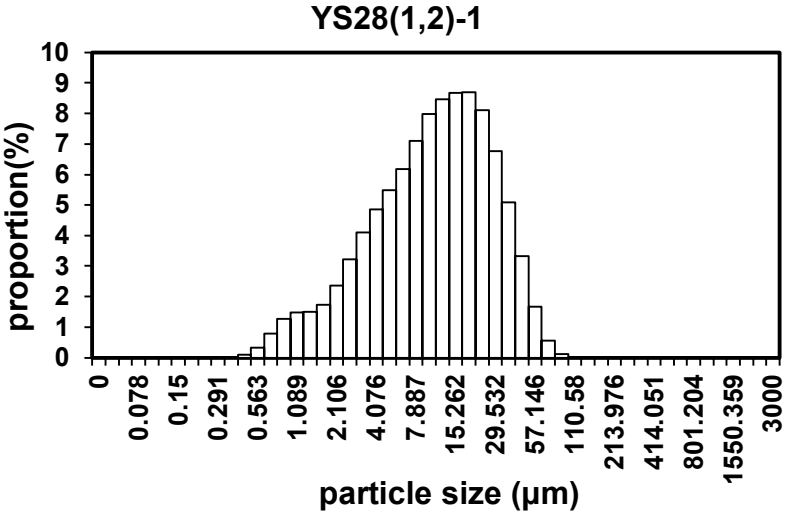

Figure 5.4 The distribution proportion of each particle size in the measured sediment sample of YS28(1,2)-1.

Assuming that each particle is perfectly spherical and with a soil particle specific gravity of 2.65×10^{-12} g/μm^3 (Winterwerp and Van Kesteren, 2004), the specific surface area of each sample can be calculated from the frequency distribution of each particle size. The specific surface area of the sediment samples can be calculated as follows:

$$m = \sum (G_s \times V \times k) \tag{5-1}$$

$$V = \frac{4}{3}\pi \left(\frac{D}{2}\right)^3 \tag{5-2}$$

$$S = \sum (S_n \times k) \tag{5-3}$$

$$S_n = 4\pi \left(\frac{D}{2}\right)^2 \tag{5-4}$$

$$S_m = \frac{S}{m} \tag{5-5}$$

where m is weight (g), G_s respects particle density equal to 2.65×10^{-12} g/μm^3, V respects volume (μm^3), k is the proportion of each particle size, D is particle size (μm), S respects surface area (μm^2), S_n is the surface area of each particle (μm^2), S_m is the specific surface area of the sediment sample.

5.2.4 Determination of mercury concentration

T-Hg concentrations in sediments were measured using the method proposed by Akagi and Nishimura (1991) and modified by Akagi et al. (1995). The accuracy and precision of the method have been calibrated in laboratories (Malm, et al., 1995). It has been repeatedly validated in the analysis of the IAEA-158 reference standard as well (Campbell and Azemard, 2008). The sediment sample, 1 mL distilled water, 2 mL nitric acid/perchloric acid (1:1, v/v), and 5 mL concentrated sulfuric acid were mixed in a 50 mL volumetric flask. After 5 minutes, the volumetric flask was heated for 20 minutes (above 200 °C). After the volumetric flask had been cooled, the volume was made up of purified water. Using $SnCl_2$ as a reducing agent, the samples were analyzed by cold vapor atomic absorption spectrometry (Hg-201, Sanso Seisakusho Co., Tokyo, Japan). The water content of the sediment is calculated from the difference in the mass of the sediment before and after drying.

5.3 Results and Discussions

5.3.1 Relationship between particle size and total mercury concentration

The relationship between particle size and total mercury concentration is shown in **Fig. 5.5**. At point YS28, the particle size is in a minor range from 6 μm to 25 μm, suggesting there is no significant change in particle size, subsequently resulting in an inconspicuous relationship between T-Hg concentration and particle size. Except for point YS28, the total mercury concentration at various sampling points was inversely proportional to the particle size of the sediments. Overall, with the increase of particle size, the T-Hg decreased gradually. It completely demonstrates that particle size has a great influence on the distribution of T-Hg. The smaller the particle size of sediments, the larger the specific surface area, which provides more effective sites for mercury absorption. On the other hand, the migration speed of sediment with smaller particle sizes is considered higher because of the gravity effect, leading to more mercury migration and accumulation. Therefore, sediments with small particle sizes have a high T-Hg concentration.

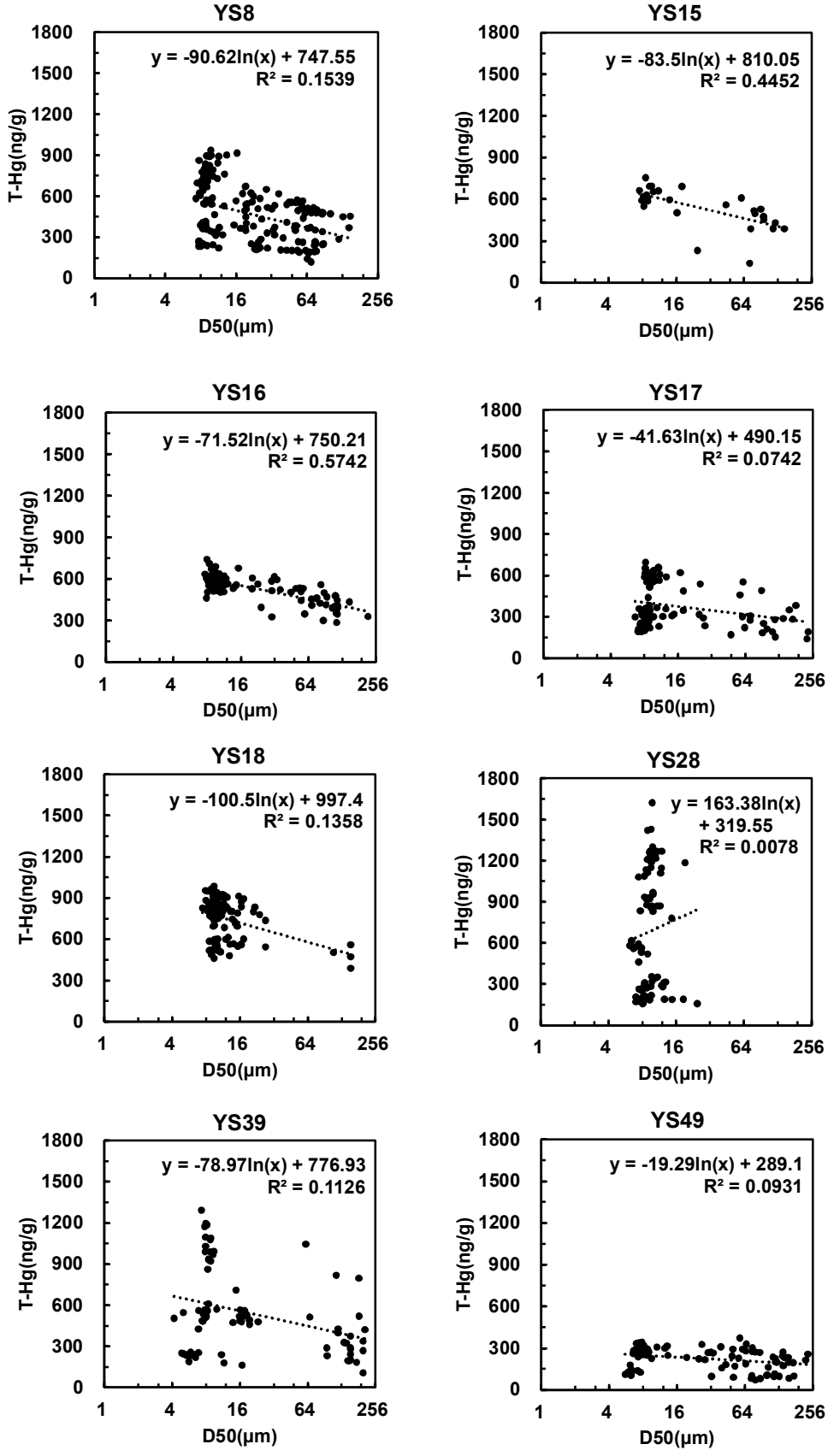

Figure 5.5 The relationship between particle size and T-Hg concentration.

5.3.2 Relationship between total mercury concentration and particle specific surface area of sediments

As shown in **Fig. 5.6**, the relationship between T-Hg concentration and particle specific surface area of sediments was obtained. It can be seen that the specific surface area at various sampling points was proportional to the total mercury concentration in the sediments. In other words, the larger the specific surface area, the higher the total mercury concentration. It indicated that the specific surface area of sediment particles has an influence on the total mercury distribution in sediments. It is mainly because of the following two reasons:

(1) Mercury can be fixed on the particle surface through adsorption in the sediment. Due to the larger specific surface area of particles, the ratio of surface area to volume is higher, and there is more surface area available for adsorption. Therefore, the larger the specific surface area of particles, the more mercury they can adsorb, leading to a higher T-Hg concentration in sediments;

(2) The larger the specific surface area of particles, the lower their settling rate, the more mercury they can carry, resulting in a higher T-Hg concentration in sediments.

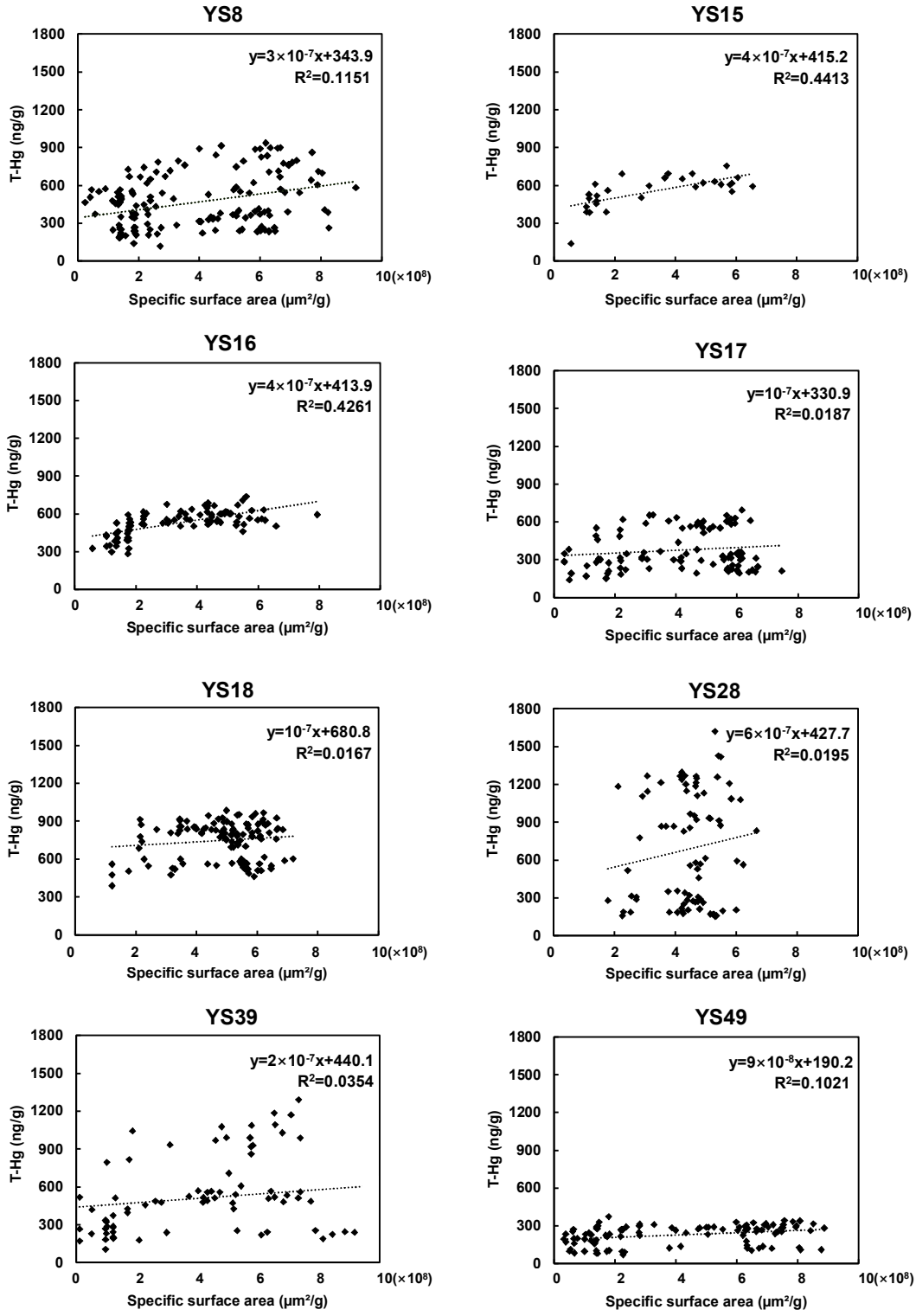

Figure 5.6 The relationship between T-Hg concentration and particle specific surface area.

5.4 Conclusions

In this study, the relationships between T-Hg concentration and particle size as well as specific surface area were investigated.

According to the experimental results, it can be seen that the particle size and specific surface of the sediment have a great influence on the concentration and distribution of mercury in the sediment.

The larger the particle size of the sediment particles, the lower the T-Hg concentration in the sediments. The migration speed of sediment with smaller particle sizes is considered higher because of the gravity effect, leading to a higher amount of Hg accumulation.

The larger the specific surface area of the sediment particles, the higher the T-Hg concentration in the sediment. The larger the specific surface area of particles, the lower their settling rate, the more mercury they can adsorb, resulting in higher T-Hg concentration in sediments.

References

Akagi, H., & Nishimura, H. (1991). Speciation of mercury in the environment. *Advances in mercury toxicology*, 53-76.

Akagi, H., Malm, O., Branches, F., Kinjo, Y., Kashima, Y., Guimaraes, J.R.D., Oliveira, R.B., Haraguchi, K., Pfeiffer, W.C., Takizawa, Y., & Kato, H. (1995). Human exposure to mercury due to gold mining in the Tapajós River Basin, Amazon, Brazil-speciation of mercury in human hair, blood and urine, *Water, Air, & Soil Pollution*, 80(1-4), 85-94.

Campbell, M. J., Oh, J., & Azemard, S. (2008). World-wide Intercomparison Exercise for the Determination of Trace Elements in IAEA-158 Marine Sediment. International Atomic Energy Agency, Marine Environment Laboratories.

Hachiya, N. (2006). The history and the present of Minamata disease. *Japan Medical Association Journal*, 49, 112-118.

Harada, M. (1995). Minamata disease: methylmercury poisoning in Japan caused by environmental pollution. *Critical reviews in toxicology*, 25(1), 1-24.

Li, P., Feng, X. B., Qiu, G. L., Shang, L. H., & Li, Z. G. (2009). Mercury pollution in Asia: a review of the contaminated sites. *Journal of hazardous materials*, 168(2-3), 591-601.

Malm, O., Branches, F.J., Akagi, H., Castro, M.B., Pfeiffer, W.C., Harada, M., Bastos, W.R., & Kato, H. (1995). Mercury and methylmercury in fish and human hair from the Tapajos River basin, Brazil, *Science of the Total Environment*, 175(2), 141-150.

Matsunoshita, K., Yano, S., Matsuyama, A., Kitaoka, T. & Tada, A. (2018). Analysis on dispersion of mercury in bottom sediments in Minamata Bay by long-term numerical simulation of sediment transport using particle size classification model. *Journal of Japan Society of Civil Engineers, Ser. B2 (Coastal Engineering)*, 74(2), I_1153-I_1158 (in Japanese).

Matsuyama, A., Yano, S., Hisano, A., Kindaichi, M., Sonoda, I., Tada, A., & Akagi, H. (2014). Reevaluation of Minamata Bay, 25 years after the dredging of mercury-polluted sediments. *Marine pollution bulletin*, 89(1-2), 112-120.

Matsuyama, A., Yano, S., Matsunoshita, K., Kindaichi, M., Tada, A., & Akagi, H. (2019). The spatial distribution of total mercury in sediments in the Yatsushiro Sea, Japan. *Marine Pollution Bulletin*, 149, 110539.

Minamata City. (2022). Minamata Disease -Its History and Lessons-2022, 66p.

Ministry of the Environment. (2006). Report of General Survey Results of Ariake Sea and Yatsushiro Sea by Survey Evaluation Committee.

Tomiyasu, T., Matsuyama, A., Eguchi, T., Fuchigami, Y., Oki, K., Horvat, M., Rajar, R. & Akagi, H. (2006). Spatial variations of mercury in sediment of Minamata Bay, Japan. *Science of the Total Environment*, 368(1), 283-290.

Tomiyasu, T., Matsuyama, A., Eguchi, T., Marumoto, K., Oki, K., & Akagi, H. (2008). Speciation of mercury in water at the bottom of Minamata Bay, Japan. *Marine Chemistry*, 112(1-2), 102-106.

Tomiyasu, T., Takenaka, S., Noguchi, Y., Kodamatani, H., Matsuyama, A., Oki, K., Kono, Y., Kanzaki, R., & Akagi, H. (2014). Estimation of the residual total mercury in marine sediments of Minamata Bay after a pollution prevention project. *Marine Chemistry*, 159, 19-24.

Winterwerp, J. C., & Van Kesteren, W. G. (2004). Introduction to the physics of cohesive sediment dynamics in the marine environment. Developments in Sedimentology, 56, Amsterdam: Elsevier, 466p.

Chapter 6
Analysis of Distribution and Migration of Mercury in Sediment in the Yatsushiro Sea Based on the Classification Experimental Method

6.1 Introduction

Mercury has a long and interesting history, stemming from its significant use in medicine and industry, and the resulting toxicity (Clifton II, 2007). Once mercury enters the food chain, it can accumulate in organisms and cause adverse effects, which in turn can seriously affect human health (Harada et al., 1999). In the 1960s, residents of Minamata City suffered severe neurosis due to eating seafood contaminated with methylmercury (MeHg). It is known as Minamata disease, and 2217 cases had been officially confirmed in the city by 1989 (Burbacher et al., 1990). To solve this problem, Kumamoto Prefecture started the Minamata Bay Pollution Prevention Project in 1977. The survey conducted after the completion of the project showed that the average T-Hg value at 84 sites in the bay had dropped to 4.7 (0.06-12) μg/g (Minamata City, 2022). However, as reported by Nishimura and Okamoto (2001), large amounts of methylmercury still exist in Minamata Bay. Moreover, the average level of mercury in fish remains still slightly higher than in other regions (Yasuda and Mori, 2010). Furthermore, some studies have reported the migration of mercury from Minamata Bay to the Yatsushiro Sea along with sediments (Rajar et al., 2004; Matsuyama et al., 2019). Therefore, it is essential to study the contra distribution of residual trace mercury in the Yatsushiro Sea, including the bay, continuously.

Mercury is mainly concentrated in sediments and migrates along with the sediments. The sediment acts as a record of deposition, and its geographic distribution of mercury could indicate the temporal behavior of discharged mercury (Tomiyasu et al., 2000). Therefore, the prediction of mercury migration based on sediments was

regarded as an effective way.

In **Chapter 3**, we developed a numerical model to simulate the migration of mercury-containing sediments from Minamata Bay to the Yatsushiro Sea. However, the particle size of the sediment used in this model is the average of the measured particle sizes. According to the research in **Chapter 5**, the particle size of the sediment has a great influence on the total mercury concentration in the sediments. Therefore, we need to study further the migration of mercury-containing sediments with different particle sizes.

In this study, dependent on sedimentation classification, the numerical simulations of sediment migration with different particle sizes were established to study the effect of particle size on the migration of mercury-containing sediments. Furthermore, based on the simulation results, combined with the relationship between total mercury and particle size, the simulation realized the distribution of T-Hg in the Yatsushiro Sea.

6.2 Model improvement

The numerical model was established using the Delft3D hydrodynamic model. The calculation domain in the model was defined to contain both the Yatsushiro Sea and the Ariake Sea. The horizontal grid is a variable grid established by Fathya et al. (2016), and the grid precision is 62.5 m, 125 m, and 250 m, respectively. The vertical grid adopts the σ-coordinate system and consists of five layers, each of which is 20% of the total depth. The water depth distribution in the calculation area is shown in **Fig. 6.1**.

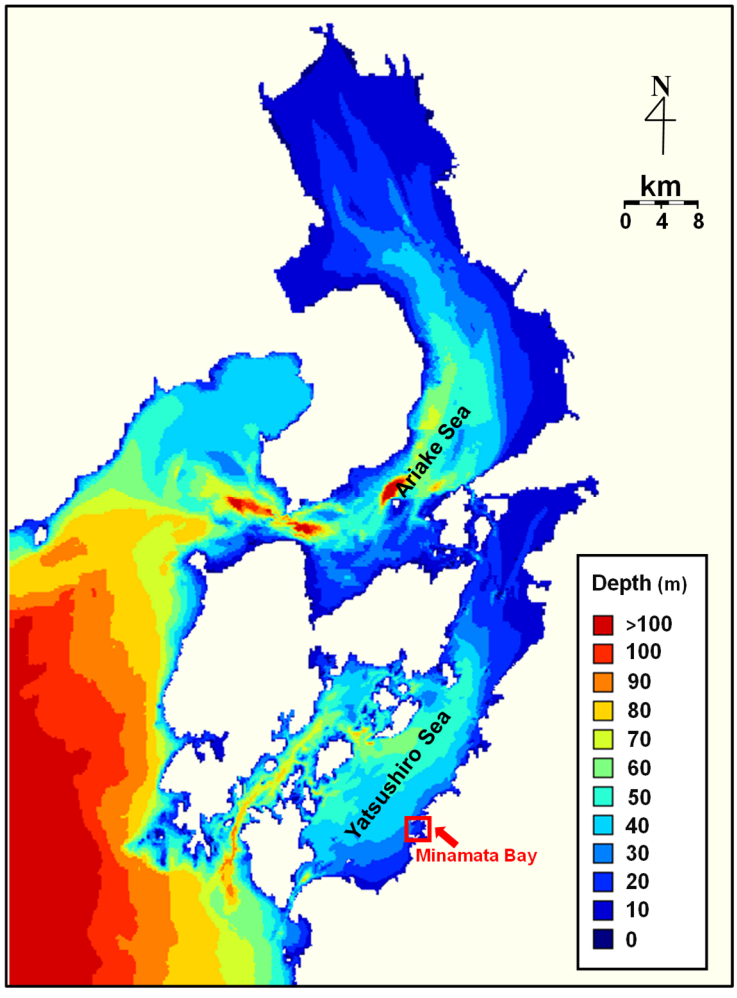

Figure 6.1 The water depth distribution in the calculation area.

The initial bottom sediment thickness was set to 1 m only in Minamata Bay (the area shown in the red box in **Fig. 6.2** and the initial bottom sediment thickness was set to 0 m elsewhere. The calculation period was one year.

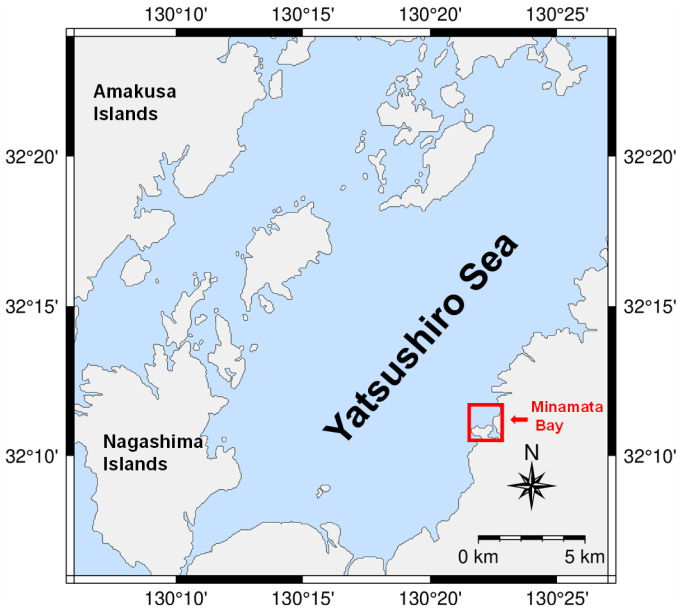

Figure 6.2 The initial sediment distribution setting.

According to the following formula, the critical shear stress was determined:

$$\tau_{*C} = \frac{\frac{\tau_{Cr,e}}{\rho}}{\left(\frac{\sigma}{\rho} - 1\right) g d_m} \tag{6-1}$$

where τ_{*C} denotes dimensionless critical tractive force, which is 0.05, $\tau_{cr,e}$ respects the critical shear stresses for erosion (Pa), σ is particle density (g/cm^2), ρ denotes water density (g/cm^3), g respects gravity acceleration (cm/s^2), d_m is the median grain size of sediment samples (μm).

The following formula can be used to calculate the sedimentation rate of suspended particles:

$$w_s = \left(\sqrt{\frac{2}{3} + \frac{36\nu^2}{d_*}} - \sqrt{\frac{36}{d_*}} \right) \sqrt{(\sigma_s - 1) g D} \tag{6-2}$$

$$d_* = \frac{(\sigma_s - 1) g D^3}{\nu^2} \tag{6-3}$$

where w_s denotes the sedimentation velocity (cm/s), ν is the kinematic viscosity coefficient (cm^2/s), D respects the median grain size (cm), g is gravity acceleration (cm/s^2), and σ_s denotes particle density (g/cm^3).

According to the distribution of particle sizes in sediments (**Fig. 6.3**, data from **Chapter 5**), several particle sizes are selected for calculation in this simulation. The critical shear stresses for erosion $\tau_{cr,e}$ and the sedimentation rate w_s of different particle sizes are shown in **Table 6.1**. In addition, the erosion rate parameters were used from **Chapter 3**, which were obtained based on *in-situ* measurements.

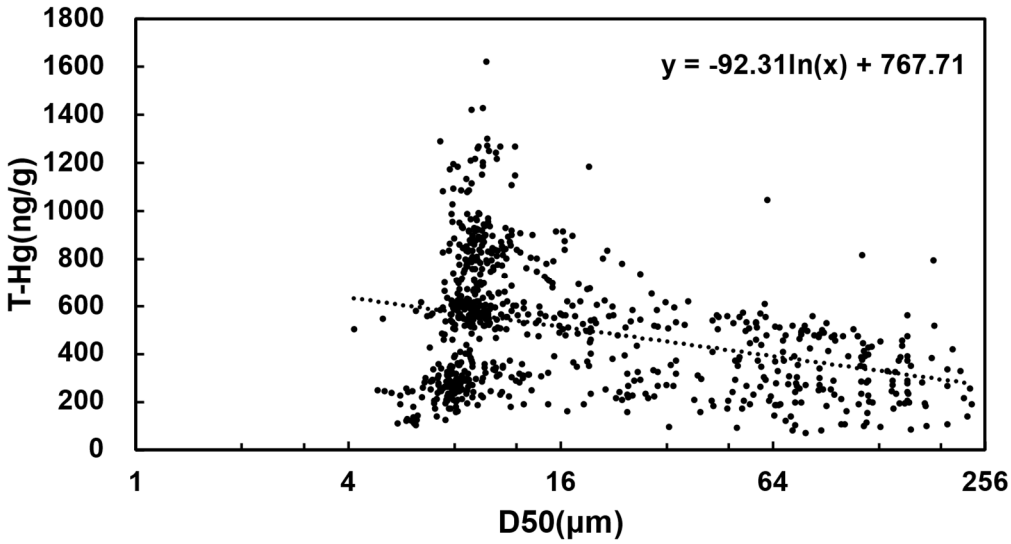

Figure 6.3 The distribution of particle sizes in sediments and the relationship between the T-Hg concentration and the particle size of the sediments as a whole.

Table 6.1 The critical shear stresses for erosion and the sedimentation rate of different particle sizes.

Particle sizes (μm)	The critical shear stresses (N/m^2)	The sedimentation rate (m/s)
5	3.97×10^{-3}	2.25×10^{-5}
10	7.94×10^{-3}	8.99×10^{-5}
15	1.19×10^{-2}	2.02×10^{-4}
25	1.99×10^{-2}	5.61×10^{-4}
50	3.97×10^{-2}	2.23×10^{-3}
75	5.96×10^{-2}	4.91×10^{-3}
100	7.95×10^{-2}	8.40×10^{-3}
200	1.59×10^{-1}	2.53×10^{-2}

For the erosion and deposition process of sediments, the Partheniades-Krone (K-P) framework was used. The formulas are as follows:

$$E = MS(\tau_{cw},\ \tau_{cr,e}) \tag{6-4}$$

$$D = wc_bS(\tau_{cw},\ \tau_{cr,d}) \tag{6-5}$$

$$S(\tau_{cw}, \tau_{cr,e}) = \left(\frac{\tau_{cw}}{\tau_{cr,e}} - 1\right), \text{when } \tau_{cw} > \tau_{cr,e} \tag{6-6}$$

$$S(\tau_{cw}, \tau_{cr,e}) = 0, \text{when } \tau_{cw} \leq \tau_{cr,e} \tag{6-7}$$

$$S(\tau_{cw}, \tau_{cr,d}) = \left(1 - \frac{\tau_{cw}}{\tau_{cr,d}}\right), \text{when } \tau_{cw} < \tau_{cr,d} \tag{6-8}$$

$$S(\tau_{cw}, \tau_{cr,d}) = 0, \text{when } \tau_{cw} \geq \tau_{cr,d} \tag{6-9}$$

where E denotes erosion flux (kg/m^2/s), M is erosion rate parameters (kg/m^2/s), D respects deposition flus (kg/m^2/s), w is settling velocity (m/s), c_b respects suspended solid concentration in the bottom layer (kg/m^3), τ_{cw} is bottom shear stress (N/m^2), $\tau_{cr,e}$ respects critical shear stresses for erosion (N/m^2) and $\tau_{cr,d}$ denotes critical shear stresses for deposition, which is 1.0 N/m^2 (Yano et al., 2014).

6.3 Results and Discussions

6.3.1 Migration of mercury-containing sediments with different particle sizes

The migration of mercury-containing sediments with different particle sizes is shown in **Fig. 6.4**. The smaller the particle size of the sediment, the faster the migration speed and the more comprehensive the migration range. This phenomenon is mainly due to the fact that the sediments in small particle sizes have a larger specific surface area, which contributes to providing the sediments with more areas to contact with the surrounding environment. It is easier to be transported and diffused under the action of water flow, and so on. Additionally, when the inertial mass of particles is smaller, the movement resistance becomes smaller, which leads to its faster movement speed as well. After one year of simulation, it can be found that sediments with a particle size greater than 50 μm migrated almost exclusively around Minamata Bay, illustrating that once the particle size is bigger than 50 μm, much longer time is needed for the sediments to transport to the Yatsushiro Sea while their migration range is also tiny. Furthermore, it confirms again that the sediments with smaller particle sizes are the main force for migration.

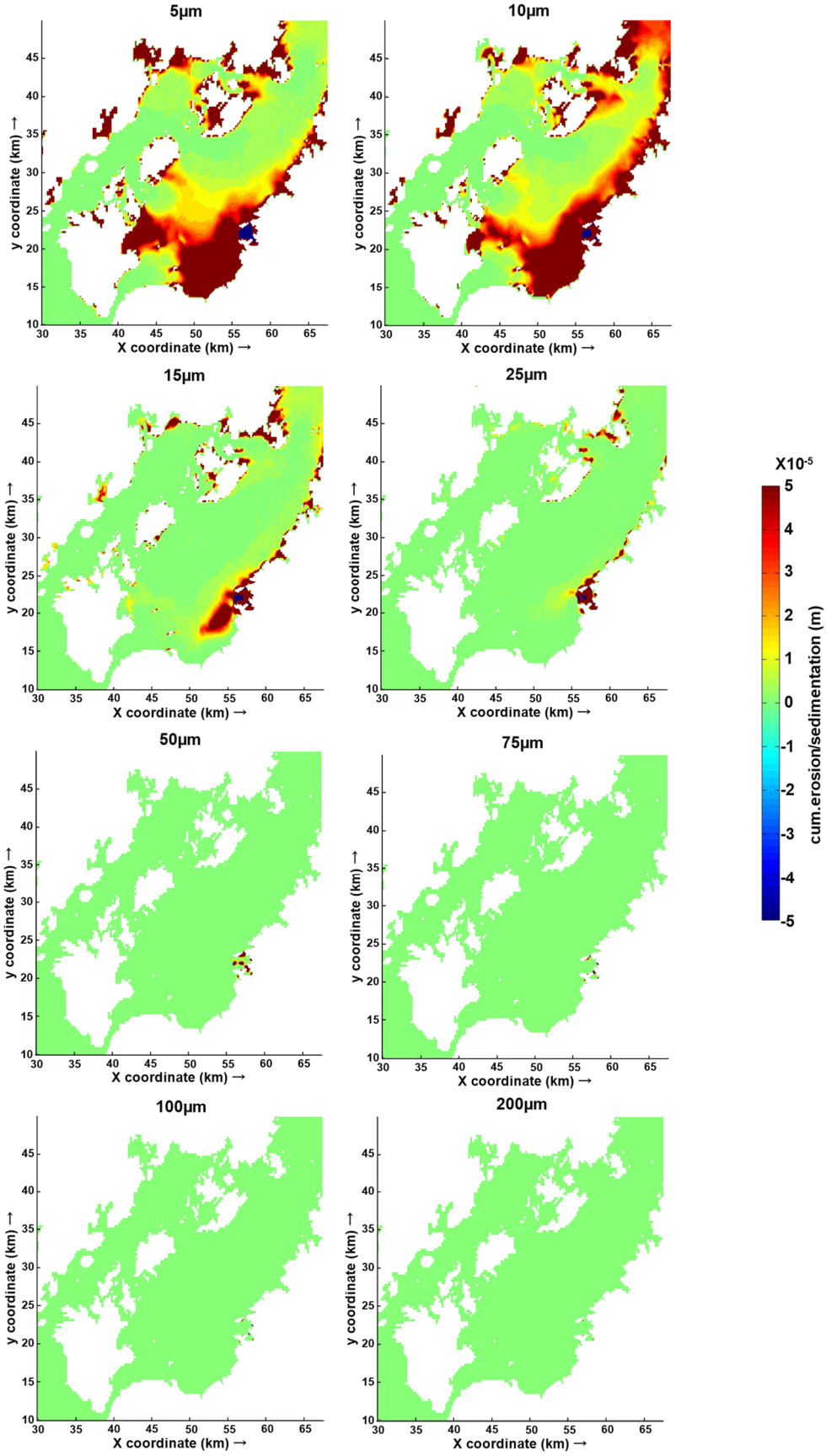

Figure 6.4 The migration of sediments with different particle sizes.

6.3.2 Mercury concentration distribution in the Yatsushiro Sea

Based on the migration simulations in **Section 6.3.1**, combined with the relationship between particle size and mercury concentration (**Fig. 6.3**), the mercury concentration distribution in the Yatsushiro Sea considering the effect of particle size (from 5 μm to 200 μm) was obtained (**Fig. 6.5**), where the distribution rules of different particle sizes and the weighted settlement were used. It can be seen that mercury is mainly distributed in the southwest and northeast of the Yatsushiro Sea near Minamata Bay. Meanwhile, the amount of mercury distributed in the southwest area of the Yatsushiro Sea is more than that in the northeast area. This may be mainly caused by the geographical differences between the two regions and the influence of different ocean currents. In addition, due to the complex topography and vegetation in the shore area, the water flow is relatively slow, which makes mercury more likely to distribute in the shore area. On the other hand, the more sediments and suspended matter in the coastal area, which are more likely to absorb mercury, may be another reason for the accumulation of mercury in the coastal area. In the earlier study, Matsuyama et al. (2019) measured the plane distribution of sediment with a T-Hg concentration range of 0.5-2.0 mg/kg dry weight in the Yatsushiro Sea. Compared with their experimental result of T-Hg distribution (**Fig. 6.6**), it concludes that the simulated distribution (**Fig. 6.5**) agreed well with the measured one.

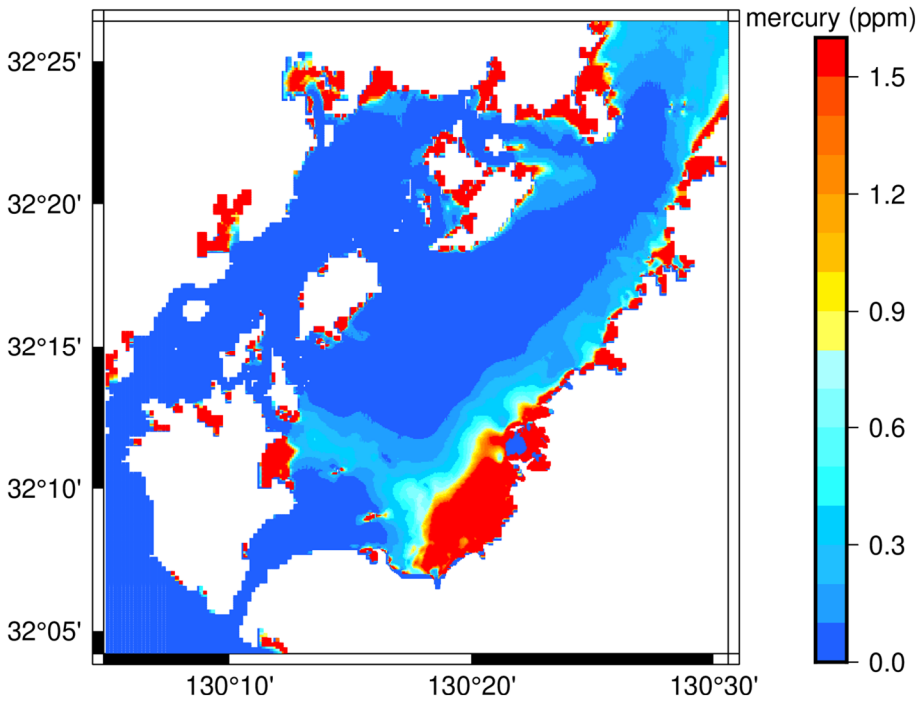

Figure 6.5 The mercury concentration distribution in the Yatsushiro Sea.

Figure 6.6 The plane distribution of sediment with T-Hg concentration range of 0.5-2.0 mg/kg dry weight (area filled with gray lines) (Matsuyama et al., 2019).

6.4 Conclusions

In this study, numerical simulations were performed on the migration of mercury-containing sediments with different particle sizes in the Yatsushiro Sea. According to the simulation results, it can be concluded that:

1. The smaller the particle size of the sediment, the faster the migration speed and the more comprehensive the migration range.

2. The sediments with smaller particle sizes are the main force of migration. Once the particle size is bigger than 50 μm, a much longer time is needed for the sediments to transport to the Yatsushiro Sea while their migration range is also tiny.

3. Based on the numerical simulation of migration, considering the relationship between particle size and mercury concentration, the concentration distribution of mercury in the Yatsushiro Sea was calculated, and it was found that mercury is mainly distributed in the southwest and northeast of the Yatsushiro Sea. Meanwhile, the amount of mercury distributed in the southwest area of the Yatsushiro Sea is more than that in the northeast area. In addition, the simulated distribution shows high agreement with the experimental measurements.

References

Burbacher, T. M., Rodier, P. M., & Weiss, B. (1990). Methylmercury developmental neurotoxicity: a comparison of effects in humans and animals. *Neurotoxicology and Teratology*, 12(3), 191-202.

Clifton II, J. C. (2007). Mercury exposure and public health. *Pediatric Clinics of North America*, 54(2), 237-249.

Fathya, E.N., Yano, S., Matsuyama, A., Tada, A. & Riogilang, H. (2016). Impact of reclamation project on mercury contaminated sediment transport from Minamata Bay into the Yatsushiro Sea. *Journal of Japan Society of Civil Engineers, Ser. B2(Coastal Engineering)*, 72(2), I_1285-I_1290.

Harada, M., Nakachi, S., Cheu, T., Hamada, H., Ono, Y., Tsuda, T., Yanagida, K., Kizaki, T. & Ohno, H. (1999). Monitoring of mercury pollution in Tanzania: relation between head hair mercury and health. *Science of the total environment*, 227(2-3), 249-256.

Matsuyama, A., Yano, S., Matsunoshita, K., Kindaichi, M., Tada, A., & Akagi, H. (2019). The spatial distribution of total mercury in sediments in the Yatsushiro Sea, Japan. *Marine Pollution Bulletin*, 149, 110539.

Minamata City. (2022). Minamata Disease -Its History and Lessons-2022, 66p.

Nishimura, H. & Okamoto, T. (2001). Minamatabyou no Kagaku (The Science of Minamata Disease), Nippon Hyoronsha (in Japanese).

Rajar, R., Žagar, D., Četina, M., Akagi, H., Yano, S., Tomiyasu, T., & Horvat, M. (2004). Application of three-dimensional mercury cycling model to coastal seas. *Ecological Modelling*, 171(1-2), 139-155.

Tomiyasu, T., Nagano, A., Yonehara, N., Sakamoto, H., Ōki, K., & Akagi, H. (2000). Mercury contamination in the Yatsushiro Sea, south-western Japan: spatial variations of mercury in sediment. *Science of the Total Environment*, 257(2-3), 121-132.

Yano, S., Kawase, H., Hisano, A. Riogilang, H., Matsuyama, A., & Tada, A. (2014). Examination on the Relationship between Bottom Sediment Transport and Baroclinic Structure by Numerical Model in Minamata Bay. *Journal of Japan Society of Civil Engineers, Ser. B2 (Coastal Engineering)*, 70(2), I_461-I_420 (in Japanese).

Yasuda, Y., & Mori, K. (2010). Mercury deposit distribution in Minamata Bay. *Coastal Marine Science*, 34(1), 223-229.

Chapter 7
Conclusions and Recommendations

Minamata disease is one of four big pollution diseases in Japan. Due to the toxicity, bioaccumulation, and environmental sustainability of mercury, the mercury entering Minamata Bay is absorbed by organisms and accumulates in the biological chain, and finally absorbed by humans, which leads to very serious consequences. Although the high concentration of mercury has been dredged after the incident, many studies have shown that the mercury concentration in water systems and organisms in Minamata Bay is still much higher than in other areas, and the mercury in the bay has migrated to the Yatsushiro Sea along with the sediment. Therefore, we studied the distribution of mercury in the sediments of the Yatsushiro Sea near the bay and the mercury migration with the sediment through a combination of simulation and experiment.

A numerical model to simulate the transport of bottom sediments from Minamata Bay to the Yatsushiro Sea was established in Delft3D based on in-situ measurement results adapting internal diffusion. According to the simulation results, we can conclude that the sediments transported from the bay to the Yatsushiro Sea significantly. Mercury-containing sediments migrated from the bay to the seas around the bay and gradually spread to the entire Yatsushiro Sea. The sediments were mainly deposited in the coastal seas of the southwest and northeast Yatsushiro Sea and the seas surrounding Nagashima Island and Amakusa over time. The mercury-containing sediments trended to deposit along the seacoast, which was mainly considered due to the terrain effect.

We develop a novel method based on particle size classification to comprehend both horizontal and vertical distribution of the total-mercury (T-Hg) concentration in sediment fractions in the Yatsushiro Sea. In the horizontal direction, the T-Hg concentration became smaller and smaller along A and B lines from the sampling point Y28, indicating the mercury transport from Minamata Bay to the Yatsushiro Sea. Moreover, it suggested that the migrated mercury was mainly deposited in the upper sediments by analyzing the vertical distribution of total mercury in sediment. In addition, according to the classification experiment results, it can be concluded that overall, the smaller the particle size, the higher the T-Hg concentration.

Furthermore, very fine silt to fine silt particles are the main particles that are transferred.

The relationships between T-Hg concentration and particle size as well as specific surface area were investigated. The particle size and specific surface of the sediment have a great influence on the content and distribution of mercury in the sediment. The larger the particle size of the sediment particles, the lower the T-Hg concentration in the sediments. The larger the specific surface area of the sediment particles, the higher the T-Hg concentration in the sediment.

Numerical simulations were performed on the migration of mercury-containing sediments with different particle sizes in the Yatsushiro Sea. According to the simulation results, it can be concluded that the smaller the particle size of the sediment, the faster the migration speed and the more comprehensive the migration range. The sediments with smaller particle sizes are the main force of migration. Based on the numerical simulation of migration, considering the relationship between particle size and mercury concentration, the concentration distribution of mercury in the Yatsushiro Sea was calculated, and it was found that mercury is mainly distributed in the southwest and northeast of the Yatsushiro Sea near Minamata Bay. Meanwhile, the amount of mercury distributed in the southwest area of the Yatsushiro Sea is more than that in the northeast area.

In this thesis, a more accurate simulation of mercury migration from Minamata Bay to the Yatsushiro Sea was obtained by developing a simulation based on measured data. Moreover, the distribution of T-Hg concentration in sediment fractions in the Yatsushiro Sea and the influence of sediment properties (such as particle size and specific surface area) on the mercury concentration in the sediment were investigated by a new particle size classification experimental method. Furthermore, the effect of particle size on mercury transport was analyzed, and a direct transformation from the accumulation and erosion of mercury-containing sediments to the distribution and transport of mercury was realized by combining experiments and simulations.

Recommendations for further research

This study was mainly conducted on the total mercury in sediments. In reality, there are many forms of mercury in nature, such as methylmercury, which has the most

toxic impact on humans. The hydrodynamic model of this study and the ecological model can be combined to continue to study the methylation and demethylation of mercury.

In the experiments of this study, the data are mainly from the main sampling points. However, the area of the Yatsushiro Sea is very wide, and the density and number of sampling points can be increased in the future to investigate the mercury pollution in the Yatsushiro Sea more accurately.